Spring 5-31-2012

Mathematical models of combustion at high pressure

Daniel Fong
New Jersey Institute of Technology

Copyright Warning & Restrictions

The copyright law of the United States (Title 17, United States Code) governs the making of photocopies or other reproductions of copyrighted material.

Under certain conditions specified in the law, libraries and archives are authorized to furnish a photocopy or other reproduction. One of these specified conditions is that the photocopy or reproduction is not to be "used for any purpose other than private study, scholarship, or research." If a, user makes a request for, or later uses, a photocopy or reproduction for purposes in excess of "fair use" that user may be liable for copyright infringement,

This institution reserves the right to refuse to accept a copying order if, in its judgment, fulfillment of the order would involve violation of copyright law.

Please Note: The author retains the copyright while the New Jersey Institute of Technology reserves the right to distribute this thesis or dissertation

Printing note: If you do not wish to print this page, then select "Pages from: first page # to: last page #" on the print dialog screen

ABSTRACT

MATHEMATICAL MODELS OF COMBUSTION AT HIGH PRESSURE

by
Daniel Fong

In this dissertation, we develop new mathematical theories of flame propagation that are valid at elevated, or extreme, pressures. Of particular interest is the regime of burning in which the pressure exceeds the critical pressure of the species undergoing chemical reaction. Fluids and flames are known to behave differently under these extreme conditions as opposed to atmospheric pressure. The focus of this dissertation is to investigate these differences by deriving reduced models that contain the unique features.

In the first part of this dissertation, we analyze the structure of laminar diffusion flames at high pressure in the limit of large activation energy for the particular configuration of a steady flame in counterflow. We consider a dense fluid in which normal Fickian diffusion of the fuel is limited, and thermal diffusion, i.e., the Soret effect, is the dominant mechanism for fuel mass transport. Temperature and species profiles, as well as flame temperature and location, are determined as a function of Damköhler number and Soret diffusion coefficient. In particular, we find that oxidant is entirely consumed by the flame, while some fuel leaks through. For light fuels, the fuel profile is found to have a local peak on the oxidant side as a result of thermal diffusion. Our analysis includes a description of extinction phenomenon, including explicit criteria in terms of the Soret diffusion coefficient, ratio of temperature of the two streams, and the Damköhler number at extinction.

In the second part of this dissertation, we derive an asymptotic theory of laminar premixed flames in high density fluids in the limit of large activation energy. The model is intended to provide insights into the structure and dynamics of deflagration

waves in high pressure, dense fluids where normal Fickian diffusion is limited. In such cases, particularly under conditions exceeding the thermodynamic critical point of the fluid, the primary mode of species transport is through thermal diffusion, i.e., the Soret effect. Such a model for diffusive transport is considered, and we derive a model with an explicit dependence on the Soret effect for a one-step overall reaction. The density is assumed sufficiently high to adopt a constant density formulation. The local reaction-diffusion structure is found to be fundamentally different from that of an ideal gas with Fickian diffusion, which results in new conditions relating the equations for thermal and mass transport in the bulk flow. The model is used to investigate the basic structure of planar flames, as well as their stability. Stability boundaries are identified that mark the transition from planar to either steady, spatially periodic structures, or time-dependent modes of propagation. The combined effects of the Soret diffusion coefficient and Lewis number are discussed. Furthermore, a weakly nonlinear analysis of the derived model is carried out, resulting in a modified Kuramoto-Sivashinsky (K-S) equation, accounting for effects of Soret Diffusion. Linear stability analysis shows that the flame front is unstable with respect to long-waves in a range of Soret diffusion coefficient that corresponds to no and weak Soret effect. However, there exists a range of Soret diffusion coefficient for which a flame front is unconditionally stable.

MATHEMATICAL MODELS OF COMBUSTION AT HIGH PRESSURE

by
Daniel Fong

A Dissertation
Submitted to the Faculty of
New Jersey Institute of Technology and
Rutgers, The State University of New Jersey – Newark
in Partial Fulfillment of the Requirements for the Degree of
Doctor of Philosophy in Mathematical Sciences,

Department of Mathematical Sciences, NJIT
Department of Mathematics and Computer Science, Rutgers-Newark

May 2012

APPROVAL PAGE

MATHEMATICAL MODELS OF COMBUSTION AT HIGH PRESSURE

Daniel Fong

Dr. John K. Bechtold, Dissertation Advisor — Date
Professor, Department of Mathematical Sciences, NJIT

Dr. Shahriar Afkhami, Committee Member — Date
Assistant Professor, Department of Mathematical Sciences, NJIT

Dr. Michael R. Booty, Committee Member — Date
Professor, Department of Mathematical Sciences, NJIT

Dr. Linda J. Cummings, Committee Member — Date
Associate Professor, Department of Mathematical Sciences, NJIT

Dr. Hong G. Im, Committee Member — Date
Professor, Department of Mechanical Engineering, University of Michigan

BIOGRAPHICAL SKETCH

Author: Daniel Fong

Degree: Doctor of Philosophy

Date: May 2012

Undergraduate and Graduate Education:

- Doctor of Philosophy in Mathematical Sciences,
  New Jersey Institute of Technology, Newark, NJ, 2012
- Bachelor of Science in Mathematical Sciences,
  New Jersey Institute of Technology, Newark, NJ, 2007
- Bachelor of Science in Computer Science,
  New Jersey Institute of Technology, Newark, NJ, 2007

Major: Mathematical Sciences

Presentations and Publications:

Refereed Publications

Fong, D., Bechtold, J. K., and Law, C. K. An Asymptotic Theory of Laminar Premixed Flames in Dense Fluids, (in preparation).

Fong, D., Bechtold, J. K., and Law, C. K. Asymptotic Structure of Laminar Diffusion Flames at High Pressure, (submitted to Phys. Fluids).

Conference Proceedings

Fong, D., Bechtold, J. K., and Law, C. K. An Asymptotic Theory of Laminar Premixed Flames in Dense Fluids (short version), *2012 Spring Technical Meeting of the Western States Section of the Combustion Institute*, Tempe, AZ, March 19-20, 2012.

Fong, D., Bechtold, J. K., and Law, C. K. Asymptotic Structure of Diffusion Flames at High Pressure (short version), *7th U.S. National Technical Meeting of the Combustion Institute*, Atlanta, GA, March 20-23, 2011.

Presentations

Fong, D., Bechtold, J. K., and Law, C. K. An Asymptotic Theory of Laminar Premixed Flames in Dense Fluids, *2012 Spring Technical Meeting of the Western States Section of the Combustion Institute*, Tempe, AZ, March 19, 2012.

Davis, D. L., and Fong, D. Turbulent Basis Functions for Flow Simulation, *37th Annual Dayton-Cincinnati Aerospace Science Symposium*, Dayton, OH, March 6, 2012.

Fong, D., and Davis, D. L. A New Method for Improving Turbulent Combustion Simulations, *Propulsion Sciences Branch Seminar – Aerospace Propulsion Division*, Air Force Research Laboratory, Wright-Patterson Air Force Base, OH, August 26, 2011.

Fong, D., Bechtold, J. K., and Law, C. K. Asymptotic Structure of Diffusion Flames at High Pressure, *NJIT Summer Program Seminar Series*, Newark, NJ, May 24 2011.

Fong, D., Bechtold, J. K., and Law, C. K. Asymptotic Structure of Diffusion Flames at High Pressure, *Combustion Branch Seminar – Turbine Engine Division*, Air Force Research Laboratory, Wright-Patterson Air Force Base, OH, April 25, 2011.

Fong, D., Bechtold, J. K., and Law, C. K. Asymptotic Structure of Diffusion Flames at High Pressure, *7th U.S. National Technical Meeting of the Combustion Institute*, Atlanta, GA, March 21 2011.

Fong, D., and Bechtold, J. K. Asymptotic Structure of Diffusion Flames at High Pressure with Soret Transport, *Society for Industrial and Applied Mathematics Annual Meeting 2010 (AN10)*, Pittsburgh, PA, July 12, 2010.

Fong, D., and Bechtold, J. K. Asymptotic Structure of Diffusion Flames at High Pressure with Soret Transport, *NJIT Summer Program Seminar Series*, Newark, NJ, July 6 2010.

This dissertation is dedicated to my parents,
Soi Tong Fong and I Lei Vong.

ACKNOWLEDGMENT

First and foremost, I offer my sincerest gratitude and appreciation to my adviser, Professor John K. Bechtold, who has supported me throughout my dissertation with his patience and encouragement. He has introduced me to the field of combustion theory and shared his immeasurable knowledge with me. Certainly, he has always been a positive influence in both my academic as well as professional career. I am truly grateful for everything he has done for me: the conferences and workshops he encouraged me to attend, the presentations he helped me prepare, and the reviewers comments he taught me how to response to. Besides I truly admire his kindness – he allowed me to take a summer off for an internship. One simply could not wish for a better and friendlier adviser than him. From the bottom of my heart, I truly thank him.

I would like to thank my committee members, Professor Shahriar Afkhami, Professor Michael R. Booty, Professor Linda J. Cummings, and Professor Hong G. Im, not only for their constructive comments and suggestions, but also for their time and interest.

I would like to extend my gratitude to Dr. Angelo J. Perna and Ms. Zara Williams of the NJIT Ronald E. McNair Post-baccalaureate Achievement program. They have been my mentor on countless occasions and for that I am extremely grateful.

I would also like to thank Dr. Douglas L. Davis, for his guidance and support during my summer 2011 internship at the Air Force Research Laboratory. Additionally, I would like to thank him for reviewing this dissertation.

Many gratitude must go to a very good friend and mentor of mine, Dr. Matt Malej, for his continuing support, encouragement and helpful advice.

In addition, I would like to thank my fellow graduate students, more specifically, Dr. Matthew Causley, Daniel Cargill, Dr. Xinxian Huang, Dr. Dongwook Kim, Te-Sheng Lin, Dr. Oleksiy Varfolomiyev, and Dr. Jacek Wrobel for being great friends and colleagues in the last five years.

Finally, I would like to thank my family for their support and encouragement. During the first two years of graduate studies, the combination of coursework and qualifying exams made my life miserable. I was totally burned out. Looking back now, I really need to thank my brother, my shopping buddy, Alberto Fong, for bringing me out of my own misery.

I would be remiss if I did not recognize my brother, the biggest sports fan I know, Humberto Fong. He has become a great hang out buddy in the last two years of graduate studies and I owe him many debts of gratitude. I enjoyed spending time dining together and attending all the sporting events he invited me to: from the NY Red Bulls to the NY Knicks. I truly thank him for the company the last two year.

I must acknowledge my, fiancé, Jing[2] Choi. I really do not know how she has put up with me for the last five years, but I am thankful for every day. Her love and support throughout the entire process (qualifying exams and dissertations) were instrumental to my success. I thank her for her love and care, plus for her positive attitude towards life – "Don't worry, everything will work out just fine."

Without the love, support and encouragement of my parents, Soi Tong Fong and I Lei Vong, I would never finish writing this dissertation. I still remember the day I called my mother in February, and asked if she could come back to NJ from Macau. Without hesitation, my mother agreed and they showed up two weeks later. I thank my father to made time in his busy schedule to travel back to visit me for two weeks. I thank my mother for staying with me to cook all of my meals and take good care of me until I am done writing. I owe many debts of gratitude to my parents and for that I dedicate this dissertation to my parents.

TABLE OF CONTENTS

TABLE OF CONTENTS
(Continued)

Chapter **Page**

LIST OF TABLES

Table **Page**

LIST OF FIGURES

LIST OF FIGURES
(Continued)

Figure **Page**

LIST OF FIGURES
(Continued)

Figure **Page**

CHAPTER 1

INTRODUCTION

1.1 Motivation and Objective

Combustion is very important in many aspects of our everyday life; our world is driven by the need to produce energy to manufacture products, for transportation (automobiles, trains, jet aircrafts, and even rockets), to heat homes and buildings, to incinerate hazardous wastes, and to produce electricity. A common source of energy in each of these applications is combustion, a chemical process in which a fuel reacts rapidly with oxidizer and gives off heat.

Some of the applications mentioned above, e.g., automobiles, jet aircrafts, and rockets have one thing in common; they employ combustion as a source of power and operate at pressures in the range of 5 to hundreds of atmospheres, which exceed the thermodynamic critical point of many species, e.g., hydrocarbons, undergoing combustion. Combustion under such conditions is more efficient, and can take place under more fuel-lean conditions, thereby reducing harmful emissions. As fossil fuels become more scarce, and attention is given to reducing emissions, engines of the future will operate at still higher pressures to exploit these benefits.

Figure 1.1 shows an example of a pressure-temperature phase diagram, which summarizes the effect of temperature and pressure on a substance. Every point in this diagram represents a possible combination of temperature and pressure for the system. The diagram identifies four distinct regions, which represent the solid, liquid, gas, and supercritical fluid (SCF) phases of the substance. A SCF, often referred to simply as a fluid, is any substance at a temperature and pressure above its critical point. The curves represent the temperatures and pressures where two phases coexist in equilibrium, e.g., the gas and liquid phases coexist along the boiling curve. By

increasing both temperature and pressure (moving upwards) along the boiling curve, then the liquid becomes less dense due to thermal expansion and the gas becomes more dense as the pressure rises. Eventually, the densities of the two phases converge and become identical, and the boiling curve comes to an end at the critical point. What truly characterizes the supercritical state is that there is no distinction between gas and liquid phases [21]. In this regime, the fluid density is closer to that of a liquid than gas, and cross-diffusion effects are known to be significant in numerous applications. In particular, the effective mass diffusivity becomes null at the critical point and the Soret effect (thermal diffusion), i.e., diffusive mass transport as a result of temperature gradients, becomes dominant [21, 20].

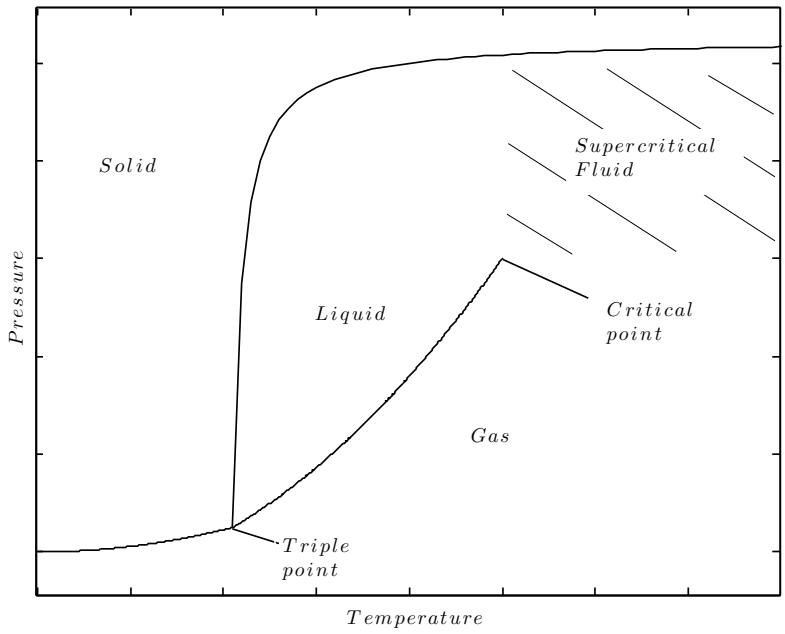

Figure 1.1 Typical pressure-temperature phase diagram of a substance.

There are many useful applications of SCF, but among the most important are industrial extraction and purification. The advantage of SCF is the liquid-like density which promotes solubility, and the gas-like viscosity and diffusivity make extraction and purification faster under supercritical conditions. For instance, supercritical fluids

have been used: for the decaffeination of green coffee beans, for the extraction of hops for beer production, for the production of essential oils and pharmaceutical products from agricultural products, for the separation of biological fluids, for bioseparation, to enhance oil recovery in mature oil fields, for recovery of organics from oil shale, for production of biodiesel, for pollution control, for dry cleaning, and many other applications.

However, this is a relatively new area for theoretical combustion research. Despite the recognized importance of the use of these combustors that actually operate in this regime. Most existing theoretical studies of flames are not able to describe this phenomenon. They are only appropriate to describe conditions at atmospheric pressure. Under such conditions, Fickian diffusion, i.e., molecular diffusion due concentration gradients, is the dominant mode of mass transport within the flame structure.

The objective of this dissertation is the development of new models for diffusion and premixed flames that incorporates features of flames that are relevant at high pressure. Asymptotic and perturbation methods, supplemented by numerical methods, are used to analyze the structure and dynamical properties of such flames. There are two main parts in this dissertation: 1) to examine the basic structure and dynamics of diffusion flames at high pressure, 2) to derive an asymptotic model of laminar premixed flames in high density fluids. The derived model is then employed to investigate the basic structure of planar flames, as well as their stability. Furthermore, a nonlinear partial differential equation, which describes the evolution of the disturbed flame front in high density fluids is derived. Finally, a linear stability analysis of the evolution equation for the flame front is carried out.

1.2 Mathematical Modeling and Activation Energy Asymptotics of Combustion Phenomena

Combustion science has been studied for centuries in order to better understand how to produce energy in a more efficient way. It is an interdisciplinary subject which involves challenging theoretical analysis, experiments and resource-intensive numerical simulations. Therefore, it is essential to have researchers with different backgrounds to work on this fascinating and complicated science. From a theoretical standpoint, the equations that govern combustion processes are the conservation equations of fluid dynamics, temperature and mass transport coupled to chemical kinetics. These nonlinear equations represent a balance between convection, diffusion and reaction. In many practical situations, these processes occur over different temporal and spatial scales. Consequently, a great deal of modern combustion theory has been developed through the use of multi-scale analysis, a standard tool of applied mathematicians, to extract reduced models that retain the essential physics of a given combustion process.

The theoretical study of combustion really took off with the discovery of the technique known as large activation energy asymptotics to resolve the highly nonlinear Arrhenius reaction rate term that appears in the governing equations. The origin of this technique dates back to 1938 where Frank-Kamenetskii [52] introduced approximations based on large activation energy to construct a steady-state thermal theory of spontaneous combustion. Around the same time, Zel'dovich exploited the modern singular perturbation theory which led to his early contributions to deflagration theory (equivalent to use of large activation energy asymptotics) [52]. Over the last 40 years, researchers have expanded on this approach to formally derive mathematical models that describe a wide variety of practical combustion processes. In particular the basic structure of premixed flames and diffusion flames have been analyzed, as well as ignition, extinction, flame-flow interactions, and instabilities. Surveys of all

these many studies can be found in several books that have been published in the last 25 years, e.g., [6, 29, 42, 50]. These books all emphasize the contributions of singular perturbation methods as one of the most important theoretical tools to advance combustion science. Given that this discussion extends earlier theory, it is appropriate to review many of these advances, which typically describe condition at atmosphere pressure. We will begin with premixed flames, then follow by diffusion flames. In addition, we describe new features that arise at high pressure and how these new features may be incorporated into the next generation of flame theory.

1.2.1 Mathematical Models of Premixed Flames

A premixed flame is a wave-like phenomena in which a chemically reacting flame front tends to propagate into, and consume, the unburned mixture where fuel and oxidizer are mixed at the molecular level. The flame front is often considered as a moving interface that separates two regions: the unburned fresh mixture region, where the temperature is low enough such that no chemical reaction has yet occurred; and the burned region, where the flame front has passed through.

The hydrodynamic model is used to describe large flames whose thickness is much smaller than the characteristic length scale of the flow field. When viewed on this length scale, the whole flame, where all transport processes and chemical reaction take place, is relatively thin. The flame may then be considered as a moving surface, which regard as the flame front. This class of model is appropriately used to study long wave instabilities for which the wavelength of a disturbance is much larger than the diffusion length.

On the other hand, the diffusional-thermal model is employed when the flame thickness is of the same order of magnitude as the characteristic length scale of the flow field, i.e., diffusion and convection are of comparable magnitude. When viewed on this length scale, the flame is like under a magnifying glass, where we can examine the

flame structure more closely to investigate the effect of diffusional-thermal interactions on the flame front.

The earliest theoretical studies of premixed flames were given by Landau [27] and Darrieus [12], often referred to as the hydrodynamic model. They treated the flame as a surface of moving density discontinuity, separating the unburned (high density) region from the burned (light density) region, thus ignoring diffusion. The fluid flow on either side of the flame is governed by the incompressible Navier-Stokes equations. In order to relate the fluid variables on either side, the Rankine-Hugoniot relations, expressing the conservation of mass, momentum and energy across the discontinuity were imposed. To close the problem, a constant flame speed, the rate of diffusion transport of heat from the flame front to the cold unburned mixture, was prescribed relative to the incoming flow. However, in contrast to experimental observations, the Darrieus-Landau model predicted that a plane flame is unconditionally unstable due to the thermal expansion across the flame (density differences between the unburned region and burned region). It was believed that the effects of diffusion in the flame structure could potentially stabilize the flame. A few years later, Markstein [33] proposed that the flame speed should be a function of curvature of the flame front. Thus, he modified the flame speed equation to include a linear dependence of curvature and introduced a phenomenological parameter to account for this dependence. He showed that curvature can indeed stabilize the flame under perturbations of sufficiently short wavelength, provided this new parameter was positive.

Matalon and Matkowsky [36], and Clavin and Williams [9] derived a model of flames as gasdynamic discontinuities for Near-Equidiffusional Flames (NEFs) – heat and mass diffuse at near equal rates. They considered the effect of flame on hydrodynamics through gas expansion. By analyzing the internal structure of the flame, they derived a set of jump conditions relating the fluid variables on the burned

and unburned regions. Matalon, Cui and Bechtold [34] later extended this model by using a two-reactant scheme, with arbitrary reaction orders, as well as variable transport coefficients. The resulting models are valid for flame of arbitrary shape in general fluid flows.

At the opposite end of the spectrum, a consistent mathematical derivation of a diffusional-thermal model was first proposed by Matkowsky and Sivashinsky [37]. This type of model is derived in the limit of large activation energy, so that the reaction zone confined to a narrow boundary layer which can be resolved asymptotically. The method of matched asymptotic is employed to analyze each region separately and matching relates the variables across the reaction zone. Thus, the nonlinear reaction rate term is effectively replaced by jump conditions. In addition to the realistic large activation energy assumption, these models also consider weak thermal expansion, in order to decouple the heat and mass transport equations from the hydrodynamic equations. Consequently, this type of model is sometimes referred to as the constant density approximation model. In addition, this has been used to derive various type of evolution equation for the flame front [47, 48]. Recently, Antoniou, Bechtold and Matalon [1] derived a new diffusional-thermal model for near-stoichiometric premixed flames in a two-reactant mixture. The derivation is carried out similar to the one-reactant model, by considering the limit of large activation energy, which enables an analytical resolution of the nonlinear reaction rate terms, and weak thermal expansion, which decouples the heat and mass transport equations from the hydrodynamic equations. They concluded that it is possible along a corrugated flame to have regions burning fuel-lean while neighboring regions burn fuel-rich. Furthermore, they provided a description of the extinction characteristics, showing that the flame response depends significantly on which of the two species is ultimately consumed at the reaction zone.

We have just briefly discussed two classes of models of laminar premixed flames: 1) the hydrodynamic model which considers the effect of the flame on the flow field, but ignores the effect of flow field on the flame, and 2) the diffusional-thermal model accounts for the effect of the flow field on the flame, but the effect of the flame on the flow field is suppressed.

However, all of these existing models mentioned above are only valid at atmospheric pressure. Therefore, it is necessary to develop a new model to account for these new features that arise at high pressure, which will be presented in Chapter 2. The objective of this dissertation is to examine these new features within the context of a diffusional-thermal model. While the hydrodynamic type model is not appropriate to capture these new features since the events taking place are on a smaller length scale. Hence, it will not be employed in this dissertation but a brief description has been given here for completeness.

1.2.2 Mathematical Models of Diffusion Flames

In the broadest sense a diffusion flame is defined, see Williams [50], as any flame in which the fuel and oxidant initially are separated before entering into the combustion chamber; the term is synonymous with non-premixed combustion. The simplest mathematical description of diffusion flames dates back to Burke and Schumann [7], who introduced infinitely fast-chemistry limit, commonly referred as Burke–Schumann limit of complete combustion. They considered the reaction zone confined to an infinitely thin sheet located where stoichiometric condition is achieved, and separating the fuel and oxidant. Their theory has successfully approximated the flame temperature, flame location and fuel consumption. Due to the over simplified reaction rate, their theory is not able to provide extinction criterion and reactants leakage.

A seminal contribution to the analysis of diffusion flames is due to Liñán [30], who derived the general asymptotic theory of steady diffusion flames with Fickian diffusion in a counterflow with unity Lewis numbers. In the limit of large activation energy, the chemical reaction zone confined to a thin reactive boundary layer, when viewed on the much larger diffusion scale, is a moving reaction sheet. His theory provides a complete description of non-premixed combustion: 1) a nearly frozen ignition regime, in which temperature and species concentrations gradients are small, 2) a partial burning regime, where both reactants cross the reaction zone, 3) a premixed flame regime, in which one of the reactants leaks through the reaction zone, and 4) a diffusion flame regime, where both reactants in the reaction zone are small. In addition, his analysis includes extinction and ignition criteria.

All of these models have been used extensively to analyze the basic structure of premixed [1, 4, 5, 36, 34, 37, 45] and diffusion flames [30], as well as ignition [28, 35], extinction [28, 25], flame-flow interactions [48], and instabilities of flames [8, 23, 24, 26]; but they have one thing in common – they are only appropriate to describe conditions at atmospheric pressure.

This dissertation is organized as follows. In Chapter 1, we give the motivation, objective and present a review of the relevant literature. In Chapter 2, we discuss the new features that arise in high pressure and what has been incorporated into our theory. In Chapter 3, we examine the asymptotic structure of laminar diffusion flames at high pressure in the limit of large activation energy for the particular configuration of a steady flame in counterflow. In addition, we study how the new effect that arises at high pressure affects the species concentration profiles, flame temperature and location, as well as the extinction phenomenon. In Chapter 4, we derive an asymptotic theory of laminar premixed flame in high density fluids in the limit of large activation energy. We then use this new model to investigate the new effect on the structure of a steady planar flame. We also examine the linear stability of the planar

flame and identify neutral stability boundaries that mark the transition from a stable, uniform, state to either non-planar or non-steady modes of propagation. In addition, a weakly nonlinear analysis is carried out, resulting in a modified Kuramoto-Sivashinsky equation, accounting for effects of Soret Diffusion. Finally, in Chapter 5, conclusions are given.

CHAPTER 2

MODELING OF COMBUSTION PHENOMENA AT HIGH PRESSURE

It should be mentioned again that all of the existing models presented in the previous chapter are only really appropriate to describe combustion systems operate at atmospheric pressure. However, in reality, as discussed above, a lot of these systems operate at much higher pressures, including pressure exceeding the critical pressure. This regime presents many new challenges as the fluid are markedly different. Fluids are known to take on peculiar properties under extreme conditions. For example, they tend to have gas-like viscosity and fluid-like densities. Mass diffusivity tends to diminish in very dense mixtures and diffusive mass transport as result of temperature gradients, the Soret effect, becomes significant.

2.1 Equation of State

At high pressures, it is well known that the behavior of real gases changes dramatically from that predicted by the ideal gas law

$$P = \frac{R^o T}{V} \tag{2.1}$$

where P is the pressure, T is the temperature, R^o is the universal gas constant and V is the molar volume. The van der Waals equation,

$$P = \frac{R^o T}{V - b} - \frac{1}{V^2} \tag{2.2}$$

where a and b are the van der Waals constants, was introduced with a correction term which can better illustrate the behavior of real gases. There are numerous number of more complex and realistic equations of state (EOS) based on the van der Waals equation, such as the Redlich-Kwong, the Soave-Redlich-Kwong and the

Peng-Robinson (P-R). P-R EOS is commonly used because of its wide application in the field of high pressure, particularly, when the pressure is sufficiently higher than the atmospheric pressure. Recently, Harstad, Miller and Bellan [22] have presented a computationally efficient form of the P-R EOS that is pretty accurate even at pressure exceeding the critical pressure. Thus, many recent studies have adopted the cubic P-R EOS to predict real gas behavior [19, 18, 20, 21, 38, 39, 40, 41]. The P-R EOS is given by

$$P = \frac{R^o T}{V - b} - \frac{a(T)}{V^2 + 2Vb - b^2} \tag{2.3}$$

where a is now a function of temperature and b is still a constant. For the sake of brevity, all details are omitted, but are reported in Miller et. al. [15] and Harstad et. al. [22].

2.2 Viscosity and Heat Capacity

Figure 2.1 is a schematic illustration showing an isotherm ($T > T_c$) of the kinematic viscosity of a substance as a function of reduced pressure. We observe that the kinematic viscosity is a monotonically decreasing function of pressure. Furthermore, we also observe that it remain fairly constant at pressure sufficiently higher than its critical pressure. Figure 2.2 is a schematic which shows the heat capacity at constant pressure as a function of reduced pressure. We can see that the heat capacity changes significantly (becomes infinite) near the critical pressure ($P_r \approx 1$). Nevertheless, it remain fairly constant at pressure sufficiently greater than its critical pressure. Therefore, in our formulation, it is reasonable to make the assumption that the viscosity and the specific heat at high pressure are constant.

2.3 Chemical Reaction Kinetics

It is very complicated to incorporate chemistry effectively into the study of reacting flow. A serious problem arises when one considers a direct approach to compute a

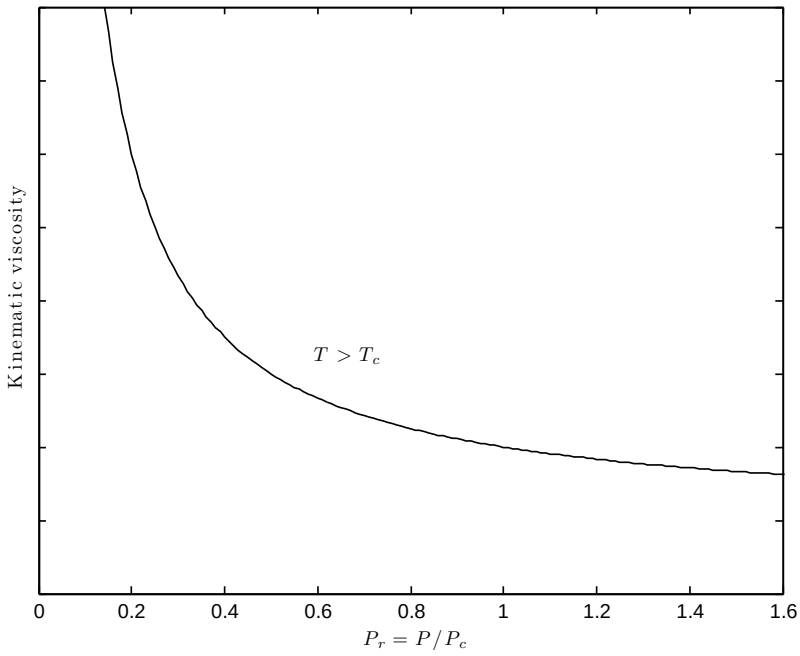

Figure 2.1 Schematic of the kinematic viscosity of a substance as a function of reduced pressure.

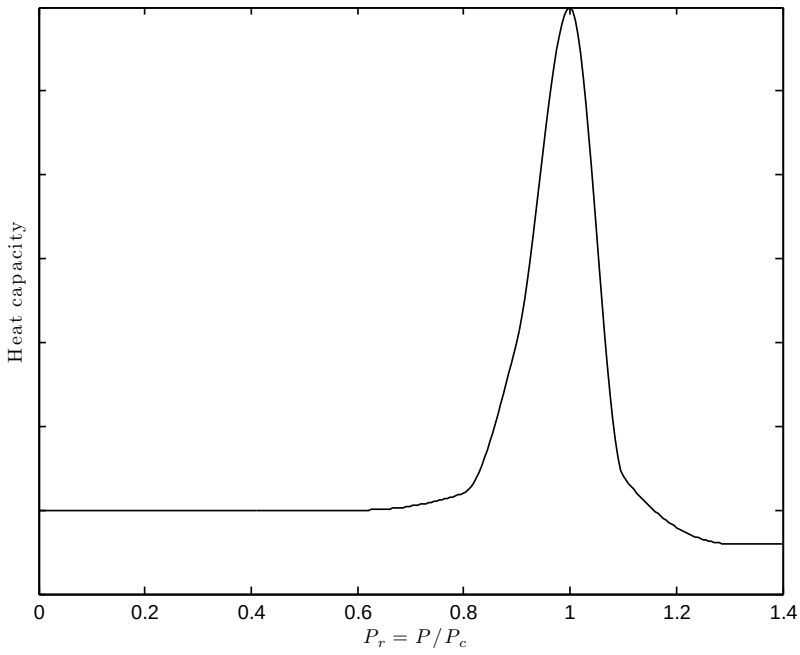

Figure 2.2 Schematic of the heat capacity at constant pressure as a function of reduced pressure.

realistic chemical kinetic mechanism since it often involve hundreds of species and thousands of reaction steps. Therefore, modern numerical simulations often consider the use of reduced chemistry models such that only a relatively small number of species and reactions are retained. We note that considerably less is known about detailed combustion chemistry at high pressure as compared to atmospheric pressure. Thus we have chosen to adopt a one-step reaction as a start toward modeling flames at high pressure, which has been used effectively to describe combustion phenomenon for 50 years. We are also guided by recent numerical studies of flames at high pressure [21, 22, 24] that have employed Arrhenius rate laws with good success. Nevertheless, this is an area that requires further investigation, both in terms of modeling and experimentation.

2.4 Diffusion

Conventional theories of flames usually consider ordinary gasses in which Fickian diffusion, i.e., molecular diffusion due to concentration gradients, is the dominant mode of mass transport within the flame structure. However, kinetic theory of gasses demonstrates cross-diffusion effects usually small at low pressure. The role of cross-diffusion on combustion at atmospheric pressure has been assessed in a number of theoretical and computational studies of both premixed [17, 16, 13, 14, 51] and diffusion [44, 49, 10, 43, 2] flames. The conclusions of each of these studies emphasize that the Soret effect, i.e., diffusion of mass as a result of temperature gradient, may be significant in many applications, especially for species that are very light or very heavy. Dufour effects, i.e., diffusion of heat caused by concentration gradients, are generally found to be negligible in most practical applications. Although most of the studies cited above are computational, there have been several notable theoretical investigations of these effects. García-Ybarra and Clavin [17] included weak cross-diffusion effects in their large activation energy theory and showed that they significantly

alter the thermo-diffusive stability limits for premixed flames. García-Ybarra, et al. [16] extended that theory to include thermal expansion, and concluded that Soret diffusion, as well as weak variations in other gas properties, modify flame dynamics by altering Markstein lengths. Arias-Zugasti and Rosner [2] analyzed a diffusion flame in counterflow in the limit of infinitely fast chemistry, in which they accounted for Soret transport of the fuel species, and obtained analytical expressions for flame temperatures and locations. This configuration is relevant in certain air-breathing engines in which temperatures may exceed the critical temperature of fuel, but not that of oxidant.

Mathematical models of flames at high pressure are relatively scarce. Daou and Rogg [11] studied convective burning of fuel pockets at supercritical pressures, in a model that assumed constant transport properties and an ideal gas equation of state. Margolis and Johnston [32] proposed a model of supercritical premixed flames to describe Supercritical Water Oxidation (SCWO), a process involving the chemical conversion of toxic wastes by injecting a stream of oxidant into a supercritical fuel/water mixture, and allowing combustion to take place. Recognizing that the effective mass diffusivity of species is greatly reduced in the transcritical regime, they assumed zero mass diffusivity. Later, an Arrhenius representation for effective mass diffusivity was adopted in models of both premixed [31] and diffusion [3] flames.

More recently, Harstad and Bellan [19, 18] have presented a generalized form of diffusion fluxes that remain valid over a wide pressure range. They demonstrated that consideration of non-equilibrium thermodynamics requires that heat and mass flux vectors include gradients of concentration, temperature and pressure. Furthermore, their derivation reveals a mass diffusion factor, a thermodynamic parameter that approaches unity at low pressure, and is reduced at high pressure, approaching zero at the critical point [20, 39, 40]. That model has since been used extensively in computational studies concerning both non-reacting [38, 39] and reacting [41, 15]

supercritical fluids, as well as the behavior of supercritical drops for different sets of binary species at large ranges of pressure [19, 18, 21].

2.4.1 Thermal Diffusion

Soret effect also called Ludwig-Soret effect, or thermo diffusion is a phenomenon in which particles experience a force in the direction of temperature gradient in mixtures. This phenomenon is first predicted by Ludwig and experimentally demonstrated by Soret more than a century ago.

Soret diffusion, i.e., the transport of species as a result of temperature gradient is very different from the familiar Fickian diffusion, which postulates that the species goes from regions of high concentration to regions of low concentration, with a magnitude that is proportional to the concentration gradient. Conversely, Soret diffusion allows species to move up or down the temperature gradient as to equalize the internal energy distribution.

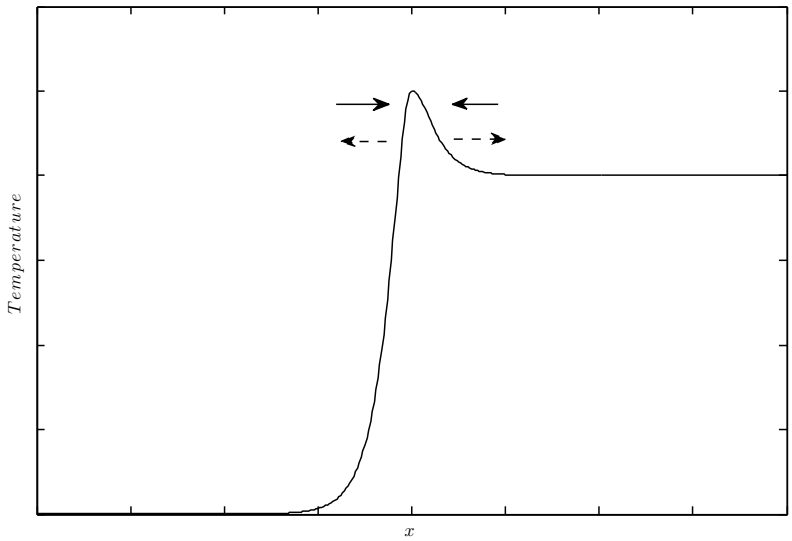

Figure 2.3 Schematic of species transport due to Soret effect. The arrows indicate the direction of fuel transport. The solid and dashed arrows represent negative and positive Soret diffusion coefficient, respectively.

The Soret diffusion coefficient for lighter fuel, e.g., hydrogen, is typically negative, so thermal diffusion tends to transport the fuel into the reaction zone, i.e., fuel moves from cold to hot region. On the other hand, for heavy fuel, e.g., hydrocarbons, the Soret diffusion coefficient is positive, suggesting fuel is being transported away from the reaction zone, i.e., from hot to cold region. Figure 2.3 is a schematic which shows the directions of species transport as a result of temperature gradient. We note that this effect is relatively small at low pressure, but becomes significant at high pressure. In some cases, it may become the dominant mechanism of the transport of fuel.

2.4.2 Transport Processes

As mentioned earlier, the transport terms enter into the conservation equations for reacting flow comprised of terms that are proportional to gradients of temperature T, concentration X_i and pressure P:

$$\hat{\mathbf{J}}_{j,T} = \hat{\mathbf{J}}^{T}_{j,T} + \hat{\mathbf{J}}^{X_1}_{j,T} + \cdots + \hat{\mathbf{J}}^{X_{N-1}}_{j,T} + \hat{\mathbf{J}}^{P}_{j,T}, \tag{2.4}$$

and

$$\hat{\mathbf{J}}_{j,X_k} = \hat{\mathbf{J}}^{T}_{j,X_k} + \hat{\mathbf{J}}^{X_1}_{j,X_k} + \cdots + \hat{\mathbf{J}}^{X_{N-1}}_{j,X_k} + \hat{\mathbf{J}}^{P}_{j,X_k}, \tag{2.5}$$

where subscript j denotes the vector component, subscript T denotes heat, subscript X_k denotes the species i, and the superscripts represent the thermodynamic gradient. For the sake of brevity, the explicit form of diffusion fluxes are shown after the assumptions in the next section are made. See, e.g., [21, 41], for derivation and discussion.

2.5 Modeling Assumptions

In the present study, we adopt Harstad and Bellan's formulation for diffusion fluxes which includes gradients of concentration, temperature and pressure. Figure (2.4)

shows the critical points for various species in a pressure vs. temperature plot. It is seen that the critical pressure for the oxidant is higher than the critical pressure for all the fuel. Therefore, we assume that the mass diffusivity of the fuel is negligible as compared to thermal diffusivity such that Soret transport is dominant, while the oxidant is an ideal, gas, which undergoes Fickian diffusion. Furthermore, we neglect Dufour effects, and assume small Mach number so that pressure-gradient induced transport is ignored. Under these conditions, the effective mass diffusivity is weak relative to thermal diffusion, and thus Soret diffusion is the dominant molecular transport mechanism for the fuel species in our theory. In the limit of large activation energy, the flame structure is comprised of outer advective-diffusive layers on either side of an inner reaction layer. As a result of this transport mechanism employed in our study, the reaction zone exhibits a balance between advection, Soret diffusion and reaction of fuel.

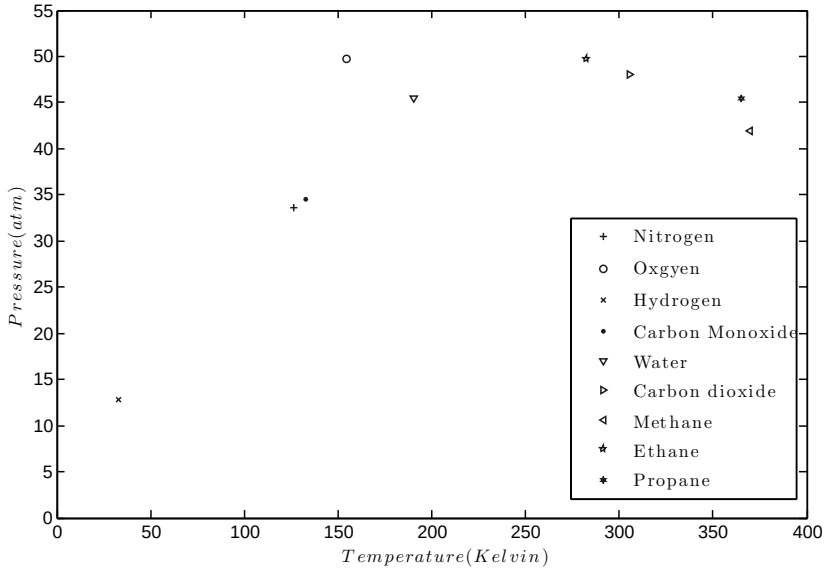

Figure 2.4 Critical points for various species are shown in a pressure vs. temperature plot.

CHAPTER 3

NEW THEORY OF DIFFUSION FLAMES AT HIGH PRESSURE

3.1 Formulation

We consider a combustion system in which fuel and oxidant are brought together separately into the combustion chamber. The fuel is assumed to be in a fluid state, in which Soret transport is dominant, while the oxidant is assumed to be an ideal gas, which undergoes Fickian diffusion. This scenario has relevance to a number of practical applications, including SCWO and burning in certain internal combustion engines. Furthermore, we assume the chemical reaction is modeled by a one-step global irreversible reaction

$$\nu_Y \mathcal{M}_Y + \nu_X \mathcal{M}_X \rightarrow \text{Products},$$

where $\mathcal{M}_i$ are the chemical symbols, and ν_i are the stoichiometric coefficients for species i, with the subscripts Y, X denoting fuel and oxidizer, respectively. The chemical reaction is assumed to be of Arrhenius type with an overall activation energy $\hat{E}_a$ and a pre-exponential factor $\mathcal{A}$, and the reaction rate Ω therefore of the form

$$\hat{\Omega} = \mathcal{A}\hat{\rho}^2 \frac{\hat{Y}_O \hat{Y}_F}{W_O W_F} e^{-\frac{\hat{E}_a}{R^o \hat{T}}}, \tag{3.1}$$

where $\hat{\rho}$ is the fluid density, W_i is the molecular weight of species i and R^o the gas constant.

The governing equations for temperature, $\hat{T}$ and mass fractions of fuel and oxidant, $\hat{X}$ and $\hat{Y}$ are coupled to the equations of fluid mechanics are

$$\frac{\partial \hat{\rho}}{\partial \hat{t}} + \nabla \cdot (\hat{\rho}\hat{\mathbf{V}}) = 0, \tag{3.2}$$

$$\hat{\rho}\left(\frac{\partial \hat{\mathbf{V}}}{\partial \hat{t}} + \hat{\mathbf{V}} \cdot \hat{\nabla}\hat{\mathbf{V}}\right) = -\nabla \hat{P} + \mu\left(\hat{\nabla}^2 \hat{\mathbf{V}} + \frac{1}{3}\hat{\nabla}(\hat{\nabla} \cdot \hat{\mathbf{V}})\right), \tag{3.3}$$

$$\hat{\rho} c_p \left(\frac{\partial \hat{T}}{\partial \hat{t}} + \hat{\mathbf{V}} \cdot \hat{\nabla} \hat{T} \right) + \hat{\nabla} \cdot (\hat{J}_T) = \hat{Q} \hat{\Omega}, \tag{3.4}$$

$$\hat{\rho} \left(\frac{\partial \hat{X}}{\partial \hat{t}} + \hat{\mathbf{V}} \cdot \hat{\nabla} \hat{X} \right) + \hat{\nabla} \cdot (\hat{J}_X) = -\nu_X W_X \hat{\Omega}, \tag{3.5}$$

$$\hat{\rho} \left(\frac{\partial \hat{Y}}{\partial \hat{t}} + \hat{\mathbf{V}} \cdot \hat{\nabla} \hat{Y} \right) + \hat{\nabla} \cdot (\hat{J}_Y) = -\nu_Y W_Y \hat{\Omega} \tag{3.6}$$

where $\hat{\mathbf{V}}$ is the velocity field (we assume two streams have equal velocity), $\hat{P}$ is the pressure, $\hat{Q}$ is the heat release, μ is the dynamic viscosity, c_p is the specific heat, and W_i is the molecular weights, respectively, of species i.

The generalized flux vectors, $\hat{\mathbf{J}}_T$, $\hat{\mathbf{J}}_X$ and $\hat{\mathbf{J}}_Y$ are comprised of terms that are proportional to gradients of temperature, concentration and pressure. However, we will restrict our analysis to zero Mach numbers, in which case pressure-induced diffusion may be ignored. We further assume a dilute mixture in which both species appear in relatively small quantities relative to an abundant inert, so that the remaining terms in the diffusive flux vectors have the form:

$$\hat{\mathbf{J}}_T = -\left(\lambda + \hat{\rho} \hat{D} \alpha_{IK} \alpha_{BK} R^o \hat{Y} \frac{\bar{W}}{W_Y} \right) \nabla \hat{T} + \hat{\rho} \hat{D} \alpha_{D_Y} \alpha_{IK} R^o \hat{T} \frac{\bar{W}}{W_Y} \nabla \hat{Y} \tag{3.7}$$

$$\hat{\mathbf{J}}_X = -\hat{\rho} \hat{D}_X \alpha_{BK} \hat{X} \frac{1}{\hat{T}} \nabla \hat{T} + \hat{\rho} \hat{D}_X \alpha_{D_X} \nabla \hat{X} \tag{3.8}$$

$$\hat{\mathbf{J}}_Y = -\hat{\rho} \hat{D}_Y \alpha_{BK} \hat{Y} \frac{1}{\hat{T}} \nabla \hat{T} + \hat{\rho} \hat{D}_Y \alpha_{D_Y} \nabla \hat{Y} \tag{3.9}$$

Here $\bar{W}$ is the average molecular weight of the mixture, and the quantities α_{IK}, α_{BK} and α_{D_i} are thermodynamic parameters whose explicit forms can be found in [19]. The parameter α_{IK} has been estimated to be very small over a wide range of pressures, including sub- and super-critical regimes. As a result, Dufour effects are negligible, and heat conduction proceeds according to Fourier's law. The first term in $\hat{J}_X$ and

$\hat{J}_Y$ corresponds to Soret diffusion, while the second corresponds to Fickian diffusion. We note the presence of the mass diffusion factor, α_{D_i}, which has a value of unity at low pressures, but is reduced at high pressures. On the other hand, the Soret coefficient, α_{BK} is small at low pressures, but may attain order one values at high pressures. Furthermore, this coefficient is typically positive at high pressures for most hydrocarbon species, but may assume negative values for light fuels, cf. [38].

To further simplify the mathematical aspects of the problem, we assume that the specific heat c_p and thermal conductivity of the mixture λ, and the mass diffusivities of the fuel $\hat{D}_Y$ and oxidizer $\hat{D}_X$ are all constant. Furthermore, we assume viscous effects to be negligible.

Equations (3.2) - (3.6) must be supplemented by appropriate initial and boundary conditions reflecting the way in which the fuel and oxidant are brought together separately into the combustion chamber. In addition, the temperature and concentration of the fuel stream may be different than the temperature and concentration of the oxidant stream. Generally, initial and boundary conditions could vary sufficiently depending on the particular configuration, e.g., jet diffusion flame, counterflow diffusion flame, liquid fuel drop and burned-generated spherical diffusion flame. In the present study, we have chosen to examine the structure of counterflow diffusion flames.

3.2 Counterflow Diffusion Flames at Elevated Pressure

To examine the basic structure of diffusion flames in dense fluids, we consider a thin flame residing in counterflowing streams of fuel and oxidant, as shown in Figure 3.1. The fuel is assumed to be a fluid, in which Soret transport is dominant, while the oxidant stream is an ideal gas that undergoes Fickian diffusion. This configuration is chosen for analytical simplicity, as it admits steady, one-dimensional solutions (We note that counterflow diffusion flames are often use experimentally due to its

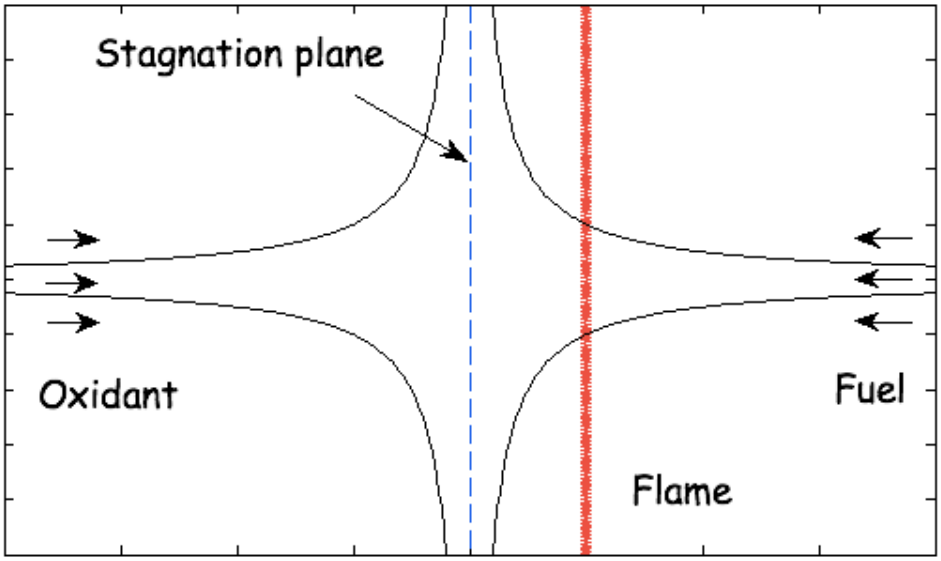

Figure 3.1 Schematic of a counterflow diffusion flame.

simplicity). We remark that Arias-Zugasti and Rosner [2] studied the same geometry with Burke-Schumann infinitely fast chemistry which is different than what we consider here, finite-rate chemistry. The density is assumed sufficiently high to adopt a constant density formulation, and thus we impose the flow field $\mathbf{V} = -\hat{k}(\hat{z}, -\hat{y})$, where $\hat{k}$ is the strain rate. For such a flow, it is possible for the combustion field to be uniform in the y-direction, with the flame located at $\hat{z} = \hat{z}_f$.

The governing equation for temperature and species concentrations, (3.4) - (3.6) under above assumptions can be simplified to

$$-\hat{\rho} c_p \hat{k} \hat{z} \frac{d\hat{T}}{d\hat{z}} = -\frac{d}{d\hat{z}}(\hat{\mathbf{J}}_T) + \hat{Q}\hat{\Omega} \tag{3.10}$$

$$-\hat{\rho} \hat{k} \hat{z} \frac{d\hat{X}}{d\hat{z}} = -\frac{d}{d\hat{z}}(\hat{\mathbf{J}}_X) - \nu_X W_X \hat{\Omega} \tag{3.11}$$

$$-\hat{\rho} \hat{k} \hat{z} \frac{d\hat{Y}}{d\hat{z}} = -\frac{d}{d\hat{z}}(\hat{\mathbf{J}}_Y) - \nu_Y W_Y \hat{\Omega} \tag{3.12}$$

with the boundary conditions

$$\hat{T} \to \hat{T}_{-\infty}; \qquad \hat{X} \to \hat{X}_{-\infty}; \qquad \hat{Y} \to 0 \qquad as \quad \hat{z} \to -\infty \tag{3.13a}$$

$$\hat{T} \to \hat{T}_{+\infty}; \qquad \hat{X} \to 0; \qquad \hat{Y} \to \hat{Y}_{+\infty} \qquad as \quad \hat{z} \to +\infty \tag{3.13b}$$

3.3 Nondimensionalization

The first step in analyzing the solution is to nondimensionalize the problem. Lengths are scaled with respect to the diffusion length, $l_D = \sqrt{\lambda/(\hat{\rho} c_p \hat{k})}$, and temperature is nondimensionalized with respect to its value far upstream on the oxidant side, $\hat{T}_{-\infty}$. We also scale the fuel and oxidant variables based on their respective fresh stream values. Upon introducing the nondimensional variables:

$$z = \frac{\hat{z}}{l_D}, \qquad T = \frac{\hat{T}}{\hat{T}_{-\infty}}$$

$$X = \frac{\hat{X}}{\hat{X}_{-\infty}}, \qquad Y = \frac{\hat{Y}}{\hat{Y}_{+\infty}}$$

our system of equations becomes

$$-z\frac{dT}{dz} = \frac{d^2T}{dz^2} + q\Omega \tag{3.14}$$

$$-z\frac{dX}{dz} = Le_X^{-1}\frac{d^2X}{dz^2} - \phi\Omega \tag{3.15}$$

$$-z\frac{dY}{dz} = Le_Y^{-1}\frac{d}{dz}\left[\alpha_{BK}\frac{Y}{T}\frac{dT}{dz} + \alpha_{D_Y}\frac{dY}{dz}\right] - \Omega \tag{3.16}$$

with the boundary conditions

$$T \to 1; \qquad X \to 1; \qquad Y \to 0 \qquad as \quad z \to -\infty \tag{3.17a}$$

$$T \to \beta; \qquad X \to 0; \qquad Y \to 1 \qquad as \quad z \to +\infty \tag{3.17b}$$

where the Lewis number

$$Le_i = \frac{\lambda}{\hat{\rho}\hat{c}_p\hat{D}_i} \tag{3.18}$$

is the ratio of thermal diffusivity to mass diffusivity, the scaled temperature

$$\beta = \frac{\hat{T}_{+\infty}}{\hat{T}_{-\infty}} \tag{3.19}$$

of the fuel stream, the mixture strength

$$\phi = \frac{\frac{Y_0}{\nu_Y W_Y}}{\frac{X_0}{\nu_X W_X}} \tag{3.20}$$

is the ratio of the fuel mass fraction supplied at the fuel boundary to the oxidizer mass fraction supplied at the oxidizer boundary normalized by the stoichiometric proportions and the heat release

$$q = \frac{\hat{Q}Y_0}{\hat{c}_p\hat{T}_{-\infty}\nu_Y W_Y}. \tag{3.21}$$

Finally, the dimensionless reaction rate term Ω has the form

$$\Omega = \hat{\mathcal{D}}XY \exp\left\{\frac{-1}{\epsilon T}\right\} \tag{3.22}$$

where the inverse of the dimensionless activation energy

$$\epsilon = \frac{R^o\hat{T}_{-\infty}}{\hat{E}} \tag{3.23}$$

is generally very small in most combustion systems, and the Damköhler number

$$\hat{\mathcal{D}} = \frac{\nu_Y\rho\hat{X}_0}{kW_X}\hat{A} \tag{3.24}$$

is the ratio of flow time to reaction time tends to very large. In the limit of large activation energy, equation (3.22) shows that the reaction is exponentially small. In order to retain the reaction, we can employ the technique of large activation energy

asymptotics to rescale the Damköhler number as

$$\hat{\mathcal{D}} = \bar{\mathcal{D}}\epsilon^{-2} \exp\left\{\frac{1}{\epsilon T_f}\right\} \tag{3.25}$$

where $\bar{\mathcal{D}} = O(1)$ is the reduced Damköhler number. Therefore, with such scaling, the reaction rate term is appreciable only when T is sufficiently close to T_f, and vanishes when $T < T_f$.

Solutions will now be constructed to the above system for negligible effective fuel mass diffusivity, $\alpha_{D_Y} \to 0$, in the limit of large activation energy, $\epsilon \ll 1$. For convenience, we will consider unity Lewis number for the oxidant, i.e. $Le_x^{-1} = 1$, and define the modified Soret and mass diffusion coefficients $\alpha_s = Le_Y^{-1}\alpha_{BK}$, $\alpha_D = Le_Y^{-1}\alpha_{D_Y}$.

3.4 Flame as a Boundary Layer

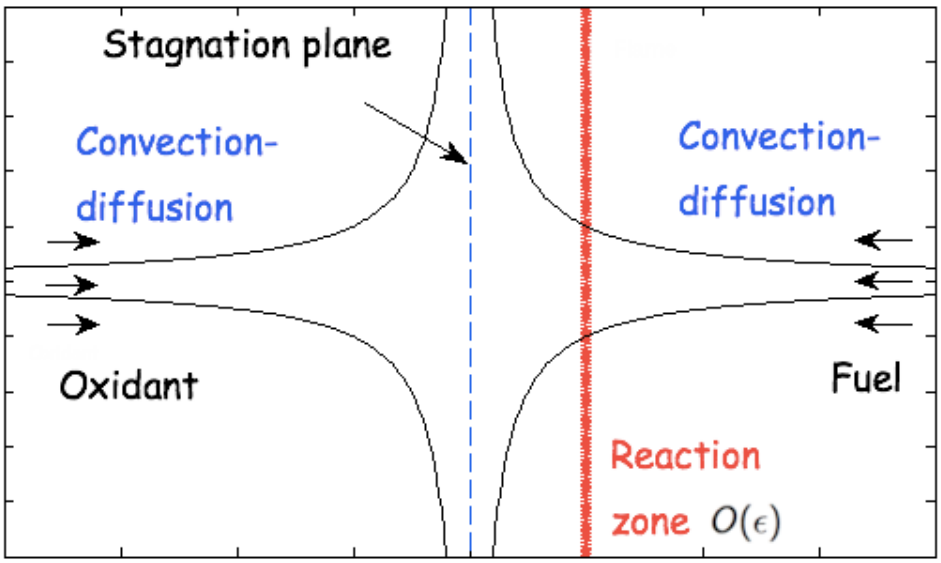

Figure 3.2 Schematic illustration of the structure of a diffusion flame which shows the boundary layer (reaction zone) and outer regions (convection-diffusion zone).

The reaction zone is confined to an infinitely thin sheet around the flame location z_f, separating fuel and oxidizer streams in the limit of large activation energy. Moreover, the reaction rate Ω in equation (3.22) is exponentially small and can be ignored when the temperature is less than the flame temperature in the limit of large activation energy E. Therefore, reaction is only appreciable when the temperature is very close to the flame temperature, in particular within $O(\epsilon)$.

The system of equations (3.14) - (3.16) for temperature and mass fractions are quite complicated, but under large activation energy asymptotics the effects of reaction are concentrated in a narrow layer near the flame location. Hence, our strategies for solving the system of equations then will be to treat the reaction zone as a boundary layer where gradients are steep and a balance between diffusion and reaction is maintained. Furthermore, in the outer regions on either side of the flame sheet (boundary layer), reaction is negligible and a balance between convection and diffusion is achieved. The structure of the flame is schematically shown in Figure 3.2. We can then use the method of matched asymptotics to analyze each region separately and matching will relate the solutions in the outer regions across the reaction zone. This procedure will provide a composite solution that is valid everywhere in the flow field.

3.5 The Outer Region

In the large activation energy limit, reaction is confined to a narrow zone of $O(\epsilon)$, separating fuel and oxidant streams. On either side of this layer, there is only a balance between diffusion and convection since temperature gradient is constant, Soret effect therefore is negligible in these regions. Hence, the leading order chemistry-free governing equations are

$$-z\frac{dT}{dz} = \frac{d^2T}{dz^2} \tag{3.26}$$

$$-z\frac{dX}{dz} = \frac{d^2X}{dz^2} \tag{3.27}$$

$$-z\frac{dY}{dz} = \alpha_s \frac{d}{dz}\left[\frac{Y}{T}\frac{dT}{dz}\right] \tag{3.28}$$

with the boundary conditions

$$T \to 1; \qquad X \to 1; \qquad Y \to 0 \qquad as \quad z \to -\infty, \tag{3.29a}$$

$$T \to \beta; \qquad X \to 0; \qquad Y \to 1 \qquad as \quad z \to +\infty. \tag{3.29b}$$

The outer solutions for temperature and oxidizer concentration are given by

$$T = \begin{cases} 1 + A_0\left[2 - erfc\left(\frac{z}{\sqrt{2}}\right)\right], & z < z_f \\ \beta + B_0 erfc\left(\frac{z}{\sqrt{2}}\right), & z > z_f \end{cases}, \tag{3.30}$$

$$X = \begin{cases} 1 + C_0\left[2 - erfc\left(\frac{z}{\sqrt{2}}\right)\right], & z < z_f \\ D_0 + \epsilon D_1 erfc\left(\frac{z}{\sqrt{2}}\right), & z > z_f \end{cases}. \tag{3.31}$$

To leading order in ϵ the constants in these expressions are given by

$$A_0 = \tfrac{T_f - 1}{2 - E},\ B_0 = \tfrac{T_f - \beta}{E},\ C_0 = \tfrac{-1}{2-E}, \text{ and } D_0 = 0$$

where we have defined

$$E = erfc(z_f/\sqrt{2}),$$

and T_f and z_f are the flame temperature and location, respectively. The solution for fuel concentration is obtained by integrating equation (3.28), which yields

$$Y = \exp\left\{\int_\infty^z \left[\frac{\alpha_s \frac{T_z}{T}(z + \frac{T_z}{T})}{z + \alpha_s \frac{T_z}{T}}\right] dz\right\}, \quad \text{for} \quad z > z_f. \tag{3.32}$$

One obtains a similar expression for Y to the left of the flame sheet $z < z_f$, but it is also necessary to account for a boundary layer of thickness $O(\alpha_D)$ in this region to satisfy the boundary condition far upstream on the oxidant side. The boundary layer analysis is presented in Appendix A and the resulting profiles will be presented shortly. It is important to note that oxidizer is entirely consumed to leading order, while there is generally an $O(1)$ amount of fuel passes through the flame remain unburned. This result in a jump in fuel concentration across the reaction layers and is typically the case when convective diffusive balance is achieved in the reaction zone, [32].

An integration of enthalpy variables across the reaction zone provide two relations for the flame temperature T_f and flame location z_f:

$$T_f = \beta + \frac{E}{2}\left\{1 + \frac{q}{\phi} - \beta\right\}, \tag{3.33}$$

$$\gamma = Y^+(1 - \alpha\gamma m) - Y^-\left(1 - \alpha\gamma(m-1)\right), \tag{3.34}$$

where

$$\gamma = \sqrt{\frac{2}{\pi}}\frac{e^{-z_f^2/2}}{z_f(2-E)\phi}, \quad \alpha = \frac{\alpha_s q}{T_f},$$

and

$$m = \frac{1 + q/\phi - T_f}{q/\phi}$$

is the ratio of heat flux to the fuel side to the total flux away from the flame. The amount of fuel entering the reaction zone, denoted by Y^+ in equation (3.34) is obtained by evaluating equation (3.32) at z_f^+. To leading order in ϵ, all quantities are now known as a function of flame temperature T_f, flame location z_f, and the amount of fuel passes through the reaction zone remain unconsumed Y^-. Equations (3.33) and (3.34) provide two relations for the flame temperature and flame position as a

function of the unburned fuel which is yet to be determined. Hence, it is necessary to analyze the reaction zone structure which will provide a relation between the amount unburned fuel Y^- and the Damköhler number $\hat{\mathcal{D}}$.

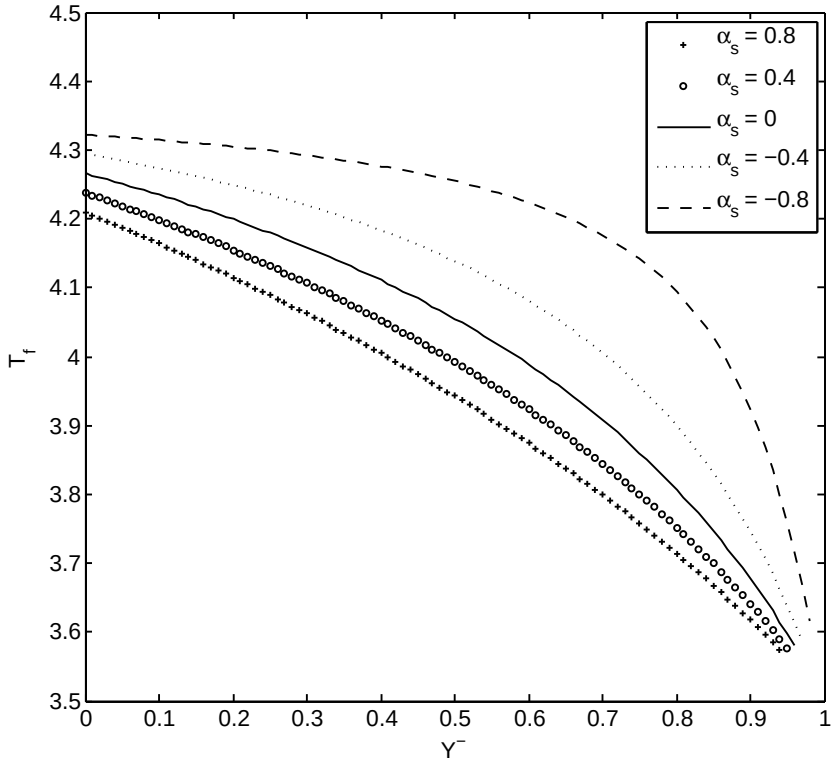

Figure 3.3 Flame temperature, T_f, as a function of the amount of unconsumed fuel, Y^- for several values of the modified Soret diffusion coefficient, α_s.

Flame temperature, T_f and flame location, z_f as a function of the amount of unconsumed fuel, Y^-, as determined from equation (3.33) and (3.34) are shown in Figures 3.3 and 3.4 for several values of the modified Soret diffusion coefficient α_s with $\phi = 1, \quad q = 5, \quad \beta = 1 + q/2\phi$. Curves are shown for Soret coefficients in the range $-\frac{T_f}{q} \leq \alpha_s$ $(-1 \leq \alpha)$, for which the structure problem, to be discussed in the next section, has physical solutions. We observe that flame temperature decreases as the

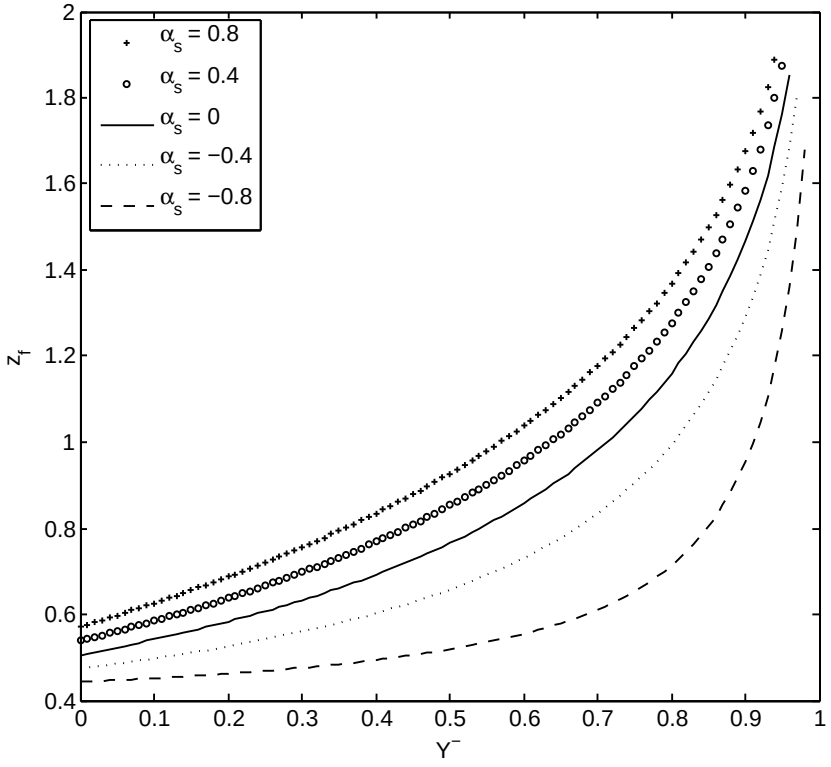

Figure 3.4 Flame location, z_f, as a function of the amount of unconsumed fuel, Y^- for several values of the modified Soret diffusion coefficient, α_s.

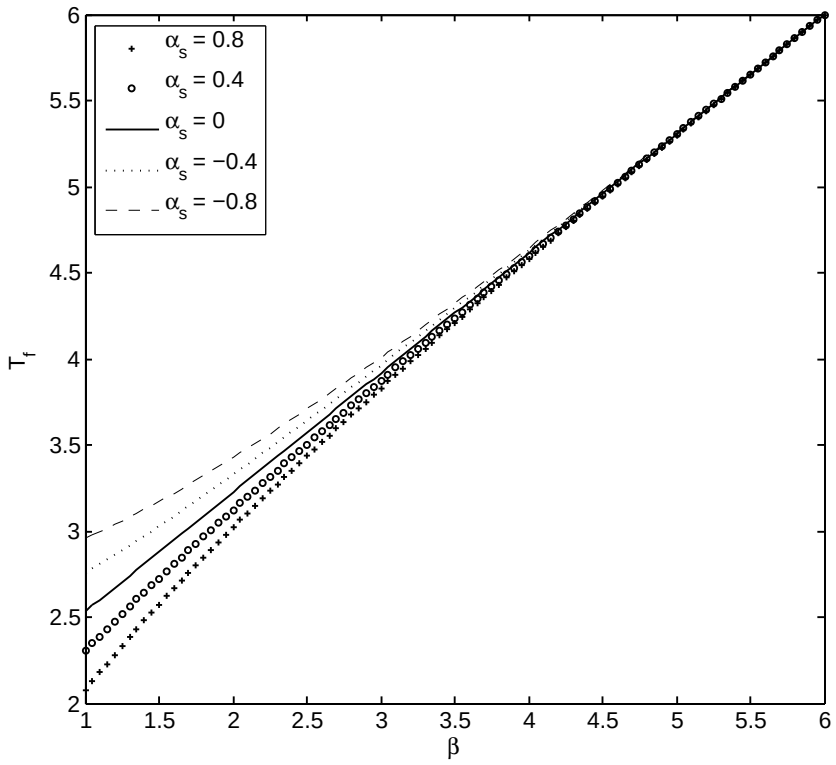

Figure 3.5 Flame temperature, T_f, as a function of the temperature of the fuel stream to the oxidant stream ratio, β for several values of the modified Soret diffusion coefficient, α_s.

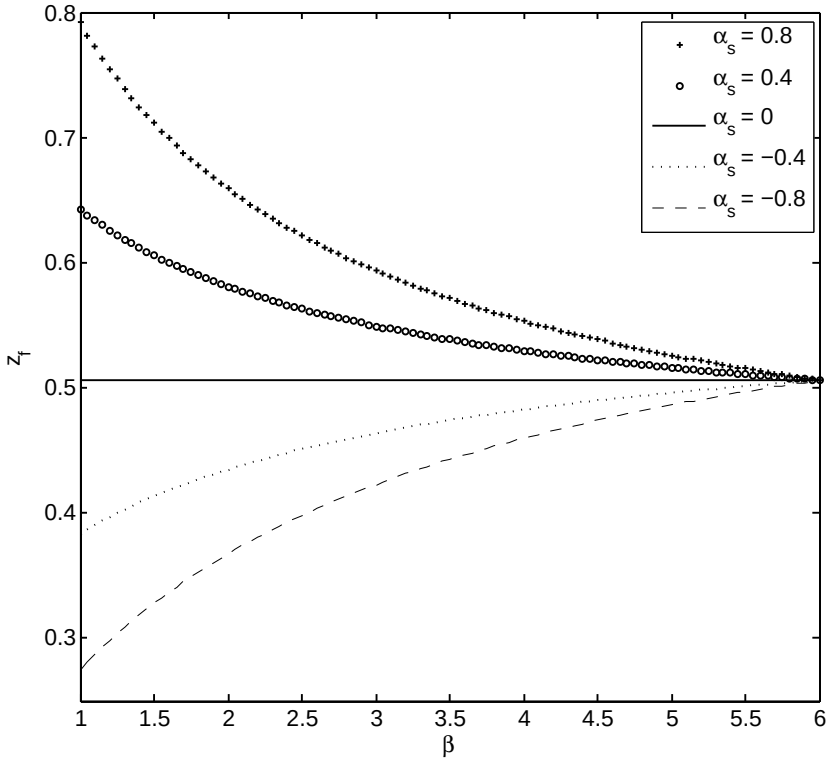

Figure 3.6 Flame location, z_f, as a function of the temperature of the fuel stream to the oxidant stream ratio, β for several values of the modified Soret diffusion coefficient, α_s.

amount of unconsumed fuel is increased, while the flame retreats further upstream on the fuel side. We anticipate that the value $Y^- \to 0$ corresponds to an intense burning limit, characterized by large Damköhler number. Figures 3.5 and 3.6 show flame temperature, T_f and flame location, z_f as a function of the temperature of the fuel stream to the oxidant stream ratio, β for several values of α_s, computed for the intense burning limit, $Y^- = 0$, with $\phi = 1$ and $q = 5$. Note that $\beta = 1$ when the temperatures of the two supply streams are equal, and $\beta = 1 + q/\phi$ corresponds to the case in which the temperature of the fuel stream is equal to the adiabatic flame temperature, $T = T_a = 1+q/\phi$. We also note that the temperature on the fuel stream is always larger than or equal to the temperature on the oxidant stream, therefore $\beta \geq 1$. All results will be shown for this range of β. When $\alpha_s = 0$, Soret effects are absent, and the flame structure is determined by a balance between advection and reaction. In this case, the flame resides at the same location, $z_f \sim .506$ for all values of β. When Soret effects are present, $\alpha_s \neq 0$, the flame is seen to reside closer to the oxidant stream when $\alpha_s < 0$, and further upstream when $\alpha_s > 0$. We also observe that the flame location always approaches the value $z_f \sim .506$ as $\beta \to 1 + q/\phi$. As shown in Figure 3.5, $T_f = T_a = \beta$ when $\beta = 1 + q/\phi$ for all values of α_s, while for lower values of β, T_f decreases with increasing values of α_s.

Typical profiles of temperature, T and species concentrations are shown in Figures 3.7 and 3.8 for several specified values of the amount of unconsumed fuel Y^-. The value of β is 1 in Figure 3.7 and $1 + q/\phi$ in Figure 3.8, with $q = 5$, $\phi = 1$ and $\alpha_s = -0.2$ in both Figures. (We remark that the curves in the region $z < z_f$ were computed using the MATLAB boundary value solver bvp4c with a very small value of $\alpha_D = 0.001$ in order to resolve the narrow mass-diffusive boundary layer in this region.) In general, the temperature achieves its maximum value at the reaction sheet, although $T \equiv T_a$ for all $z > z_f$ when $\beta = 1 + q/\phi$, as shown in Figure 3.8. The oxidant is entirely consumed to leading order, while some fuel may pass through the

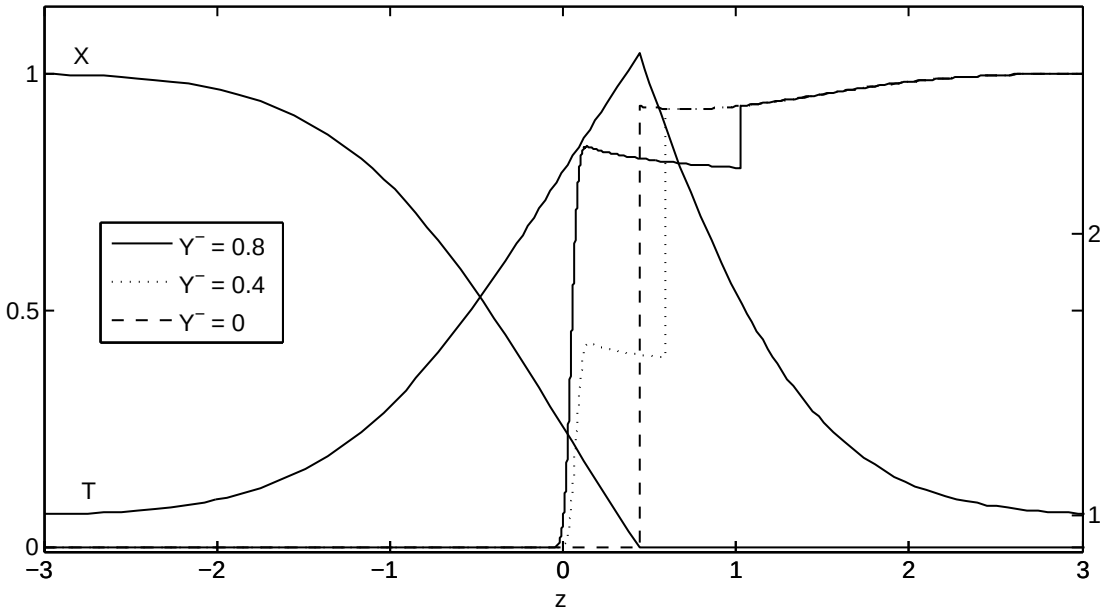

Figure 3.7 Profiles of temperature, T and species concentrations, X, and Y, with temperature of the fuel stream to the oxidant stream ratio, $\beta = 1$, heat release, q = 5, fuel to oxidant ratio, $\phi = 1$, modified Soret diffusion coefficient, $\alpha_s = -0.2$ and several values of the amount of unconsumed fuel, Y^-. Profiles for T and X are only shown for the single case $Y^- = 0$.

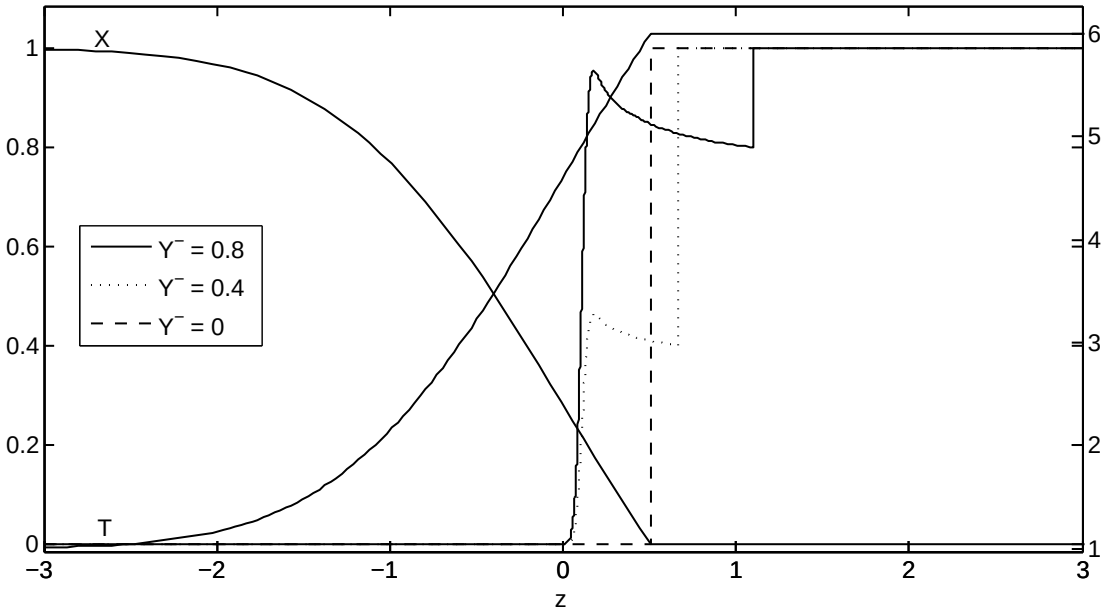

Figure 3.8 Profiles of temperature, T and species concentrations, X, and Y, with temperature of the fuel stream to the oxidant stream ratio, $\beta = 1 + q/\phi$, heat release, q = 5, fuel to oxidant ratio, $\phi = 1$, modified Soret diffusion coefficient, $\alpha_s = -0.2$ and several values of the amount of unconsumed fuel, Y^-. Profiles for T and X are only shown for the single case $Y^- = 0$.

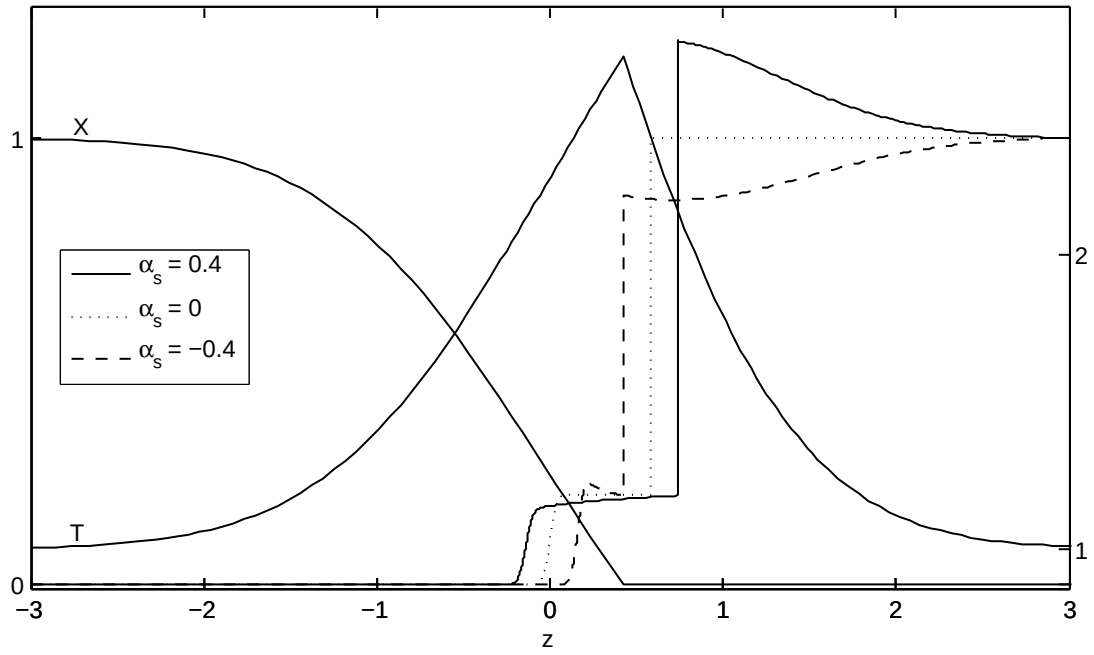

Figure 3.9 Profiles of temperature, T and species concentrations, X, and Y with temperature of the fuel stream to the oxidant stream ratio, $\beta = 1$, heat release, q = 5, fuel to oxidant ratio, $\phi = 1$, amount of unconsumed fuel, $Y^- = 0.2$ and several values of the modified Soret diffusion coefficient, α_s. Profiles for T and X are only shown for the single case $\alpha_s = -0.4$.

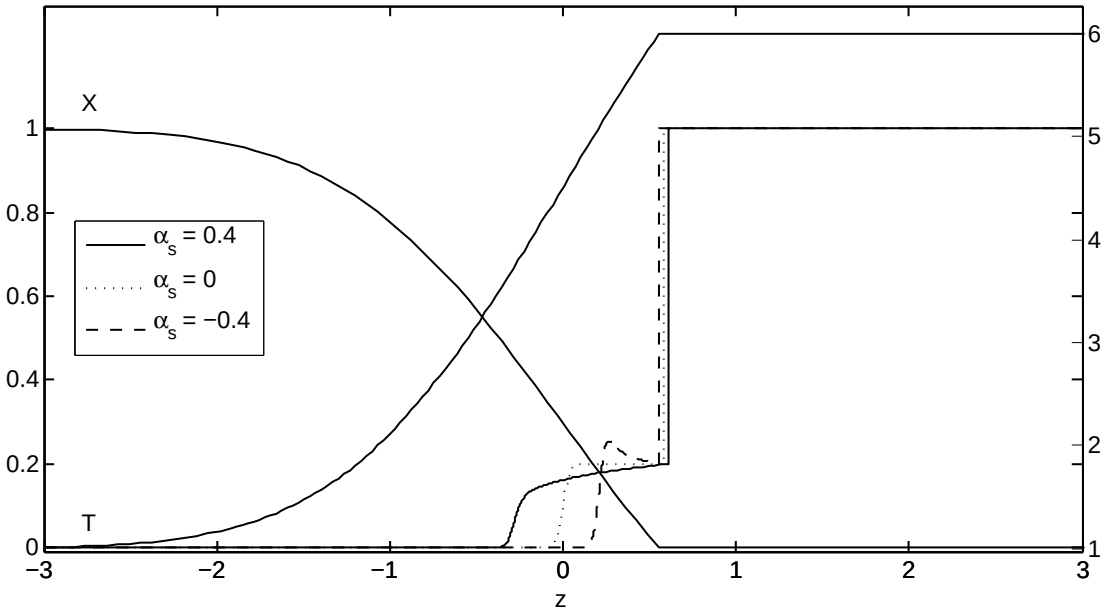

Figure 3.10 Profiles of temperature, T and species concentrations, X, and Y with temperature of the fuel stream to the oxidant stream ratio, $\beta = 1 + q/\phi$, heat release, q = 5, fuel to oxidant ratio, $\phi = 1$, amount of unconsumed fuel, $Y^- = 0.2$ and several values of the modified Soret diffusion coefficient, α_s. Profiles for T and X are only shown for the single case $\alpha_s = -0.4$.

reaction zone unburned. The fuel concentration profile is seen to achieve a localized peak on the oxidant side of the reaction zone. This is a result of competing effects of advection, that wants to transport the fuel further toward the stagnation plane, and the Soret effect, which has a tendency to distribute the fuel back toward the peak temperature location. As seen in these Figures, an increase in Y^- causes the flame to move further upstream on the fuel side.

Figures 3.9 and 3.10 show the same profiles as in Figures 3.7 and 3.8, but with Y^- fixed and varying α_s. For the same amount of unconsumed fuel, the flame moves closer toward the oxidant stream when the Soret coefficient is decreased.

The above profiles were all generated by specifying Y^-, the amount of fuel left unconsumed by the reaction. However, this quantity, and hence T_f and z_f, are functions of the Damköhler number. Thus, in order to completely construct our response curves, it is necessary to resolve the reaction zone structure.

3.6 The Reaction Zone

The species concentration profiles in the outer regions presented in the previous section indicate that the oxidizer is entirely consumed to leading order, while there is an $O(1)$ amount of fuel enters into the reaction zone. This suggests an inner structure with similarities to Liñán's "premixed regime" - the flow is frozen on the oxidizer side, and the flow is near-equilibrium on the fuel side are separated by an infinitely thin reaction zone [30]. The temperature and concentration profiles are given to all orders by equations (3.30) - (3.32). In the fuel stream, we expand the coefficients B_0 and D_0 in equations (3.30) - (3.31) in a power series in ϵ to account for the small amount of oxidant that may leak through.

To examine the structure of the reaction zone, we introduce the stretched spatial coordinate

$$\xi = \frac{z - z_f}{\epsilon}, \tag{3.35}$$

and the expansion for the temperature and species concentration

$$T \sim T_f + \epsilon\theta(\xi) + \cdots ,$$

$$X \sim 0 + \epsilon x(\xi) + \cdots ,$$

$$Y \sim y(\xi) + \epsilon y_1(\xi) + \cdots .$$

so that the local equations take the form:

$$\frac{d^2\theta}{d\xi^2} = -q\bar{\mathcal{D}}xye^{\theta/T_f^2} \tag{3.36}$$

$$\frac{d^2x}{d\xi^2} = \phi\bar{\mathcal{D}}xye^{\theta/T_f^2} \tag{3.37}$$

$$z_f\frac{dy}{d\xi} + \frac{\alpha_s}{T_f}\frac{d}{d\xi}\left[y\frac{d\theta}{d\xi}\right] = \bar{\mathcal{D}}xye^{\theta/T_f^2}. \tag{3.38}$$

The matching conditions are derived by expanding the outer solution as a Taylor series about $z = z_f$ in terms of the inner variable, ξ, to yield

$$T(z = z_f + \epsilon\xi) \sim T_0^{\pm} + \epsilon\left(\frac{dT_0^{\pm}}{dz}\xi + T_1^{\pm}\right) + \cdots , \tag{3.39}$$

$$X(z = z_f + \epsilon\xi) \sim X_0^{\pm} + \epsilon\left(\frac{dX_0^{\pm}}{dz}\xi + X_1^{\pm}\right) + \cdots , \tag{3.40}$$

$$Y(z = z_f + \epsilon\xi) \sim Y^{\pm} + \epsilon\left(\frac{dY^{\pm}}{dz}\xi + Y_1^{\pm}\right) + \cdots . \tag{3.41}$$

where we have used the notation $T_0^{\pm} = T_0(0\pm)$.

Matching to the outer solution written in terms of the stretched coordinate ξ provides the relations

$$\theta \sim \begin{cases} A_0\Gamma\xi, & \xi \to -\infty \\ T_1^{+} - B_0\Gamma\xi, & \xi \to +\infty \end{cases} , \tag{3.42}$$

$$x \sim \begin{cases} C_0\Gamma\xi, & \xi \to -\infty \\ X_1^+, & \xi \to +\infty \end{cases}, \tag{3.43}$$

$$y \sim \begin{cases} Y^-, & \xi \to -\infty \\ Y^+, & \xi \to +\infty \end{cases} \tag{3.44}$$

where $\Gamma = \sqrt{2/\pi}\exp\{-z_f^2/2\}$, $T_1^+ = B_1E$, $X_1^+ = D_1E$, Y^+ is the amount of fuel entering the reaction zone, and Y^- is the amount of fuel remain unconsumed.

The local enthalpy equation corresponding to the oxidizer species can be integrated to yield the following expression for x explicitly in terms of θ:

$$\theta + \frac{q}{\phi}x = -B_0\Gamma\xi. \tag{3.45}$$

Similarly, a linear combination of equations (3.36) and (3.38) can be directly integrated to determine y_0 in terms of θ, namely

$$\frac{d\theta}{d\xi} + \left(qz_f + \alpha\frac{d\theta}{d\xi}\right)y = A_0\Gamma. \tag{3.46}$$

We can now insert equations (3.45) and (3.46) into equation (3.36) to provide a single equation for the local temperature perturbation. Upon making the transformation

$$\theta = T_f^2(-\varphi - m\eta), \qquad \xi = \frac{T_f^2}{qz_f\gamma}\eta$$

our system of equations becomes

$$\frac{d^2\varphi}{d\eta^2} = \frac{\mathcal{D}}{4}\varphi y e^{-\varphi - m\eta} \tag{3.47}$$

$$y = \frac{Y^+ (1 - \alpha\gamma m) + \gamma d\varphi/d\eta}{1 - \alpha\gamma(d\varphi/d\eta + m)}, \tag{3.48}$$

with the boundary conditions

$$\frac{d\varphi}{d\eta} \sim \begin{cases} -1, & \eta \to -\infty \\ 0, & \eta \to +\infty \end{cases} \tag{3.49}$$

where the further reduced Damköhler number is given by

$$\mathcal{D} = \frac{4T_f^2 \phi \bar{\mathcal{D}}}{(q z_f \gamma)^2}. \tag{3.50}$$

In addition, matching provides the limiting values

$$\lim_{\eta \to -\infty} (\varphi + \eta) = 0, \tag{3.51}$$

$$\lim_{\eta \to +\infty} \varphi = \frac{q}{\phi T_f^2} X_1^+, \tag{3.52}$$

with the latter condition determining the oxidizer leakage across the reaction zone.

In general, the solution to equations (3.47) - (3.49) are computed numerically in order to resolve the local structure and also determine the eigenvalue $\mathcal{D}$ (the reduced Damköhler number) in terms of other parameters. In the limit $\gamma \to 0$, Liñán's "premixed regime" structure for ideal gases is recovered, which occurs under very rich conditions, for example as $\phi \to \infty$ or $z_f \to \infty$.

This system can be integrated exactly when the scaled fuel temperature is equal to the adiabatic flame temperature, $\beta = T_a = 1 + q/\phi$, in which case $m = 0$, and $T = T_a$ for all $z > z_f$ as shown in Figures 3.8 and 3.10. As a result of constant temperature for all $z > z_f$, the value of the fuel concentration entering the reaction zone is determined from equation (3.32), $Y^+ = 1$ ($Y_0 \equiv 1$ for all $z > z_f$), and our

system of equations reduces to

$$\frac{d^2\varphi}{d\eta^2} = \frac{\mathcal{D}}{4}\varphi\left(\frac{1+\gamma\frac{d\varphi}{d\eta}}{1-\alpha\gamma\frac{d\varphi}{d\eta}}\right)e^{-\varphi} \tag{3.53}$$

with the boundary conditions

$$\frac{d\varphi}{d\eta} \sim \begin{cases} -1, & \eta \to -\infty \\ 0, & \eta \to +\infty \end{cases} \tag{3.54}$$

along with

$$\lim_{\eta\to-\infty}(\varphi+\eta) = 0, \tag{3.55}$$

$$\lim_{\eta\to+\infty}\varphi = 0 \tag{3.56}$$

which is identical to the limiting values that describe the reaction zone structure in premixed flames. We note that $\frac{d\varphi}{d\eta} = 0$ as $\eta \to +\infty$ implies that $\varphi = 0$ as $\eta \to +\infty$ for consistency with the differential equation (3.53). This condition also implies that there is no leakage of oxidant across the reaction zone. We integrate the above equation and impose the boundary conditions to obtain

$$\mathcal{D} = \frac{4}{\mu}, \tag{3.57}$$

where

$$\mu = \frac{-2\gamma}{\alpha\gamma + 2(1+\alpha)\left\{1+\ln|1-\gamma|/\gamma\right\}}. \tag{3.58}$$

We remark that the above system (with $m = 0$) is translationally invariant in η, and thus the profile in the structure is known only to within an arbitrary constant. However, as demonstrated by Liñán [30], this constant can be calculated by requiring bounded solutions in an expansion for small m, and then passing to the limit $m \to 0$. To analyze this limit we expand φ in a power series in m with the leading order solution given by equations (3.53) - (3.58) above. We also expand the Damköhler number

$$\mathcal{D} = \mathcal{D}_0(1 + m\mathcal{D}_1 + \cdots), \tag{3.59}$$

where $\mathcal{D}_0$ is given by equation (3.57) and the requirement that solutions be bounded at $O(m)$ leads to the following expression for the Damköhler number correction:

$$\mathcal{D}_1 = \frac{4}{\mathcal{D}_0}\left\{\alpha + \frac{\alpha}{\gamma}\ln(1-\gamma) - (Y_1^+ - \alpha\gamma)\left[\frac{\alpha+1}{\gamma(1-\gamma)} + \frac{\alpha}{\gamma} + \frac{1+2\alpha}{\gamma^2}\ln(1-\gamma)\right]\right\}$$

$$- \int_{-\infty}^{\infty} \varphi_0 \frac{d\varphi_0}{d\eta} e^{-\varphi_0}\, \eta\, d\eta. \tag{3.60}$$

For $\gamma \ll 1$, this expression yields $\mathcal{D}_1 = -1.344 + \gamma[(\alpha+1)1.965 - \alpha/2] + \cdots$, thus obtaining Liñán's result as $\gamma \to 0$.

An explicit representation for Damköhler number $\hat{\mathcal{D}}$ as a function of flame position z_f can be obtained by inserting equations (3.50) and (3.57) into (3.25), and yields

$$\hat{\mathcal{D}} = \frac{(qz_f\gamma)^2}{\epsilon^2 T_f^2 \phi\mu} \exp\left\{\frac{1}{\epsilon T_f}\right\}. \tag{3.61}$$

We note that $m = 0$ corresponds to the temperature of the fuel stream to the oxidant stream ratio β is equal to the adiabatic flame temperature T_a, i.e., $\beta = 1 + q/\phi$. We can readily see that the flame temperature is constant from equation (3.33), hence response curves of flame temperature are not shown here. Response curves of z_f

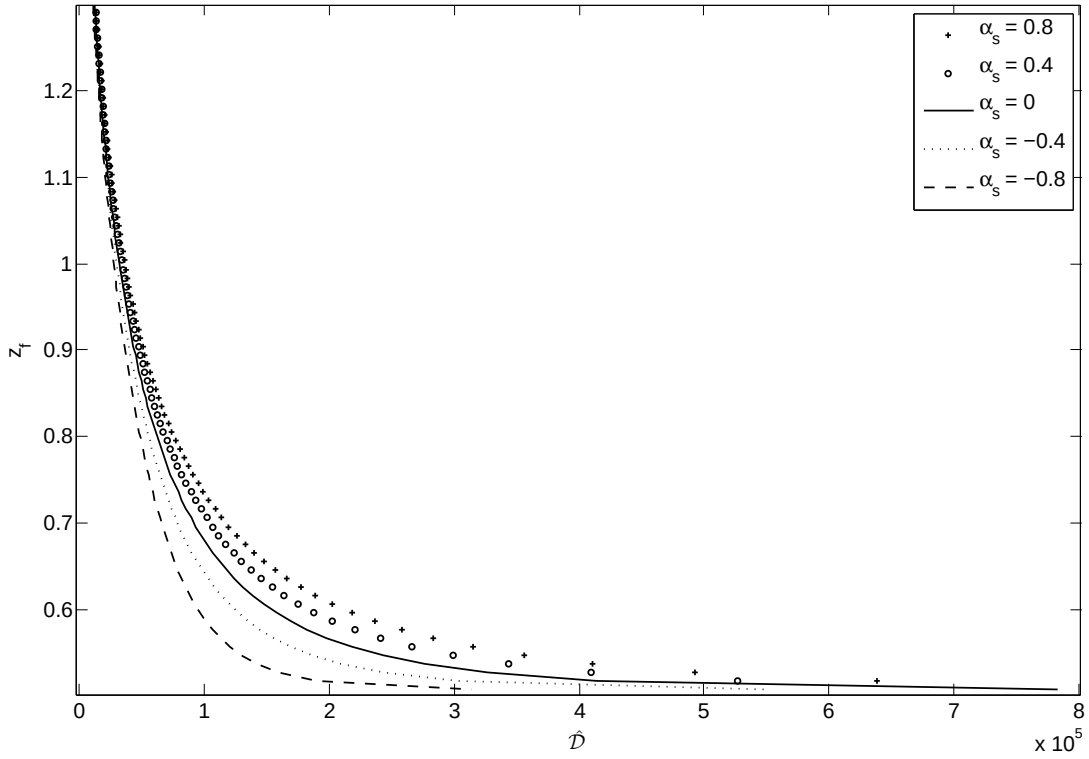

Figure 3.11 Flame location, z_f as a function of Damköhler number, $\hat{\mathcal{D}}$ for several values of the modified Soret diffusion coefficient, α_s, with fuel to oxidant ratio, $\phi = 1$, and heat release, q = 5.

vs. $\hat{\mathcal{D}}$ are shown in Figure 3.11 for several values of the modified Soret diffusion coefficient α_s, with $\phi = 1$. Flame position decreases monotonically with Damköhler number, and asymptotes to a finite value $z_f \sim .506$ as burning intensity increases. Along these response curves we can identify a weak burning limit $\gamma \to 0, \quad z_f \to \infty, \quad Y^- \to 1, \quad \mathcal{D} \to 2$, with minimal fuel consumption, and an intense burning limit, $\gamma \to 1, \quad z_f \to .506, \quad Y^- \to 0, \quad \mathcal{D} \to \infty$, in which fuel is entirely consumed. Physical solutions, corresponding to positive values of the local mass fraction, only exist for the range of values $-1 < \alpha$. For $\alpha < -1$, the large magnitude of the Soret effect inhibits mixing of fuel with oxidant, such that reaction cannot be sustained.

In general, to compute solutions to equations (3.47) - (3.49) for arbitrary β, it is convenient to write

$$\mathcal{D} = \frac{4}{\mu} e^{-nm}, \tag{3.62}$$

and make the translation $\eta \to \eta - n$ so that our system becomes

$$\mu \frac{d^2\varphi}{d\eta^2} = \varphi y e^{-\varphi - m\eta} \tag{3.63}$$

$$y = \frac{Y^+(1 - \alpha\gamma m) + \gamma d\varphi/d\eta}{1 - \alpha\gamma(d\varphi/d\eta + m)}, \tag{3.64}$$

with the boundary conditions

$$\frac{d\varphi}{d\eta} \sim \begin{cases} -1 & \eta \to -\infty \\ 0 & \eta \to \infty \end{cases}. \tag{3.65}$$

In addition, matching provides the conditions

$$\lim_{\eta \to -\infty} (\varphi + \eta) = n, \tag{3.66}$$

$$\lim_{\eta \to +\infty} \varphi = \frac{q}{\phi T_f^2} X_1^+, \tag{3.67}$$

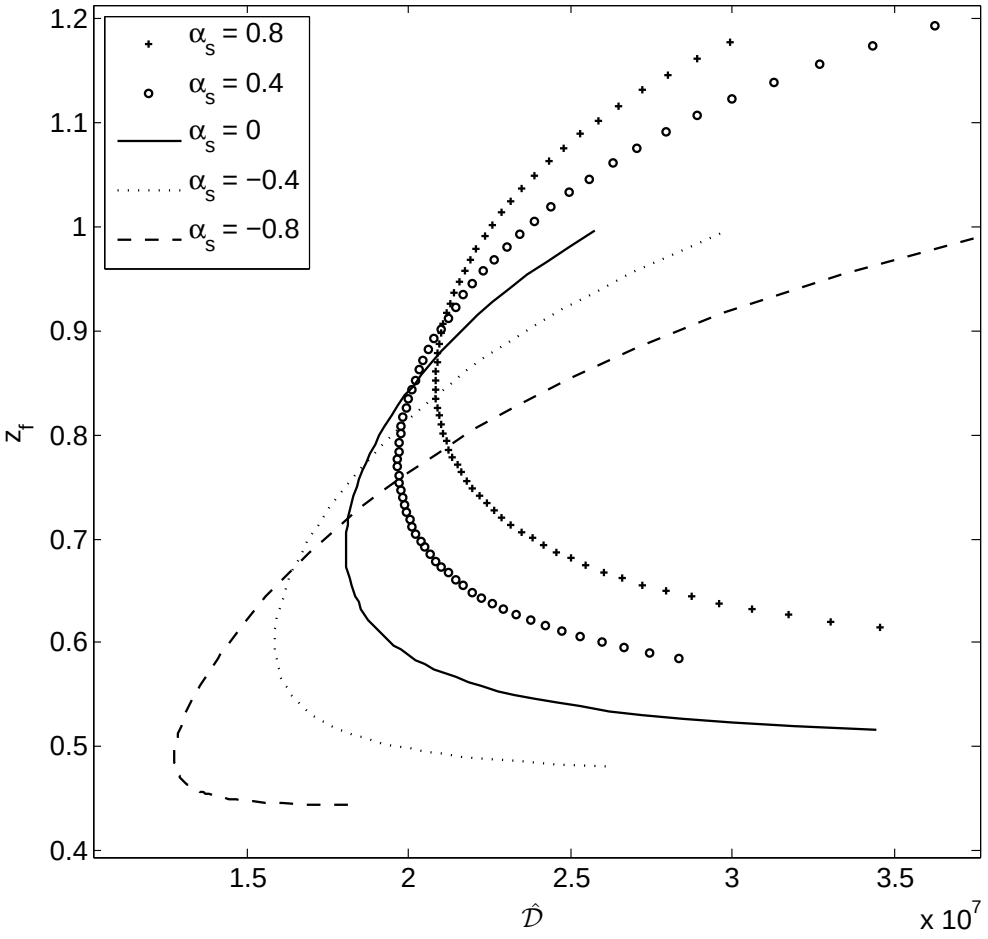

Figure 3.12 Flame location, z_f as a function of Damköhler number, $\hat{\mathcal{D}}$ for several values of the modified Soret diffusion coefficient, α_s, with fuel to oxidant ratio, $\phi = 1$, heat release, q = 5, and temperature of the fuel stream to the oxidant stream ratio, $\beta = 1 + q/2$.

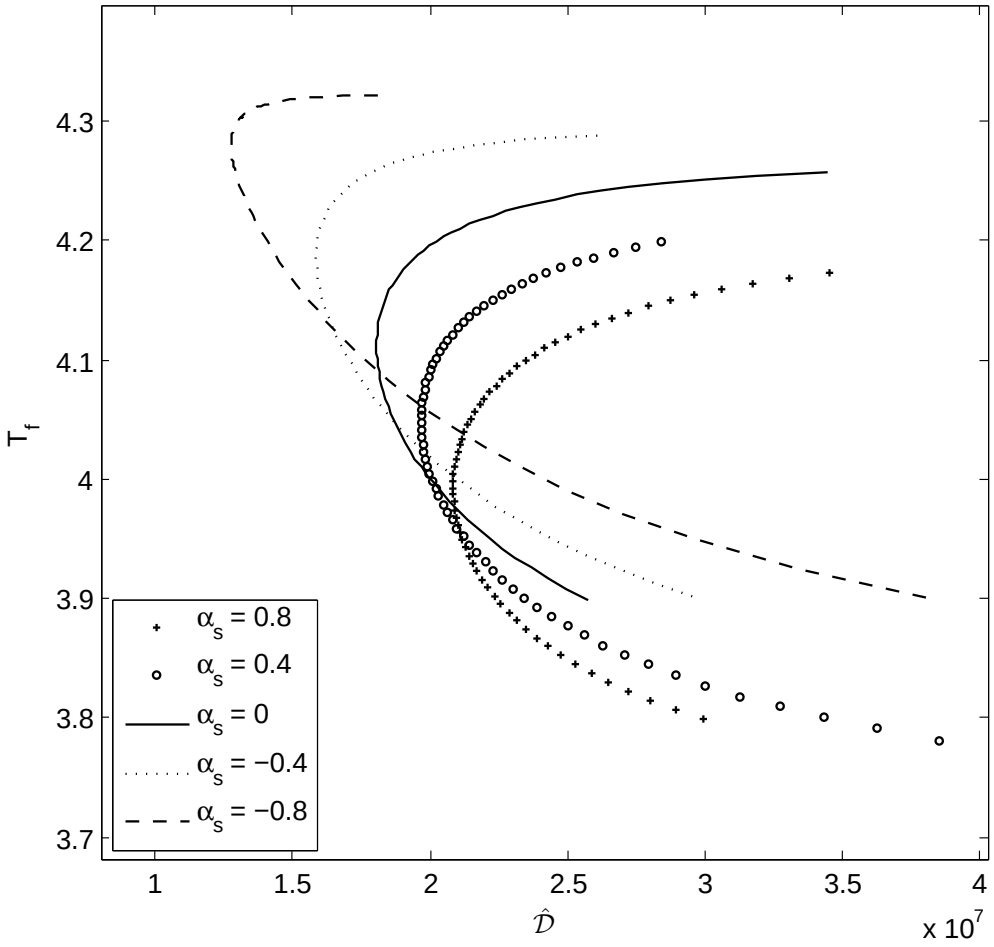

Figure 3.13 Flame temperature, T_f as a function of Damköhler number, $\hat{\mathcal{D}}$ for several values of the modified Soret diffusion coefficient, α_s, with fuel to oxidant ratio, $\phi = 1$, heat release, q = 5, and temperature of the fuel stream to the oxidant stream ratio, $\beta = 1 + q/2$.

which determine the burning rate eigenvalue, i.e., the Damköhler number, and the amount of oxidant leakage, respectively. We note that comparing the expansion in equation (3.59) for small m to equation (3.57) reveals that $n \sim -\mathcal{D}_1$, as $m \to 0$. The above boundary value problems, equations (3.63) - (3.65) were solved using nonlinear shooting with Newton's Method and fourth-order Runge-Kutta method.

Figures 3.12 and 3.13 show the flame location z_f, and flame temperature T_f, respectively, as a function of Damköhler number $\hat{\mathcal{D}}$, for several values of the modified Soret diffusion coefficient $\alpha_s > -T_f/q$, with $q = 5$, $\phi = 1.0$ and $\beta = 1+q/2$. Note that for a given $\hat{\mathcal{D}}$, there exists two solution branches. Figure 3.13 shows all curves exhibit a high temperature branch corresponding to large Damköhler numbers, and a turning point, indicating extinction, at a finite value of $\hat{\mathcal{D}}$. Only the high temperature branch is physical, as it corresponds to increasing temperatures with increasing reaction strength. Thus, the flame profiles shown in Figures (3.7) - (3.10) are for the physical branch only. From Figure 3.12, the turning point is seen to shift further toward the oxidant stream as the value of the Soret coefficient is decreased. This suggests that Soret diffusion enables flames in light fuels to withstand greater strain rates before extinguishing (We note that the Damköhler number is inversely proportional to the strain rate).

3.7 Concluding Remarks

We have analyzed the asymptotic structure of a laminar diffusion flame residing in a counterflow of a fluid fuel stream and a gaseous oxidant. The oxidant undergoes Fickian diffusion, while the fuel diffuses primarily as a result of temperature gradients, i.e., the Soret effect. We adopt a constant density approximation, and pursue a large activation energy limit. As a result of our novel transport mechanism, appropriate for high pressure and/or density, the local structure equations are substantially different from those discovered by Liñán for ideal gas streams. Temperature and concentration

profiles are determined, and the fundamental flame properties of flame temperature and location are found explicitly as a function of Soret diffusion coefficient, ratio of temperature of the two streams, and the Damköhler number.

Our model predicts that the flame resides on the fuel side of the stagnation plane, although it moves closer to the oxidant stream as the Soret coefficient assumes negative values of larger magnitude. The exact solution of the structure problem, for the case when the temperature of the fuel supply stream equals the adiabatic flame temperature ($\beta = 1 + q/\phi$), shows a monotonic decreases in flame position with Damköhler number. However, for lower values of fuel stream temperature, computation of the local structure problem determines explicit extinction conditions, characterized by turning points in response curves of flame location and temperature as a function of Damköhler number.

CHAPTER 4

NEW THEORY OF PREMIXED FLAMES IN HIGH DENSITY FLUIDS

4.1 Formulation

Consider a homogeneous premixed combustible mixture, consisting of two reactants. The fuel F is assumed to be in supercritical condition, while the oxidant O is assumed to be an ideal gas. The reaction proceeds according to

$$\nu_F \mathcal{M}_F + \nu_O \mathcal{M}_O \rightarrow \text{Products},$$

where $\mathcal{M}_i$ are the chemical symbols, and ν_i are the stoichiometric coefficients for species i.

The governing equations for temperature $\hat{T}$ and species mass fractions $\hat{X}$, and $\hat{Y}$ are coupled to the conservation of mass and momentum equations are

$$\hat{\rho} c_p \left(\frac{\partial \hat{T}}{\partial \hat{t}} + \hat{\mathbf{V}} \cdot \hat{\nabla} \hat{T} \right) - \hat{\nabla} \cdot (\lambda \hat{\nabla} \hat{T}) = \hat{Q} \hat{\Omega}, \tag{4.1}$$

$$\hat{\rho} \left(\frac{\partial \hat{Y}_O}{\partial \hat{t}} + \hat{\mathbf{V}} \cdot \hat{\nabla} \hat{Y}_O \right) - \hat{\nabla} \cdot (\hat{\rho} D_O \hat{\nabla} \hat{Y}_O) = -\nu_O W_O \hat{\Omega}, \tag{4.2}$$

$$\hat{\rho} \left(\frac{\partial \hat{Y}_F}{\partial \hat{t}} + \hat{\mathbf{V}} \cdot \hat{\nabla} \hat{Y}_F \right) - \hat{\nabla} \cdot \left(\hat{\rho} D_F \alpha_{BK} \hat{Y}_F \frac{\hat{\nabla} \hat{T}}{\hat{T}} + \hat{\rho} D_F \alpha_{D_F} \hat{\nabla} \hat{Y}_F \right) = -\nu_F W_F \hat{\Omega}, \tag{4.3}$$

$$\frac{\partial \hat{\rho}}{\partial \hat{t}} + \nabla \cdot (\hat{\rho} \hat{\mathbf{V}}) = 0, \tag{4.4}$$

$$\hat{\rho} \left(\frac{\partial \hat{\mathbf{V}}}{\partial \hat{t}} + \hat{\mathbf{V}} \cdot \hat{\nabla} \hat{\mathbf{V}} \right) = -\nabla \hat{P} + \mu \left(\hat{\nabla}^2 \hat{\mathbf{V}} + \frac{1}{3} \hat{\nabla} (\hat{\nabla} \cdot \hat{\mathbf{V}}) \right) \tag{4.5}$$

where $\hat{\rho}$ is the fluid density, $\hat{\mathbf{V}}$ is the velocity field, $\hat{P}$ is the pressure, α_D is the mass diffusion factor, α_{BK} is the Soret diffusion factor, λ is the thermal conductivity, $\hat{Q}$ is the heat release, μ is the dynamic viscosity, c_p is the specific heat, and D_i, and W_i are the mass diffusivities, and molecular weights, respectively, of species i.

Reaction proceeds at a rate that obeys the Arrhenius law with an overall activation energy $\hat{E}_a$ and a pre-exponential factor $\mathcal{A}$, and thus the reaction rate term, $\hat{\Omega}$ has the form,

$$\hat{\Omega} = \mathcal{A}\hat{\rho}^2 \frac{\hat{Y}_O \hat{Y}_F}{W_O W_F} e^{-\frac{\hat{E}_a}{R^o \hat{T}}}, \tag{4.6}$$

with R^o the gas constant.

4.2 Nondimensionalization

The governing equations can be nondimensionalized by using the adiabatic flame speed, S_f^0 and thermal thickness, $l_D = \lambda/\hat{\rho} c_p S_f^0$, as the characteristic velocity and length, respectively. The time scale is chosen to be l_D/S_f^0. All other variables are scaled with respect to their values in the fresh mixture, which are denoted by the subscript u. Upon introducing the nondimensional variables

$$\mathbf{x} = \frac{\hat{\mathbf{x}}}{l_D}, \qquad t = \frac{\hat{t}}{l_D/S_f^0},$$

$$Y_O = \frac{\hat{Y}_O}{\hat{Y}_{O,u}}, \qquad Y_F = \frac{\hat{Y}_F}{\hat{Y}_{F,u}}, \qquad T = \frac{\hat{T}}{\hat{T}_u},$$

$$\mathbf{V} = \frac{\hat{\mathbf{V}}}{S_f^0}, \qquad \rho = \frac{\hat{\rho}}{\hat{\rho}_u}, \qquad P = \frac{\hat{P}}{\hat{P}_u},$$

our system of equations become

$$\rho\left(\frac{\partial T}{\partial t} + \mathbf{V}\cdot\nabla T\right) - \nabla^2 T = q\Omega, \tag{4.7}$$

$$\rho\left(\frac{\partial Y_O}{\partial t}+\mathbf{V}\cdot\nabla Y_O\right)-Le_O^{-1}\nabla^2 Y_O=-\Omega, \tag{4.8}$$

$$\rho\left(\frac{\partial Y_F}{\partial t}+\mathbf{V}\cdot\nabla Y_F\right)-Le_F^{-1}\nabla\cdot\left(\alpha_{BK}Y_F\frac{\nabla T}{T}+\alpha_{D_F}\nabla Y_F\right)=-\frac{1}{\phi}\Omega, \tag{4.9}$$

$$\frac{\partial\rho}{\partial t}+\nabla\cdot(\rho\mathbf{V})=0, \tag{4.10}$$

$$\rho\left(\frac{\partial\mathbf{V}}{\partial t}+\mathbf{V}\cdot\nabla\mathbf{V}\right)=-\frac{1}{\gamma M_a^2}\nabla P+Pr\left(\nabla^2\mathbf{V}+\frac{1}{3}\nabla(\nabla\cdot\mathbf{V})\right), \tag{4.11}$$

where

$$q=\frac{\hat{Q}\hat{Y}_{O,u}}{c_p\hat{T}_u\nu_O W_O} \tag{4.12}$$

is the dimensionless heat release. Additional dimensionless parameter in the above system of equations are the Lewis number

$$Le_i=\frac{\lambda}{\hat{\rho}c_p\hat{D}_i} \tag{4.13}$$

is the ratio of thermal diffusivity of the mixture to mass diffusivity of species i, the equivalence ratio

$$\phi=\frac{\hat{Y}_{F,u}/\nu_F W_F}{\hat{Y}_{O,u}/\nu_O W_O} \tag{4.14}$$

is the ratio of the mass fraction of the fuel to oxidizer in the fresh mixture to their stoichiometric ratio, the Prandtl number

$$Pr=\frac{\mu c_p}{\lambda} \tag{4.15}$$

is the ratio of viscous to thermal effects, the Mach number

$$M_a=\frac{S_f^0}{\sqrt{\gamma\hat{P}_u/\hat{\rho}_u}} \tag{4.16}$$

is the ratio of the speed of the flame to sound and γ is the ratio of specific heats. The reaction rate term on the right-hand side of (4.7) - (4.9) has the form

$$\Omega = \mathcal{D}\rho^2 Y_O Y_F exp\left\{ \frac{\beta T_a^2}{q}\left(\frac{1}{T_a} - \frac{1}{T}\right)\right\} \tag{4.17}$$

where $\mathcal{D}$ is the Damköhler number, a ratio of the flow time to the chemical time, given by

$$\mathcal{D} = \frac{\lambda \nu_O \hat{Y}_{F,u}\mathcal{A}}{c_p (S_f^0)^2 W_F} e^{-\beta T_a/q}. \tag{4.18}$$

The Zel'dovich number

$$\beta = \frac{E}{R^o \hat{T}_a^2}(\hat{T}_a - \hat{T}_u) \tag{4.19}$$

is a nondimensional measure of the temperature sensitivity of the reaction rate (Note: The small parameter in activation energy asymptotics is the reciprocal of the Zel'dovich number). Here $\hat{T}_a$ is the adiabatic flame temperature, which in dimensionless form is expressed as $T_a = 1 + q$.

4.3 Analysis of Planar Flame Structure in High Density Fluids

The objective in this section is to obtain a relation for the Damköhler number and the laminar flame speed, also known as the laminar burning velocity. We adopt the constant density approximation, and thus the temperature and mass transport equations are completely decoupled from the equations of fluid dynamics. We consider a steady, planar flame travels in the negative x-direction at unit speed in the laboratory frame, so that the fresh, unburned mixture is approached as $x \to -\infty$ and the burned mixture is approached as $x \to +\infty$. For convenience, we will consider unity Lewis number for the oxidant, and define the modified Soret diffusion coefficient $\alpha_s = Le_F^{-1}\alpha_{BK}$. We note that Fickian diffusion is insignificant in high pressure, $\alpha_{D_F} \ll 1$, therefore we let $\alpha_{D_F} = 0$ for simplicity.

In the limit $\beta \to \infty$, the reaction rate term is confined to a narrow boundary layer in the flow field separating the unburned and burned mixture. On either side of this boundary layer, reaction can be ignored and equations (4.7) - (4.9) are now chemistry-free,

$$\frac{dT}{dx} - \frac{d^2T}{dx^2} = 0, \tag{4.20}$$

$$\frac{dY_O}{dx} - \frac{d^2Y_O}{dx^2} = 0, \tag{4.21}$$

$$\frac{dY_F}{dx} - \alpha_s \frac{d}{dx}\left(\frac{Y_F}{T}\frac{dT}{dx}\right) = 0, \tag{4.22}$$

with the boundary conditons

$$T \to 1; \qquad Y_O \to 1; \qquad Y_F \to 1, \qquad x \to -\infty, \tag{4.23}$$

$$T \to T_a; \qquad Y_O \to 0, \qquad x \to +\infty. \tag{4.24}$$

The differential equation for the fuel is only first order, thus we can only impose one boundary condition.

The outer solution on either side of the reaction zone can be expanded in the form

$$T = T^{(0)} + \beta^{-1}T^{(1)} + \cdots,$$

$$Y_O = Y_O^{(0)} + \beta^{-1}Y_O^{(1)} + \cdots,$$

$$Y_F = Y_F^{(0)} + \beta^{-1}Y_F^{(1)} + \cdots.$$

Since we have adopted constant density approximation, it is common to consider weak thermal expansion $q \ll 1$. We introduce the expansion

$$T^{(0)} = 1 + q\tau,$$

to obtain

$$\frac{d\tau}{dx} - \frac{d^2\tau}{dx^2} = 0, \tag{4.25}$$

with the boundary condition

$$\tau = \begin{cases} 0, & x < 0 \\ (T_a - 1)/q, & x > 0. \end{cases} \tag{4.26}$$

The solutions of the above system in the outer region is given by

$$\tau = \begin{cases} e^x, & x < 0 \\ 1, & x > 0 \end{cases}, \tag{4.27}$$

$$Y_O^{(0)} = \begin{cases} 1 - e^x, & x < 0 \\ 0, & x > 0 \end{cases}, \tag{4.28}$$

$$Y_F^{(0)} = \begin{cases} (1 - \alpha e^x)^{-1}, & x < 0 \\ Y_F^{(0)}(0+), & x > 0 \end{cases}, \tag{4.29}$$

where $\alpha = \alpha_s q/T_a$ and $Y_F^{(0^+)}$ will be determined by matching to the inner solution.

In order to achieve balance between reaction and Soret diffusion in the reaction zone, it is necessary to allow an $O(1)$ amount of fuel enters into the reaction zone. To examine the internal structure of the reaction zone, we make the stretching transformation

$$x = \beta^{-1}\xi,$$

and introduce the expansions

$$T = T_a + \beta^{-1} q\theta + \cdots,$$

$$Y_O = \beta^{-1} y_O + \cdots ,$$

$$Y_F = y_F + \cdots ,$$

so that the local equations take the form:

$$\frac{d^2\theta}{d\xi^2} = -\Lambda y_O y_F e^{\theta}, \tag{4.30}$$

$$\frac{d^2 y_O}{d\xi^2} = \Lambda y_O y_F e^{\theta}, \tag{4.31}$$

$$-\frac{dy_F}{d\xi} + \alpha \frac{d}{d\xi}\left(y_F \frac{d\theta}{d\xi} \right) = \frac{1}{\phi} \Lambda y_O y_F e^{\theta}, \tag{4.32}$$

where $\Lambda = D\rho^2/\beta^2$. At the interface between zones, we enforce the matching conditions obtained by expanding the coefficients of the outer asymptotic solutions as a Taylor series about $x = 0$ expressed in terms of ξ, matching coefficients of powers of β^{-1}, we obtain

$$T(x = \beta^{-1}\xi) \sim T^{(0)}(0\pm) + \beta^{-1}\left(\frac{dT}{dx}^{(0)}(0\pm)\xi + T^{(1)}(0\pm) \right) + \cdots , \tag{4.33}$$

$$Y_O(x = \beta^{-1}\xi) \sim Y_O^{(0)}(0\pm) + \beta^{-1}\left(\frac{dY_O^{(0)}}{dx}(0\pm)\xi + Y_O^{(1)}(0\pm) \right) + \cdots , \tag{4.34}$$

$$Y_F(x = \beta^{-1}\xi) \sim Y_F^{(0)}(0\pm) + \beta^{-1}\left(\frac{dY_F^{(0)}}{dx}(0\pm)\xi + Y_F^{(1)}(0\pm) \right) + \cdots . \tag{4.35}$$

Thus, matching to the outer solution provides the local relations

$$\theta = \begin{cases} \xi + T^{(1)}(0-), & \xi \to -\infty \\ 0 + T^{(1)}(0+), & \xi \to +\infty \end{cases}, \tag{4.36}$$

$$y_O = \begin{cases} -\xi + Y_O^{(1)}(0-), & \xi \to -\infty \\ 0 + Y_O^{(1)}(0+), & \xi \to +\infty \end{cases}, \tag{4.37}$$

$$y_F = \begin{cases} (1-\alpha)^{-1}, & \xi \to -\infty \\ Y_F^{(0)}(0+), & \xi \to +\infty \end{cases}. \tag{4.38}$$

The local enthalpy equation corresponding to the oxidant species can be integrated to yield the following expression for y_O explicitly in terms of θ. Upon matching to both the burned side $\xi \to +\infty$ and the unburned side $\xi \to -\infty$, yield

$$\theta + y_O = 0. \tag{4.39}$$

Similarly, a linear combination of equations (4.30) and (4.32) can be directly integrated to determine y_F in terms of θ. Matching to the burned side $\xi \to +\infty$, yields

$$\frac{d\theta}{d\xi} + \phi\left\{ - y_F + \alpha\left(y_F \frac{d\theta}{d\xi}\right)\right\} = -\phi Y_F^{(0)}(0+). \tag{4.40}$$

Finally, matching to the unburned side $\xi \to -\infty$, yield

$$Y_F^{(0)}(0+) = 1 - 1/\phi. \tag{4.41}$$

We now solve for y_O and y_F in equation (4.39) - (4.41), respectively, to obtain

$$y_O = -\theta, \tag{4.42}$$

and

$$y_F = \frac{Y_F^{(0)}(0+) + (1/\phi)d\theta/d\xi}{1 - \alpha d\theta/d\xi}. \tag{4.43}$$

These may now be inserted into equation (4.32) to provide a single equation for the local temperature perturbation,

$$\frac{d^2\theta}{d\xi^2} = \Lambda\theta \left(\frac{Y_F^{(0)}(0+) + (1/\phi)d\theta/d\xi}{1 - \alpha d\theta/d\xi} \right) e^{\theta}. \tag{4.44}$$

Now we can multiply equation (4.44) by $d\theta/d\xi$ to obtain the first integral

$$\phi\Bigg\{ \frac{1}{2}\left(\phi Y_F^{(0)}(0+) + \frac{d\theta}{d\xi}\right)\left(\alpha\left(3\phi Y_F^{(0)}(0+) - \frac{d\theta}{d\xi}\right) + 2\right) -$$

$$\phi Y_F^{(0)}(0+)\Big(1 + \alpha\phi Y_F^{(0)}(0+)\Big)\ln\left|\phi Y_F^{(0)}(0+) + \frac{d\theta}{d\xi}\right| \Bigg\} = \Lambda\Big(\big(\theta - 1\big)e^{\theta}\Big) + \text{const.}$$

By applying the matching conditions yield an expression for the burning rate eigenvalue, Λ, namely

$$\Lambda = -\frac{\alpha\phi}{2} + \phi\Big(1 + \alpha(\phi - 1)\Big)\left(1 - (\phi - 1)\ln\left(\frac{\phi}{\phi - 1}\right)\right). \tag{4.45}$$

Using equations (4.18) and (4.45), the flame speed can be expressed as

$$S_f^0 = \left\{ \frac{\lambda\nu_O\mathcal{A}\rho^2}{c_p W_F}\beta^{-2}\Lambda^{-1}\hat{Y}_{F,u} \right\}^{1/2} e^{-\beta T_a/2q}, \tag{4.46}$$

and thus the Damköhler number can be written as

$$\mathcal{D} = \frac{\beta^2\Lambda}{\rho^2}. \tag{4.47}$$

We note the above solutions are valid for $-\infty < \alpha < 1$. For larger values of α, the transport of fuel away from the reaction sheet toward the unburned region (the Soret effect) exceeds the rate at which convection delivers fuel toward the flame. Characteristic profiles of reduced temperature and species concentrations are shown in Figures 4.1 and 4.2 for several values of α. The value of α is negative in Figure 4.1

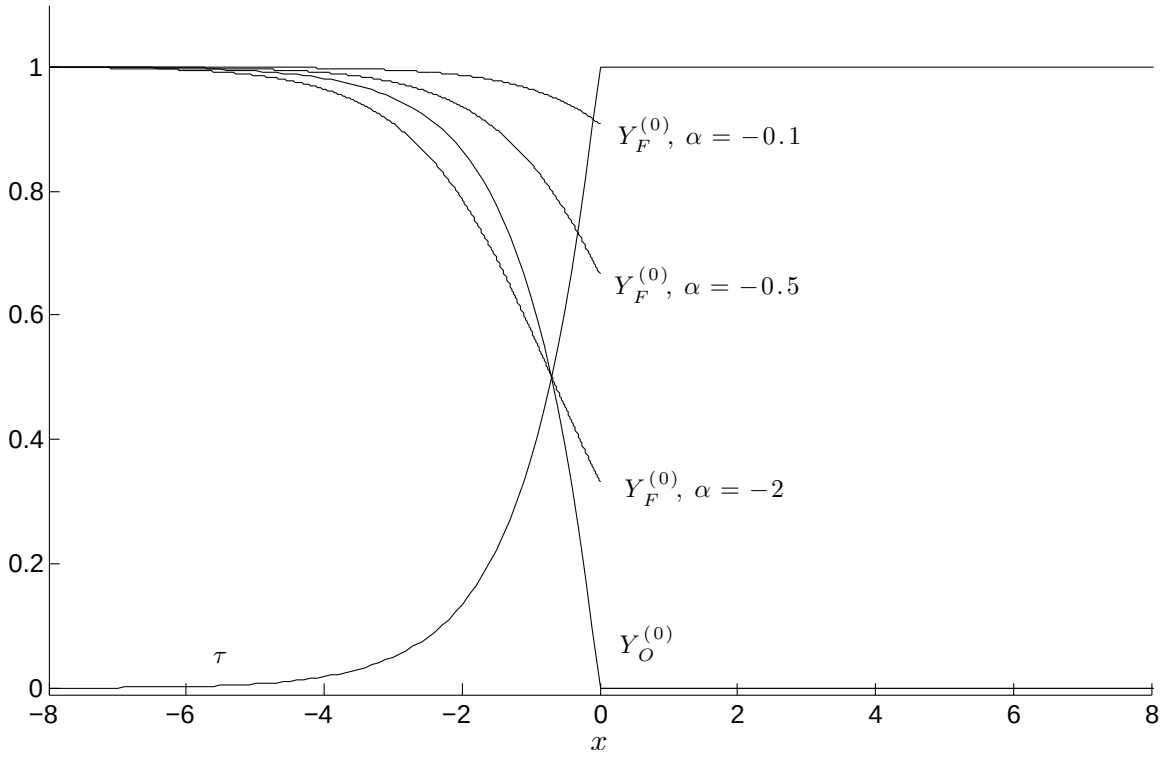

Figure 4.1 Profiles of reduced temperature, τ and species concentrations, $Y_F^{(0)}$ and $Y_O^{(0)}$ with stoichiometric condition, $\phi = 1$ and several values of the modified Soret diffusion coefficient, $\alpha < 0$.

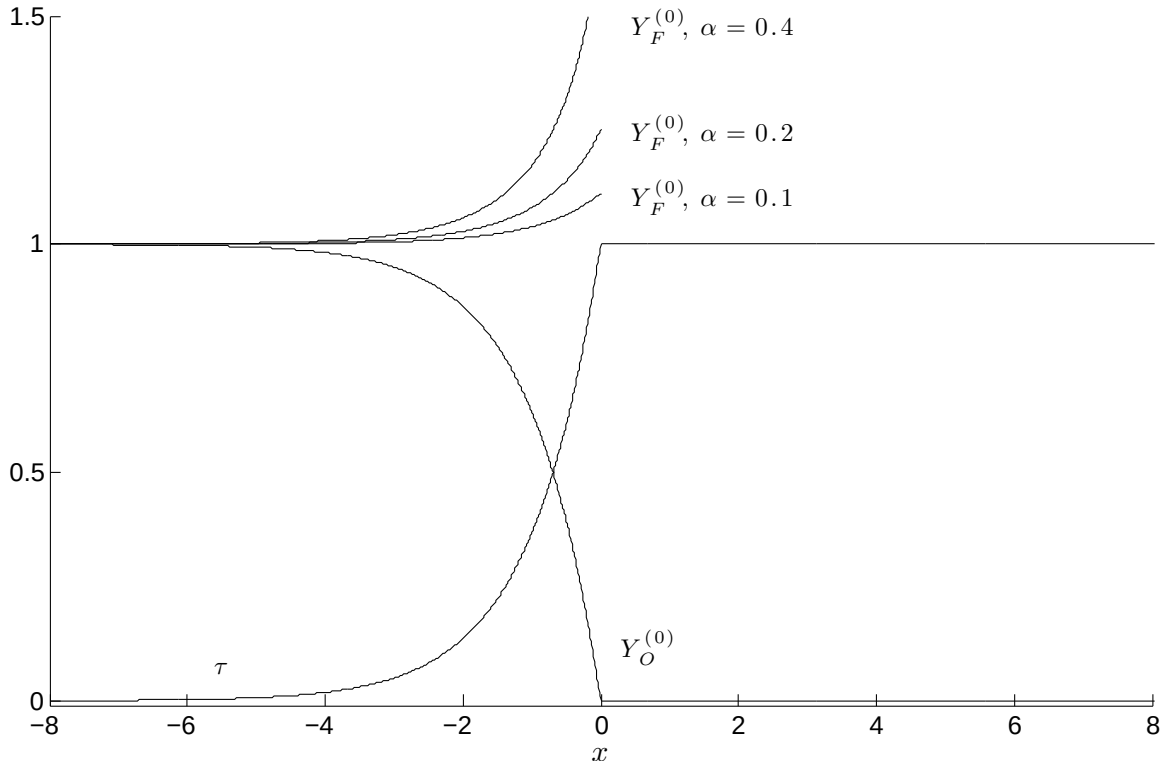

Figure 4.2 Profiles of reduced temperature, τ and species concentrations, $Y_F^{(0)}$ and $Y_O^{(0)}$ with stoichiometric condition, $\phi = 1$ and several values of the modified Soret diffusion coefficient, $\alpha > 0$.

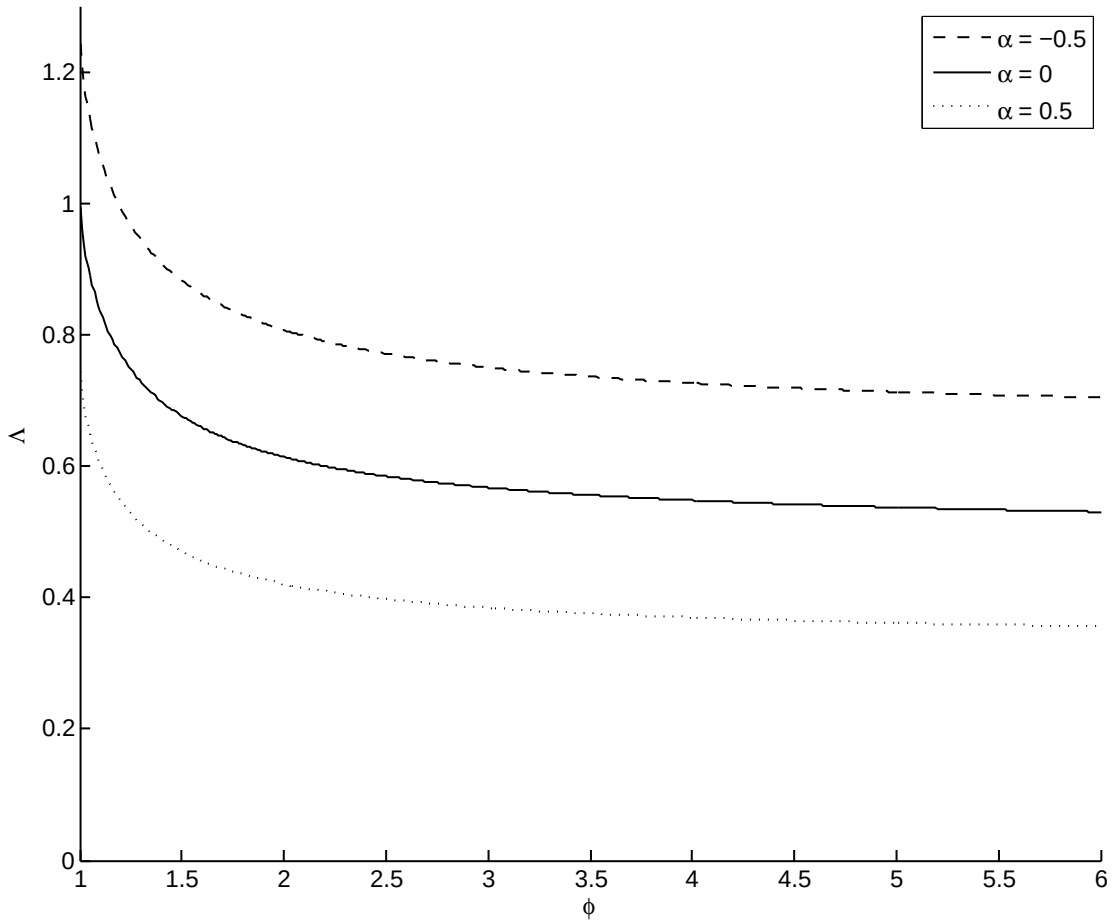

Figure 4.3 Burning rate eigenvalue, Λ shown as a function of equivalence ratio ϕ with several values of the modified Soret diffusion coefficient, α.

and positive in Figure 4.2, with $\phi = 1$ in both Figures (When stoichiometric condition is being assumed, by equation (4.41), we deduce that $Y_F^{(0)}(0+) = 1 - 1/\phi = 0$).

Figure 4.1 shows three different values of α. When $\alpha < 0$, the tendency of Soret effect is to diffuse more rapidly towards the higher temperature region. As a result, larger negative value of α shows that the local fuel concentration decreases.

The profile in Figure 4.2 illustrates the accumulation of excess fuel immediately ahead of the reaction sheet. For $\alpha > 0$, thermal diffusion causes the fuel to diffuse in the direction opposite that of the incoming flow, creating a peak in the local fuel profile upstream of the reaction sheet.

We note that temperature and oxidant mass fraction are continuous through the flame, while the fuel suffers a jump discontinuity as a direct result of limited mass diffusion. We note that this jump is in the outer profile only. The analysis of the reaction zone, which led to the above model, demonstrates that fuel undergoes rapid and complete consumption within the reaction zone, and the composite profile is indeed continuous.

The burning rate eigenvalue Λ as a function of the equivalence ratio ϕ is plotted in Figure 4.3 for several values of α. We observe that Λ decreases monotonically with ϕ for all α, and asymptotes to a finite value as $\phi \to \infty$. We note that the curve shifts up for negative value of α, indicating higher value of Λ, which means smaller value of flame speed. Whereas when α is positive the curve shifts down, suggesting smaller value of Λ which corresponds to larger value of flame speed. In general, the trend is as α increases, the burning rate eigenvalue decreases, therefore the adiabatic flame speed increases.

4.4 Generalized theory of Multidimensional Flame Structure in High Density Fluids

In this section we generalize our theory for flames of arbitrary shape. The equations for thermal and mass transport are coupled to the equations of hydrodynamics. But the two sets of equations can be decoupled by considering weak thermal expansion $q \ll 1$. For convenience, we will consider unity Lewis number for the oxidant

$$Le_O^{-1} = 1 - \beta^{-1} l, \tag{4.48}$$

and define the modified Soret and mass diffusion coefficients $\alpha_s = Le_F^{-1}\alpha_{BK}$, $\alpha_D = Le_F^{-1}\alpha_{D_F}$ Thus, the governing equations that we shall consider are

$$\rho\left(\frac{\partial T}{\partial t} + \mathbf{V}\cdot\nabla T\right) - \nabla^2 T = q\beta^2 \Lambda Y_O Y_F exp\left\{\frac{\beta T_a^2}{q}\left(\frac{1}{T_a} - \frac{1}{T}\right)\right\}, \tag{4.49}$$

$$\rho\left(\frac{\partial Y_O}{\partial t} + \mathbf{V}\cdot\nabla Y_O\right) - (1-\beta^{-1}l)\nabla^2 Y_O = -\beta^2 \Lambda Y_O Y_F exp\left\{\frac{\beta T_a^2}{q}\left(\frac{1}{T_a} - \frac{1}{T}\right)\right\}, \tag{4.50}$$

$$\begin{aligned}\rho\left(\frac{\partial Y_F}{\partial t} + \mathbf{V}\cdot\nabla Y_F\right) \;&-\; \nabla\cdot\left(\alpha_s Y_F \frac{\nabla T}{T} + \alpha_D \nabla Y_F\right) = \\ &-\; \beta^2 \frac{1}{\phi}\Lambda Y_O Y_F exp\left\{\frac{\beta T_a^2}{q}\left(\frac{1}{T_a} - \frac{1}{T}\right)\right\}.\end{aligned} \tag{4.51}$$

It is convenient in our formulation to introduce the enthalpy function for the oxidant

$$H_O = T + qY_O. \tag{4.52}$$

An equation for H_O can be written that is free of the nonlinear reaction rate term, and when equation (4.52) is used to eliminate Y_O in favor of H_O we obtain

$$\rho\left(\frac{\partial H_O}{\partial t} + \mathbf{V}\cdot\nabla H_O\right) - \nabla^2 H_O = -\beta^{-1} l \nabla^2 (H_O - T). \tag{4.53}$$

Temperature gradients behind the flame are assumed small, i.e., $O(\beta^{-1})$, and corresponding only an $O(\beta^{-1})$ amount of oxidant can leak through.

In the limit $\beta \to \infty$ the reaction zone is confined to a moving narrow reactive-diffusion boundary layer, which we regard as the flame front. In cartesian coordinates, the flame front can be described by the function

$$x - f(y, z, t) = 0, \tag{4.54}$$

such that $x < f$ corresponds to the unburned mixture, and $x > f$ to the burned mixture. The outer solution on either side of the flame, $x = f(y, z, t)$ is sought in the form of a power series in β^{-1}, i.e.

$$\rho = \rho^{(0)} + \beta^{-1}\rho^{(1)} + \cdots ,$$

$$T = T^{(0)} + \beta^{-1}T^{(1)} + \cdots ,$$

$$H_O = H_O^{(0)} + \beta^{-1}qh_O + \cdots ,$$

$$Y_F = Y_F^{(0)} + \beta^{-1}Y_F^{(1)} + \cdots .$$

These are inserted into above system of equations and at leading order we obtain the following transport equations on either side of the flame zone

$$\rho^{(0)}\left(\frac{\partial T^{(0)}}{\partial t} + \mathbf{V}\cdot\nabla T^{(0)}\right) - \nabla^2 T^{(0)} = 0, \qquad x < f, \tag{4.55}$$

$$T^{(0)} = 1 + q, \qquad x > f, \tag{4.56}$$

$$\rho^{(0)}\left(\frac{\partial Y_F^{(0)}}{\partial t} + \mathbf{V}\cdot\nabla Y_F^{(0)}\right) - \nabla\cdot\left(\alpha_s Y_F^{(0)}\frac{\nabla T^{(0)}}{T^{(0)}} + \alpha_D \nabla Y_F^{(1)}\right) = 0, \qquad x \neq f. \tag{4.57}$$

Proceeding to $O(\beta^{-1})$, we obtain

$$\rho^{(1)}\left(\frac{\partial T^{(0)}}{\partial t} + \mathbf{V}\cdot\nabla T^{(0)}\right) + \rho^{(0)}\left(\frac{\partial T^{(1)}}{\partial t} + \mathbf{V}\cdot\nabla T^{(1)}\right) - \nabla^2 T^{(0)} = 0, \qquad x \neq f, \tag{4.58}$$

$$\rho^{(0)}\left(\frac{\partial h_O}{\partial t}+\mathbf{V}\cdot\nabla h_O\right)-\nabla^2 h_O = l\nabla^2 T^{(0)}, \qquad x\neq f. \tag{4.59}$$

In order to properly relate the solutions of these equations across the flame zone it is necessary to analyze the reaction zone structure.

It is convenient to adopt a coordinate system attached to the flame front by introducing

$$\xi = x - f(y,z,t), \qquad y=y, \qquad z=z, \qquad t=t,$$

such that $\xi<0$ refers to the unburned region, and $\xi>0$ to the burned region. In this new coordinate system, the derivative with respect to time and the gradient are written as

$$\frac{\partial}{\partial t}\rightarrow\frac{\partial}{\partial t}-f_t\frac{\partial}{\partial\xi},$$

$$\nabla\rightarrow\left(\frac{\partial}{\partial\xi},\frac{\partial}{\partial y}-f_y\frac{\partial}{\partial\xi},\frac{\partial}{\partial z}-f_z\frac{\partial}{\partial\xi}\right),$$

the convective and the Laplacian operators take the form

$$\frac{\partial}{\partial t}+\mathbf{V}\cdot\nabla=\frac{\partial}{\partial t}-f_t\frac{\partial}{\partial\xi}+\mathbf{V}\cdot\left(\frac{\partial}{\partial\xi},\frac{\partial}{\partial y}-f_y\frac{\partial}{\partial\xi},\frac{\partial}{\partial z}-f_z\frac{\partial}{\partial\xi}\right),$$

$$\nabla^2=(1+f_y^2+f_z^2)\frac{\partial^2}{\partial\xi^2}+\frac{\partial^2}{\partial y^2}+\frac{\partial^2}{\partial z^2}-(f_{yy}+f_{zz})\frac{\partial}{\partial\xi}-2f_y\frac{\partial^2}{\partial\xi\partial y}-2f_z\frac{\partial^2}{\partial\xi\partial z}.$$

In the reaction zone, we stretch the spatial variable

$$\xi=\beta^{-1}\zeta$$

and seek inner solutions of the form

$$T=T_a+\beta^{-1}\theta+\cdots,$$

$$H_O=T_a+\beta^{-1}q\psi+\cdots,$$

$$Y_O = \beta^{-1} q y_O + \cdots ,$$

$$Y_F = y_F + \cdots .$$

These expansions are substituted into equation (4.49), (4.53), and (4.51) and at leading order we obtain the following equations in the reaction zone

$$-N^2 \frac{\partial^2 \theta}{\partial \zeta^2} = q \Lambda y_O y_F e^{\theta/q} \tag{4.60}$$

$$\frac{\partial^2 \psi}{\partial \zeta^2} = 0 \tag{4.61}$$

$$(u - \mathbf{v}_\perp \cdot \nabla f - f_t) \frac{\partial y_F}{\partial \zeta} - N^2 \frac{\alpha_s}{T_a} \frac{\partial}{\partial \zeta} \left(y_F \frac{\partial \theta}{\partial \zeta} \right) = -\frac{1}{\phi} \Lambda y_O y_F e^{\theta/q} \tag{4.62}$$

where $N = \sqrt{1 + |\nabla_\perp f|^2}$ is the surface normal. Solutions to these equations must match to the outer solutions of equations (4.55) - (4.59).

The matching conditions are derived by expanding the assumed form of the outer solution in terms of the inner variable, $\xi = \beta^{-1}\zeta$, to yield

$$T(\xi = \beta^{-1}\zeta) \sim T^{(0)}(0\pm) + \beta^{-1} \left(\frac{\partial T^{(0)}}{\partial \xi}(0\pm)\zeta + T^{(1)}(0\pm) \right) + \cdots , \tag{4.63}$$

$$Y_O(\xi = \beta^{-1}\zeta) \sim Y_O^{(0)}(0\pm) + \beta^{-1} \left(\frac{\partial Y_O^{(0)}}{\partial \xi}(0\pm)\zeta + Y_O^{(1)}(0\pm) \right) + \cdots , \tag{4.64}$$

$$Y_F(\xi = \beta^{-1}\zeta) \sim Y_F^{(0)}(0\pm) + \beta^{-1} \left(\frac{\partial Y_F^{(0)}}{\partial \xi}(0\pm)\zeta + Y_F^{(1)}(0\pm) \right) + \cdots , \tag{4.65}$$

Since temperature gradient and mass fraction of oxidizer behind flame is small, we deduce that

$$\frac{\partial T^{(0)}}{\partial \xi}(0+) = 0, \tag{4.66}$$

$$Y_O^{(0)}(0+) = 0, \tag{4.67}$$

and thus the matching conditions become

$$\theta = \begin{cases} \partial T^{(0)}/\partial\xi(0-)\zeta + T^{(1)}(0-), & \zeta \to -\infty \\ T^{(1)}(0+), & \zeta \to +\infty \end{cases}, \tag{4.68}$$

$$q\psi = \begin{cases} \left(\partial T^{(0)}/\partial\xi(0-) + \partial Y_O^{(0)}/\partial\xi(0-)\right)\zeta + T^{(1)}(0-) + qY_O^{(1)}(0-), & \zeta \to -\infty \\ T^{(1)}(0+), & \zeta \to +\infty \end{cases}, \tag{4.69}$$

$$y_F = \begin{cases} Y_F^{(0)}(0-), & \zeta \to -\infty \\ Y_F^{(0)}(0+), & \zeta \to +\infty \end{cases}. \tag{4.70}$$

Equation (4.61) can be readily be integrated to yield

$$\psi = h_O(0+) = h_O(0-) \tag{4.71}$$

which implies that the outer solution h_O of equation (4.59) must be continuous across the reaction zone. Also, we note that the leading order outer temperature profile must be continuous at the reaction zone, i.e. $T^{(0)}(0+) = T^{(0)}(0-) = T_a$. Thus,

$$\left[T^{(0)}\right]_{\xi=0} = 0 \tag{4.72}$$

$$\left[h_O\right]_{\xi=0} = 0 \tag{4.73}$$

An expression for the jump in the gradient of the outer solution h_O can be derived by a single integration of equation (4.59) across the reaction zone, yielding

$$\left[\frac{\partial h_O}{\partial\xi}\right]_{\xi=0} + \frac{l}{q}\left[\frac{\partial T^{(0)}}{\partial\xi}\right]_{\xi=0} = 0 \tag{4.74}$$

The local enthalpy equation corresponding to the fuel species (equation (4.60) + $q\phi$ (4.62)) can be directly integrated to yield the following expression for y_F explicitly in

terms of θ. Upon matching to the burned side, $\zeta \to +\infty$, yields

$$N\frac{\partial\theta}{\partial\zeta} - q\phi S y_F + \alpha\phi N y_F \frac{\partial\theta}{\partial\zeta} = -q\phi S Y_F^{(0)}(0+). \tag{4.75}$$

where

$$S = \frac{u - \mathbf{v}_\perp \cdot \nabla f - f_t}{\sqrt{1 + |\nabla_\perp f|^2}}$$

is the flame speed (justification will be presented shortly) and $\alpha = q\alpha_s/T_a$. Matching to the unburned side, $\zeta \to -\infty$, yields

$$q\phi S\left(Y_F^{(0)}(0+) - Y_F^{(0)}(0-)\right) = -N\left(1 + \alpha\phi Y_F^{(0)}(0-)\right)\frac{\partial T^{(0)}}{\partial\xi}(0-). \tag{4.76}$$

Since temperature gradient is assumed to be small behind the flame, $\partial T^{(0)}/\partial\xi(0+) = 0$, we can now write this in the form of jump condition for the outer solution $Y_F^{(0)}$, namely

$$q\phi S\left[Y_F^{(0)}\right]_{\xi=0} = N\left(1 + \alpha\phi Y_F^{(0)}(0-)\right)\left[\frac{\partial T^{(0)}}{\partial\xi}\right]_{\xi=0}. \tag{4.77}$$

Recall the local enthalpy variable corresponds to the oxidant is

$$q\psi = \theta + q y_O. \tag{4.78}$$

We now solve for y_F and y_O in equation (4.75) and (4.78), respectively, to obtain

$$y_F = \frac{S Y_F^0(0+) + (N/q\phi)\partial\theta/\partial\zeta}{S - (\alpha N/q)\partial\theta/\partial\zeta}, \tag{4.79}$$

and

$$y_O = \frac{q\psi - \theta}{q}. \tag{4.80}$$

These may now be inserted into equation (4.60) to provide a single equation for the local temperature perturbation. Upon making the transformation $\theta \to q\theta$, our

equation takes the form

$$-N^2\frac{\partial^2\theta}{\partial\zeta^2} = \Lambda(\psi-\theta)\left\{\frac{SY_F^{(0)}(0+)+(N/\phi)\partial\theta/\partial\zeta}{S-\alpha N\partial\theta/\partial\zeta}\right\}e^{\theta}. \tag{4.81}$$

Now we can multiply equation (4.81) by $\partial\theta/\partial\zeta$ to obtain the first integral.

$$\frac{\alpha\phi N^2}{2}\left(\frac{\partial\theta}{\partial\zeta}\right)^2 - \phi NS\left(1+\alpha\phi Y_F^{(0)}(0+)\right)\frac{\partial\theta}{\partial\zeta}$$

$$+\phi^2S^2Y_F^{(0)}(0+)\left(1+\alpha\phi Y_F^{(0)}(0+)\right)\ln\left|\phi SY_F^{(0)}(0+)+N\frac{\partial\theta}{\partial\zeta}\right| = \Lambda\Big(\big(\psi-\theta+1\big)e^{\theta}\Big)+\text{const.} \tag{4.82}$$

Matching to the burned side, $\zeta\to+\infty$, yields

$$\phi^2S^2Y_F^{(0)}(0+)\left(1+\alpha\phi Y_F^{(0)}(0+)\right)\ln\left|\phi SY_F^{(0)}(0+)\right| = \Lambda e^{h_O(0+)}+\text{const} \tag{4.83}$$

where $h_O(0+) = T^{(1)}(0+)/q$. Similarly, matching to the unburned side, $\zeta\to-\infty$, gives second expression

$$\frac{\alpha\phi N^2}{2q^2}\left(\frac{\partial T^{(0)}}{\partial\xi}(0-)\right)^2 - \left(1+\alpha\phi Y_F^{(0)}(0+)\right)\frac{\phi NS}{q}\frac{\partial T^{(0)}}{\partial\xi}(0-)$$

$$+\phi^2S^2Y_F^{(0)}(0+)\left(1+\alpha\phi Y_F^{(0)}(0+)\right)\ln\left|\phi SY_F^{(0)}(0+)+\frac{N}{q}\frac{\partial T^{(0)}}{\partial\xi}(0-)\right| = \text{const.} \tag{4.84}$$

The above expressions can now be used to write a jump condition for the outer temperature gradient, namely

$$\frac{\alpha\phi N^2}{2q^2}\left[\left(\frac{\partial T^{(0)}}{\partial\xi}\right)^2\right]_{\xi=0} - \left(1+\alpha\phi Y_F^{(0)}(0+)\right)\frac{\phi NS}{q}\left[\frac{\partial T^{(0)}}{\partial\xi}\right]_{\xi=0}$$

$$-\phi^2S^2Y_F^{(0)}(0+)\left(1+\alpha\phi Y_F^{(0)}(0+)\right)\ln\left|1+\frac{N}{q\phi SY_F^{(0)}(0+)}\frac{\partial T^{(0)}}{\partial\xi}(0-)\right| = \Lambda e^{h_O(0+)}. \tag{4.85}$$

The problem has now been reduced to solving the outer transport equations (4.55) - (4.57) and (4.59) subject to the jump conditions (4.72) - (4.74), (4.77) and

(4.85). In particular, the local analysis has revealed that the temperature $T^{(0)}$ and enthalpy function corresponds to h_O are continuous across the reaction zone, while their gradients suffer a discontinuity. Moreover, the effect of high pressure gives rise to a completely new balance in the reaction zone, namely, a balance between convection, Fickian diffusion, Soret diffusion and reaction has to be achieved. As a result, there is an order one jump in the fuel mass fraction across the reactions zone. The local analysis has also revealed a new jump condition for the fuel species, which has a dependence on the Soret diffusion coefficient α, equivalence ratio ϕ, the flame speed S and also the chemistry. This is a crucial difference from previous models as we will see in the next section. By exploiting the limit of large activation energy, we have essentially replaced the nonlinear reaction rate term that appeared in the original equations by a localized heat source on the flame-front, namely, $\Lambda e^{h_O(0+)}$.

These jump conditions can now be generalized by first considering that all transport processes and chemical reaction are confined to a moving surface

$$F(\mathbf{X}, t) = x - f(y, z, t) = 0. \tag{4.86}$$

called the flame front, separating the unburned mixture $F < 0$ from the burned mixture $F > 0$. On the surface

$$\frac{dF}{dt} = F_t + \nabla F \cdot \frac{d\mathbf{X}}{dt} = 0 \tag{4.87}$$

where $d\mathbf{X}/dt$ is the velocity of the surface. The unit surface normal to the flame front pointing toward the burned mixture is given by

$$\mathbf{n} = \frac{\nabla F}{|\nabla F|} = \frac{(1, -f_y, -f_z)}{\sqrt{1 + |\nabla_\perp f|^2}}, \tag{4.88}$$

and thus the normal velocity of the surface is given by

$$\frac{d\mathbf{X}}{dt} \cdot \mathbf{n} = -\frac{F_t}{|\nabla F|} = \frac{f_t}{\sqrt{1 + |\nabla_\perp f|^2}}. \tag{4.89}$$

We can now write the flame speed

$$S = \mathbf{V}\cdot\mathbf{n} + \frac{F_t}{|\nabla F|} = \frac{u - \mathbf{v}_\perp\cdot\nabla f - f_t}{\sqrt{1+|\nabla_\perp f|^2}} \tag{4.90}$$

where $\mathbf{V}$ is evaluated just ahead of the flame front, i.e., at $x = f(-)$. The normal derivative in terms of the transformed coordinate ξ is given by

$$\frac{\partial}{\partial\mathbf{n}} = \mathbf{n}\cdot\nabla = N\frac{\partial}{\partial\xi} - N^{-1}\left(f_y\frac{\partial}{\partial y} + f_z\frac{\partial}{\partial z}\right). \tag{4.91}$$

where the surface normal $N = \sqrt{1+|\nabla_\perp f|^2} = |\nabla F|$ can be written in terms of the surface F. Since there are no jumps in the transverse components, y and z, directions it follows that

$$N\left[\frac{\partial}{\partial\xi}\right] = \left[\frac{\partial}{\partial\mathbf{n}}\right]. \tag{4.92}$$

Thus our jump conditions can be written in the generalized coordinate-free form

$$\left[T^{(0)}\right] = 0, \tag{4.93}$$

$$\left[h_O\right] = 0, \tag{4.94}$$

$$\left[\frac{\partial h_O}{\partial\mathbf{n}}\right] + \frac{l}{q}\left[\frac{\partial T^{(0)}}{\partial\mathbf{n}}\right] = 0, \tag{4.95}$$

$$q\phi S\left[Y_F^{(0)}\right] = \left(1+\alpha\phi Y_F^{(0)}(-)\right)\left[\frac{\partial T^{(0)}}{\partial\mathbf{n}}\right], \tag{4.96}$$

$$\frac{\alpha\phi}{2q^2}\left[\left(\frac{\partial T^{(0)}}{\partial\mathbf{n}}\right)^2\right] - \left(1+\alpha\phi Y_F^{(0)}(+)\right)\frac{\phi S}{q}\left[\frac{\partial T^{(0)}}{\partial\mathbf{n}}\right]$$

$$-\phi^2 S^2 Y_F^{(0)}(+)\left(1+\alpha\phi Y_F^{(0)}(+)\right)\ln\left|1+\frac{1}{q\phi S Y_F^{(0)}(+)}\frac{\partial T^{(0)}}{\partial\mathbf{n}}(-)\right| = \Lambda e^{h_O(+)}. \tag{4.97}$$

Here we use the notation $(-)$ and $(+)$ to denote the location ahead and behind the flame front.

4.5 Diffusional-Thermal Instability of Planar Flames in High Density Fluids

Although we have succeeded in simplifying the nonlinear reaction rate terms appearing in the original governing equations, solutions of the resulting model are still difficult to obtain due to the coupling of the hydrodynamics and transport processes. We can assume the density changes across the flame are small, and thus the temperature and mass transport equations are decoupled from the hydrodynamics equations. This is a rather crude approximation from a physical standpoint, but it has been proven to be useful to gain qualitative insights in theoretical combustion. In this way we can study the effect of the flow field on the flame, but the effect of the flame on the flow field is suppressed.

When the constant density approximation is adopted. It is common to consider weak thermal expansion $q \ll 1$. We introduce the expansion

$$T^{(0)} = 1 + q\tau + \cdots,$$

$$\rho^{(0)} = 1 + qR^o + \cdots,$$

$$Y_F^{(0)} = y_f,$$

$$h_O = h_o.$$

which are inserted into equations (4.55) - (4.57) and (4.59) and jump conditions (4.93) - (4.97) to yeild

$$\frac{\partial \tau}{\partial t} + \mathbf{V} \cdot \nabla \tau - \nabla^2 \tau = 0, \qquad F < 0, \tag{4.98}$$

$$\tau = 1, \qquad F > 0, \tag{4.99}$$

$$\frac{\partial h_o}{\partial t} + \mathbf{V}\cdot\nabla h_o - \nabla^2 h_o = l\nabla^2\tau, \qquad F \neq 0, \tag{4.100}$$

$$\frac{\partial y_f}{\partial t} + \mathbf{V}\cdot\nabla y_f - \alpha\nabla\cdot(y_f\nabla\tau) = 0, \qquad F \neq 0, \tag{4.101}$$

$$\Big[\tau\Big] = 0, \tag{4.102}$$

$$\Big[h_o\Big] = 0, \tag{4.103}$$

$$\left[\frac{\partial h_o}{\partial \mathbf{n}}\right] + l\left[\frac{\partial \tau}{\partial \mathbf{n}}\right] = 0, \tag{4.104}$$

$$\phi S\Big[y_f\Big] = (1+\alpha\phi y_f(-))\left[\frac{\partial\tau}{\partial\mathbf{n}}\right], \tag{4.105}$$

$$\frac{\alpha\phi}{2}\left[\left(\frac{\partial\tau}{\partial\mathbf{n}}\right)^2\right] - (1+\alpha\phi y_f(+))\,\phi S\left[\frac{\partial\tau}{\partial\mathbf{n}}\right]$$

$$-\phi^2 S^2 y_f(+)\,(1+\alpha\phi y_f(+))\ln\left|1+\frac{1}{\phi S y_f(+)}\frac{\partial\tau}{\partial\mathbf{n}}(-)\right| = \Lambda e^{h_o(+)} \tag{4.106}$$

where $S = \frac{F_t}{|\nabla F|} + \mathbf{V}\cdot\mathbf{n}$.

This model will now be used to study the dynamic behavior of a planar flame in a uniform flow field and assuming stoichiometric condition $\phi = 1$. Thus, under such condition, by equation (4.41), we deduce that $y_f(0+) = Y_F^{(0+)} = 1 - 1/\phi = 0$. In addition, the last two jump conditions are now simplified and are given by

$$S\Big[y_f\Big] = (1+\alpha y_f(-))\left[\frac{\partial\tau}{\partial\mathbf{n}}\right], \tag{4.107}$$

$$\frac{\alpha}{2}\left[\left(\frac{\partial\tau}{\partial\mathbf{n}}\right)^2\right] - S\left[\frac{\partial\tau}{\partial\mathbf{n}}\right] = \Lambda e^{h_o(+)}. \tag{4.108}$$

With the prescribed flow field $\mathbf{V} = (1, 0, 0)$, we deduce the flame speed $S = (1 - f_t)/N$, a steady one dimensional solution of the above system is given by

$$f^s = 0, \tag{4.109}$$

$$\tau^s = \begin{cases} e^x, & x < 0 \\ 1, & x > 0 \end{cases}, \tag{4.110}$$

$$h_o^s = \begin{cases} -lxe^x, & x < 0 \\ 0, & x > 0 \end{cases}, \tag{4.111}$$

$$y_f^s = \begin{cases} (1 - \alpha e^x)^{-1}, & x < 0 \\ 0, & x > 0 \end{cases}. \tag{4.112}$$

We now suppose that the steady, planar flame are slightly perturbed such that the solutions are written as the sum of the steady basic solution and the infinitesimal disturbance:

$$f = f^s + \epsilon\tilde{f}, \tag{4.113}$$

$$\tau = \tau^s + \epsilon\tilde{\chi}, \tag{4.114}$$

$$h_o = h_o^s + \epsilon\tilde{\psi}, \tag{4.115}$$

$$y_f = y_f^s + \epsilon\tilde{\vartheta}, \tag{4.116}$$

where ϵ is a small parameter. Solutions of the perturbed quantities are sought in the normal mode form

$$\tilde{\chi} = \chi(x)exp(ik_1y + ik_2z + \omega t), \tag{4.117}$$

$$\tilde{\psi} = \psi(x) exp(ik_1 y + ik_2 z + \omega t), \tag{4.118}$$

$$\tilde{\vartheta} = \vartheta(x) exp(ik_1 y + ik_2 z + \omega t), \tag{4.119}$$

$$\tilde{f} = A exp(ik_1 y + ik_2 z + \omega t), \tag{4.120}$$

where ω is the complex growth rate and $k = \sqrt{k_1^2 + k_2^2}$ is the wavenumber of the disturbance. If there are any values of ω having positive real part for any k, then the perturbation will grow in time, and the steady flame structure is unstable. The expressions (4.117) - (4.120) are then inserted into equations (4.98) - (4.104), (4.107) and (4.108). The resulting linearized system are

$$\chi'' - \chi' - (\omega + k^2)\chi = 0, \qquad x < 0, \tag{4.121}$$

$$\chi \equiv 0, \qquad x > 0, \tag{4.122}$$

$$\psi'' - \psi' - (\omega + k^2)\psi = -l(\chi'' - k^2\chi), \qquad x \neq 0, \tag{4.123}$$

$$\vartheta' + \left(\frac{\omega - \alpha e^x}{1 - \alpha e^x}\right)\vartheta = \left(\frac{\alpha^2 e^x}{(1 - \alpha e^x)^3}\right)\chi' + \left(\frac{\alpha}{(1 - \alpha e^x)^2}\right)(\chi'' - k^2\chi), \qquad x < 0, \tag{4.124}$$

$$\vartheta \equiv 0, \qquad x > 0, \tag{4.125}$$

$$\big[\chi\big] = A, \tag{4.126}$$

$$\big[\psi\big] = -lA, \tag{4.127}$$

$$l\big[\chi'\big] + \big[\psi'\big] = -lA, \tag{4.128}$$

$$\frac{\partial \tilde{f}}{\partial t} = -(1 - \alpha)\tilde{f} - \tilde{\chi}'(0-) + (1 - \alpha)^2\tilde{\vartheta}(0-), \tag{4.129}$$

$$(2-\alpha)\left[\chi'\right] + \Lambda\psi(0+) + (1-\alpha)^2\vartheta(0-) = 2A(1-\alpha). \tag{4.130}$$

where $\Lambda = 1-\alpha/2$. Here the jump conditions are to be evaluated at the unperturbed location $x = 0$. We seek solution with $Re(\omega) > 0$, and boundedness is imposed at $x \to \pm\infty$.

The solution of the above linearized system is given by

$$\chi = \begin{cases} c_1 e^{r_1 x}, & x < 0 \\ 0, & x > 0 \end{cases}, \tag{4.131}$$

$$\psi = \begin{cases} c_2 e^{r_1 x} + lA(r_1^2 - k^2)(r_1 - r_2)^{-1} x e^{r_1 x}, & x < 0 \\ c_3 e^{r_2 x}, & x > 0 \end{cases}, \tag{4.132}$$

$$\vartheta = \begin{cases} -Ae^{-x}(e^{-x} - \alpha)^{\omega-1}(I_1 + I_2), & x < 0 \\ 0, & x > 0 \end{cases} \tag{4.133}$$

where I_1 and I_2 are

$$I_1 = \alpha^2 r_1 \int_{-\infty}^{x} e^{(r_1-1)x'}(e^{-x'} - \alpha)^{-\omega-2} dx', \tag{4.134}$$

$$I_2 = \alpha(r_1^2 - k^2) \int_{-\infty}^{x} e^{(r_1-1)x'}(e^{-x'} - \alpha)^{-\omega-1} dx', \tag{4.135}$$

respectively, and r_1 and r_2 are given by

$$r_{1,2} = \frac{1}{2}\left(1 \pm \sqrt{1 + 4(\omega + k^2)}\right) \tag{4.136}$$

such that $Re(r_1) > 0$ and $Re(r_2) < 0$. The constants can be determined by applying the jump conditions (4.126), (4.127), and (4.128) to yield:

$$c_1 = -A, \tag{4.137}$$

$$c_2 = c_3 + lA, \tag{4.138}$$

$$c_3 = lA\,(r_1 - r_2)^{-2}\left(r_1 - r_2 - r_1^2 + k^2\right), \tag{4.139}$$

and by applying jump condition (4.130) yields the last relation to determine the growth rate

$$c_3 = \frac{2}{2-\alpha}\Big\{2A(1-\alpha) - (1-\alpha)^2\vartheta(0-)\Big\} - 2Ar_1. \tag{4.140}$$

Manipulating equations (4.139) – (4.140) leads to a cubic integro-algebraic dispersion relation for the growth rate ω:

$$64\omega^3 + \Big\{192k^2 + 32 + 8l - l^2 + 16(1-\Gamma)(l+4\Gamma)\Big\}\omega^2$$

$$+\Big\{2(2+8k^2+l)(1+12k^2) + (1-\Gamma)\big\{4l(3+4k^2) + 32\Gamma(1+4k^2)\big\}\Big\}\omega$$

$$+(2+8k^2+l)^2k^2 + (1-\Gamma)\big\{2l(1+4k^2) + \Gamma(2+8k^2)^2\big\} = 0, \tag{4.141}$$

where

$$\Gamma = \frac{1-\alpha}{2-\alpha}\Big\{2 + (1-\alpha)^{\omega}\big(I_1(0-) + I_2(0-)\big)\Big\}.$$

In general, for nonzero α, this integro-algebraic equation must be computed numerically. However, the limiting case, $\alpha = 0$ ($\Gamma = 1$) yields the following explicit relation for ω:

$$64\omega^3 + \Big\{192k^2 + 32 + 8l - l^2\Big\}\omega^2 + \Big\{2(2+8k^2+l)(1+12k^2)\Big\}\omega$$

$$+(2+8k^2+l)^2k^2 = 0. \tag{4.142}$$

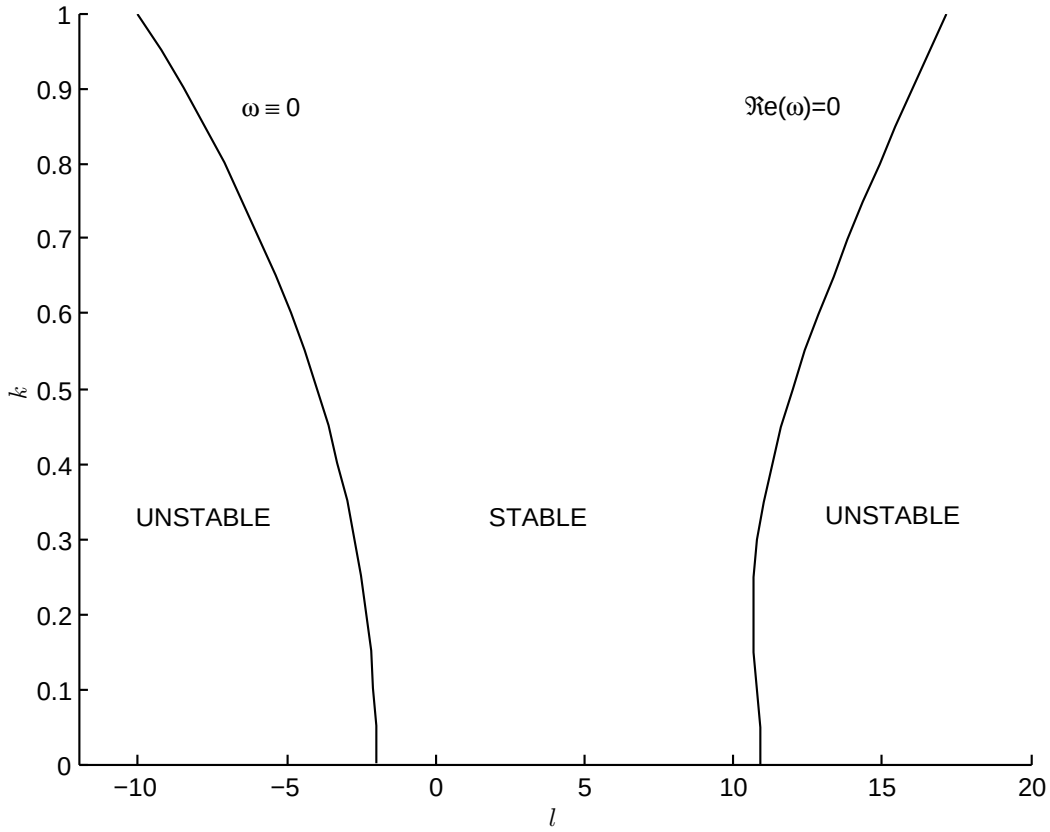

Figure 4.4 Neutral stability boundaries for $\alpha = 0$.

This is the diffusion-less limit in which fuel is transported through the flame by convection only. Thus it is the same as previous expressions derived for diffusional-thermal model [46].

The neutral stability boundaries of the above dispersion relation, determined by setting $Re(\omega) = 0$ when $\alpha = 0$, are shown in Figure 4.4. There exists a range of Lewis number

$$-2 < l < 4(1 + \sqrt{3}) \tag{4.143}$$

for which planar flames are stable to disturbances of all wavelength. The left boundary is given by $l = -2 - 8k^2$, and it is commonly referred to as the cellular boundary because $Im(\omega) = 0$ as well. As l decreased below -2 the plane flame will lose stability to a stationary cellular structure. Along the right stability boundary, $Im(\omega) \neq 0$, and thus the planar flame will lose stability to pulsations or traveling waves.

Stability boundaries computed for several specified values of $\alpha \leq 0$ are shown in Figures 4.5 and 4.6. We can see from Figure 4.5, the general shape of both neutral stability curves are the same and do not appear to differ very much for small negative values of α ($\alpha \ll 1$ and $\alpha < 0$). We note that both boundaries slowly shift to the right as the value of α decreases. In addition, it is worth mentioning that for sufficiently large negative values of α, the cellular branch can be extended into the regime of $Le_O > 1$ as shown in Figure 4.6. We note that light fuels, e.g., hydrogen typically has values of $\alpha < 0$, and the present theory suggests that cellular instability may be observed even when $Le_O > 1$.

Figure 4.7 shows similar stability boundaries as in Figures 4.5 and 4.6, but for values of $\alpha \geq 0$. Similarly, for small positive α ($\alpha \ll 1$ and $\alpha > 0$), both boundaries are relatively immobile and the general shape holds the same shape as $\alpha = 0$. We note that both boundaries also shift to the right as the value of α increases. However, the cellular boundary cannot cross the $k-$axis, suggesting cellular instability can only

be observed for $Le_O < 1$. We will now carry out a nonlinear analysis to trace the evolution from planar to cellular flames as the left stability is crossed.

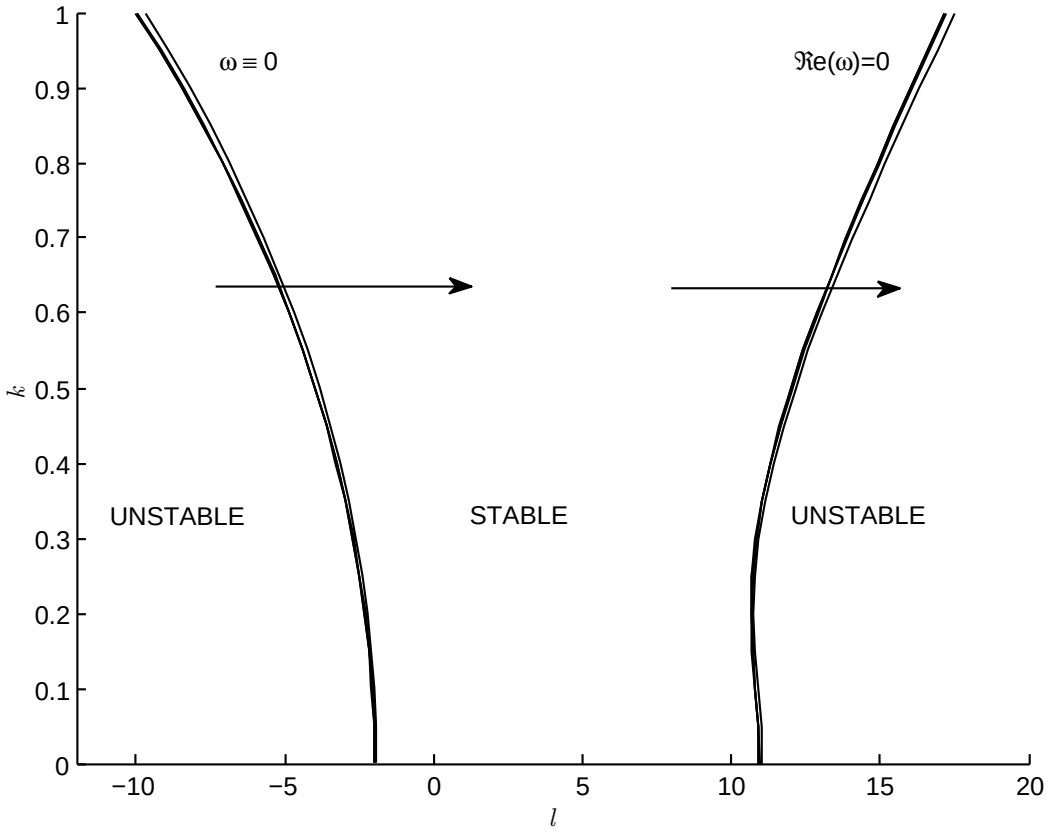

Figure 4.5 Neutral stability boundaries for $\alpha \leq 0$, $\alpha = 0$, -0.1, -0.2 and -0.5. The arrows indicate decreasing values of α.

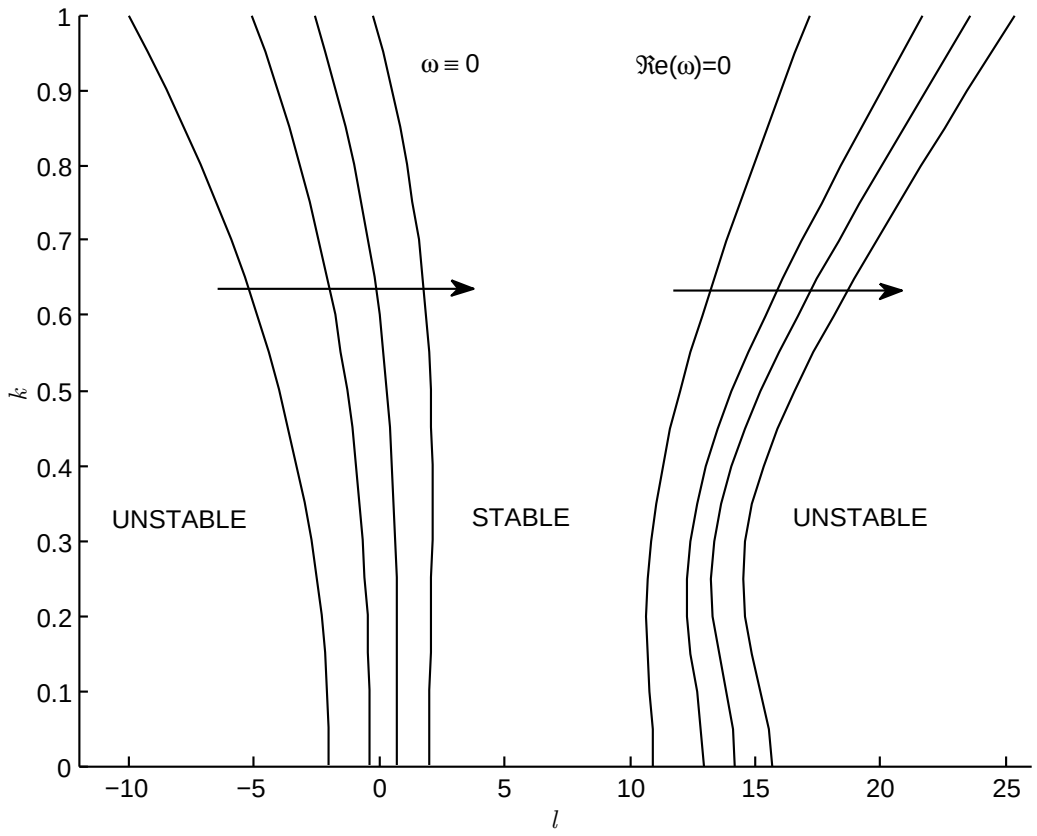

Figure 4.6 Neutral stability boundaries for $\alpha \leq 0$, $\alpha = 0$, -5, -10 and -20. The arrows indicate decreasing values of α.

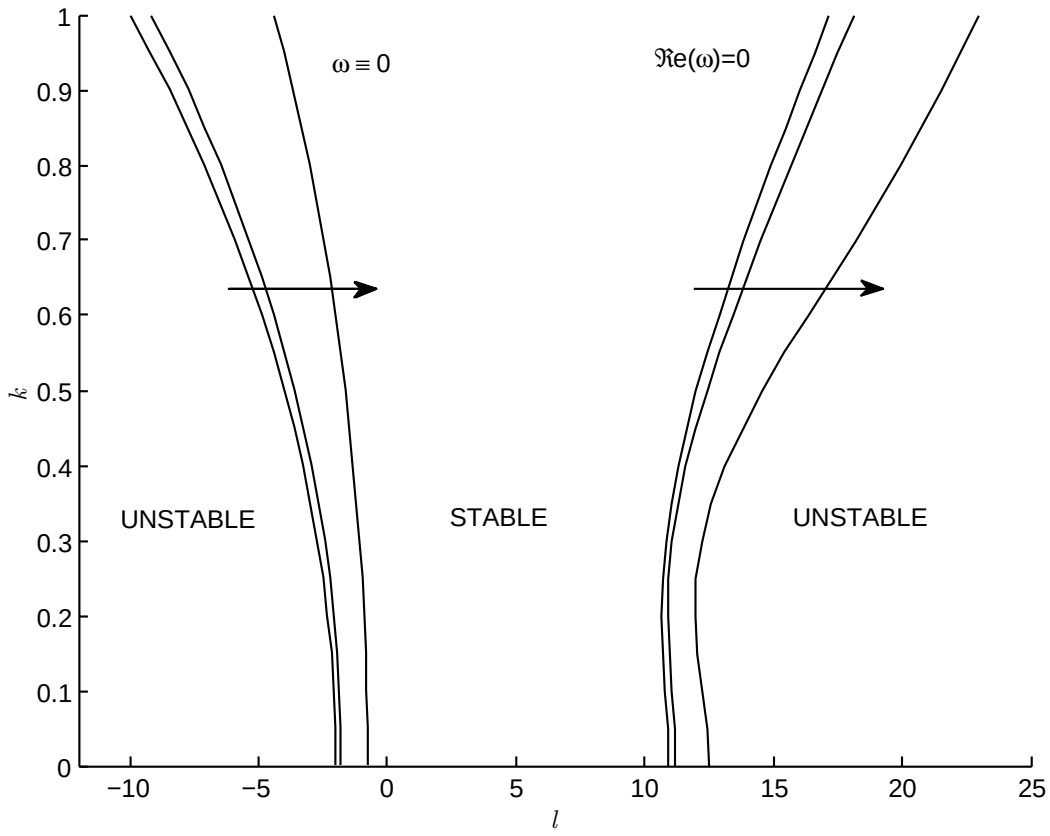

Figure 4.7 Neutral stability boundaries for $\alpha \geq 0$, $\alpha = 0$, 0.1 and 0.9. The arrows indicate increasing values of α.

4.6 Evolution Equation for the Perturbed Flame Front in High Density Fluids

In this section, we will derive a nonlinear partial differential equation that describes the evolution of the flame front in the vicinity of the cellular stability boundary. For simplicity we will first consider the planar flame in two-dimension. The linear stability analysis revealed that the flame first lose stability to long-wave disturbances ($k \to 0$) at $l = l_c$.

We first define a small parameter ϵ by

$$\epsilon = (l - l_c)/l_c. \tag{4.144}$$

Along the cellular boundary we have the relation

$$(2 + 8k^2 + l)^2 k^2 + (1 - \Gamma)\big\{2l(1 + 4k^2) + \Gamma(2 + 8k^2)^2\big\} = 0 \tag{4.145}$$

where

$$\Gamma = \frac{1 - \alpha}{2 - \alpha}\Big\{2 + (1 - \alpha)^{\omega}\big(I_1(0-) + I_2(0-)\big)\Big\},$$

and it follows that

$$k^2 \sim l - l_c = O(\epsilon) \tag{4.146}$$

where

$$l_c = -\frac{2(1 - \alpha)}{2 - \alpha}\big(2 - \ln(1 - \alpha)\big). \tag{4.147}$$

Let us assume that the characteristic amplitude of the disturbed flame front is of $O(\epsilon)$,

$$F = \epsilon f.$$

Equation (4.146) suggests that we introduce scaled variable for the time and spatial variable as

$$t_1 = \epsilon^2 t, \qquad \eta = \sqrt{\epsilon} y.$$

Solutions of all quantities are sought in the form of a power series in ϵ, i.e.

$$f = f^s + \epsilon(F^0 + F^1 + \cdots), \tag{4.148}$$

$$\tau = \tau^s + \epsilon^2(\chi^0 + \chi^1 + \cdots), \tag{4.149}$$

$$h = h_o^s + \epsilon^2(\psi^0 + \psi^1 + \cdots), \tag{4.150}$$

$$y = y_f^s + \epsilon^2(\vartheta^0 + \vartheta^1 + \cdots), \tag{4.151}$$

where the steady state solutions are given by equations (4.109) - (4.112). It is convenient to adopt a coordinate system attached to the flame front by introducing

$$\xi = x - f(\eta, t_1), \qquad \eta = \eta, \qquad t_1 = t_1.$$

The above expressions are inserted into equations (4.98) - (4.104), (4.107), and (4.108) and expanded for small ϵ to yield systems of equations to be solved at each order.

At $O(\epsilon^2)$, the appropriate system has the form

$$\frac{\partial \chi^0}{\partial \xi} - \frac{\partial^2 \chi^0}{\partial \xi^2} = -F_{\eta\eta}^0 \frac{d\tau^s}{d\xi}, \qquad \xi < 0, \tag{4.152}$$

$$\chi^0 = 0, \qquad \xi > 0, \tag{4.153}$$

$$\frac{\partial \psi^0}{\partial \xi} - \frac{\partial^2 \psi^0}{\partial \xi^2} = l_c \frac{\partial^2 \chi^0}{\partial \xi^2} - l_c F_{\eta\eta}^0 \frac{d\tau^s}{d\xi} - F_{\eta\eta}^0 \frac{dh_o^s}{d\xi}, \qquad \xi < 0, \tag{4.154}$$

$$\frac{\partial \psi^0}{\partial \xi} - \frac{\partial^2 \psi^0}{\partial \xi^2} = 0, \qquad \xi > 0, \tag{4.155}$$

$$\frac{\partial}{\partial\xi}\left(\left(1-\alpha\frac{d\tau^s}{d\xi}\right)\vartheta^0\right)=\alpha\left\{\frac{\partial}{\partial\xi}\left(y_f^s\frac{\partial\chi^0}{\partial\xi}\right)-F^0_{\eta\eta}y_f^s\frac{d\tau^s}{d\xi}\right\},\qquad \xi<0, \tag{4.156}$$

$$\vartheta^0=0,\qquad \xi>0, \tag{4.157}$$

At $\xi=0$, the following jump conditions must be satisfied:

$$\left[\chi^0\right]=0, \tag{4.158}$$

$$\left[\psi^0\right]=0, \tag{4.159}$$

$$l_c\left[\frac{\partial\chi^0}{\partial\xi}\right]+\left[\frac{\partial\psi^0}{\partial\xi}\right]=0, \tag{4.160}$$

$$2\left[\frac{\partial\chi^0}{\partial\xi}\right]+\psi^0(0+)+\Lambda^{-1}(1-\alpha)^2\vartheta^0(0-)=0 \tag{4.161}$$

where $\Lambda=(2-\alpha)/2$. The perturbation quantities χ^0,ψ^0 and ϑ^0 must vanish as $\xi\to-\infty$ and must be bounded as $\xi\to+\infty$. Hence

$$\chi^0\to 0;\qquad \psi^0\to 0;\qquad \vartheta^0\to 0,\qquad\qquad \xi\to-\infty, \tag{4.162}$$

$$\chi^0,\ \ \psi^0,\ \ \vartheta^0\qquad \text{bounded},\qquad\qquad \xi\to+\infty. \tag{4.163}$$

The solution of the $O(\epsilon^2)$ system is given by

$$\chi^0=\begin{cases} F^0_{\eta\eta}\xi e^{\xi}, & \xi<0\\ 0, & \xi>0\end{cases}, \tag{4.164}$$

$$\psi^0=\begin{cases} -l_cF^0_{\eta\eta}(1+\xi^2)e^{\xi}, & \xi<0\\ -l_cF^0_{\eta\eta}, & \xi>0\end{cases}, \tag{4.165}$$

$$\vartheta^0 = \begin{cases} F^0_{\eta\eta}\Big(\alpha(1-\alpha e^{\xi})^{-2}(1+\xi)e^{\xi} + (1-\alpha e^{\xi})^{-1}\ln(1-\alpha e^{\xi})\Big), & \xi < 0 \\ 0, & \xi > 0 \end{cases}. \tag{4.166}$$

The above solution clearly is a function of the perturbed flame front location F^0 and the modified Soret diffusion coefficient α. However, we have yet to determine an equation for the perturbed flame front F^0. In order to do this, it is necessary to go to the next order in our perturbation scheme.

The next order, $O(\epsilon^3)$ system is simply an inhomogeneous form of the $O(\epsilon^2)$ system and has the form

$$\frac{\partial \chi^1}{\partial \xi} - \frac{\partial^2 \chi^1}{\partial \xi^2} = \frac{\partial^2 \chi^0}{\partial \eta^2} + \Big(F^0_{t_1} + (F^0_{\eta})^2 - F^1_{\eta\eta}\Big)\frac{d\tau^s}{d\xi}, \qquad \xi < 0, \tag{4.167}$$

$$\chi^1 = 0, \qquad \xi > 0, \tag{4.168}$$

$$\frac{\partial \psi^1}{\partial \xi} - \frac{\partial^2 \psi^1}{\partial \xi^2} = l_c\frac{\partial^2 \chi^1}{\partial \xi^2} + l_c\frac{\partial^2 \chi^0}{\partial \xi^2} + l_c\frac{\partial^2 \chi^0}{\partial \eta^2} + \frac{\partial^2 \psi^0}{\partial \eta^2} - l_c\Big(F^0_{t_1} + (F^0_{\eta})^2\Big)e^{\xi}$$

$$-l_c\Big(F^0_{t_1} + (F^0_{\eta})^2 - F^0_{\eta\eta} - F^1_{\eta\eta}\Big)\xi e^{\xi}, \qquad \xi < 0, \tag{4.169}$$

$$\frac{\partial \psi^1}{\partial \xi} - \frac{\partial^2 \psi^1}{\partial \xi^2} = \frac{\partial^2 \psi^0}{\partial \eta^2}, \qquad \xi > 0, \tag{4.170}$$

$$\frac{\partial}{\partial \xi}\left(\Big(1 - \alpha\frac{d\tau^s}{d\xi}\Big)\vartheta^1\right) = F^0_{t_1}\frac{dy^s_f}{d\xi} + \alpha\Bigg\{\frac{\partial}{\partial \xi}\left(y^s_f\frac{\partial \chi^1}{\partial \xi}\right) + y^s_f\frac{\partial^2 \chi^0}{\partial \eta^2}$$

$$-F^1_{\eta\eta}y^s_f\frac{d\tau^s}{d\xi} + (F^0_{\eta})^2\frac{\partial}{\partial \xi}\Big(y^s_f\frac{d\tau^s}{d\xi}\Big)\Bigg\}, \qquad \xi < 0, \tag{4.171}$$

$$\vartheta^1 = 0, \qquad \xi > 0, \tag{4.172}$$

At $\xi = 0$, the following jump conditions must hold:

$$\big[\chi^1\big] = 0, \tag{4.173}$$

$$\left[\psi^1\right] = 0, \tag{4.174}$$

$$l_c\left[\frac{\partial \chi^1}{\partial \xi}\right] + \left[\frac{\partial \psi^1}{\partial \xi}\right] = -l_c\left[\frac{\partial \chi^0}{\partial \xi}\right], \tag{4.175}$$

$$2\left[\frac{\partial \chi^1}{\partial \xi}\right] + \psi^1(0+) + \Lambda^{-1}(1-\alpha)^2\vartheta^1(0-) = (F^0_\eta)^2. \tag{4.176}$$

The perturbation quantities χ^1, ψ^1 and ϑ^1 must vanish as $\xi \to -\infty$. Hence

$$\chi^1 \to 0; \qquad \psi^1 \to 0; \qquad \vartheta^1 \to 0, \qquad\qquad \xi \to -\infty. \tag{4.177}$$

The solution of the $O(\epsilon^3)$ system is given by

$$\chi^1 = \begin{cases} -\Big(F^0_{t_1} + (F^0_\eta)^2 - F^0_{\eta\eta\eta\eta} - F^1_{\eta\eta}\Big)\xi e^\xi - \frac{1}{2}F^0_{\eta\eta\eta\eta}\xi^2 e^\xi, & \xi < 0 \\ 0, & \xi > 0 \end{cases}, \tag{4.178}$$

$$\psi^1 = \begin{cases} -l_c\Big(F^0_{\eta\eta} + 5F^0_{\eta\eta\eta\eta} + F^1_{\eta\eta}\Big)e^\xi + l_c\Big(F^0_{t_1} + (F^0_\eta)^2 + 3F^0_{\eta\eta\eta\eta}\Big)\xi e^\xi \\ +l_c\Big(F^0_{t_1} + (F^0_\eta)^2 - F^0_{\eta\eta} - \frac{3}{2}F^0_{\eta\eta\eta\eta} - F^1_{\eta\eta}\Big)\xi^2 e^\xi \\ +\frac{1}{2}l_c F^0_{\eta\eta\eta\eta}\xi^3 e^\xi, & \xi < 0 \\ -l_c\Big(F^0_{\eta\eta} + 5F^0_{\eta\eta\eta\eta} + F^1_{\eta\eta}\Big) - l_c F^0_{\eta\eta\eta\eta}\xi, & \xi > 0 \end{cases}, \tag{4.179}$$

$$\vartheta^1 = \begin{cases} \alpha(1-\alpha e^\xi)^{-2}\Big(\big(F^0_{\eta\eta\eta\eta} + F^1_{\eta\eta}\big)e^\xi - \big(F^0_{t_1} + (F^0_\eta)^2 - F^1_{\eta\eta}\big)\xi e^\xi - \frac{1}{2}F^0_{\eta\eta\eta\eta}\xi^2 e^\xi\Big) \\ +(1-\alpha e^\xi)^{-1}\Big(F^0_{\eta\eta\eta\eta}\int_{-\infty}^{\xi}\ln(1-\alpha e^{\bar\xi})d\bar\xi + F^1_{\eta\eta}\ln(1-\alpha e^\xi)\Big), & \xi < 0 \\ 0, & \xi > 0 \end{cases} \cdot \tag{4.180}$$

Nontrivial solutions exist provided that the flame front location F^0 satisfies the partial differential equation

$$F^0_{t_1} + \mathcal{B}F^0_{\eta\eta} + \mathcal{C}F^0_{\eta\eta\eta\eta} + \frac{1}{2}(F^0_\eta)^2 = 0 \tag{4.181}$$

where

$$\mathcal{B} = -\frac{l_c}{2}, \tag{4.182}$$

and

$$\mathcal{C} = -1 - \frac{5l_c}{2} + \alpha(2-\alpha)^{-1} + (1-\alpha)(2-\alpha)^{-1}\int_{-\infty}^{0} \ln(1-\alpha e^{\bar{\xi}})d\bar{\xi}. \tag{4.183}$$

The above equation can be generalized to three-dimensional

$$F^0_{t_1} + \mathcal{B}\nabla^2 F^0 + \mathcal{C}\nabla^4 F^0 + \frac{1}{2}|\nabla F^0|^2 = 0. \tag{4.184}$$

We note that for the particular case, $\alpha = 0$ ($\mathcal{B} = 1$ and $\mathcal{C} = 4$), we recovered the Kuramoto-Sivashinsky (K-S) equation.

The coefficients $\mathcal{B}$ and $\mathcal{C}$ in equation (4.184) as a function of the modified Soret diffusion coefficient, α, as determined from equation (4.182) and (4.183) is shown in Figure 4.8. We note the solutions in the previous chapter are valid for $-\infty < \alpha < 1$. Without losing the capability to capture all the information, curves are only shown for Soret coefficients in the range $-20 < \alpha < 1$. We observe that both coefficients $\mathcal{B}$ and $\mathcal{C}$ are positive in the range $\alpha_{c_1} \equiv -6.389056 < \alpha < 1$ and approach zero as $\alpha \to 1$. Therefore, when $\alpha = 1$ equation (4.184) reduces to

$$F^0_{t_1} + \frac{1}{2}|\nabla F^0|^2 = 0. \tag{4.185}$$

When $\alpha = 0$, Soret effects are absent, and both coefficients $\mathcal{B}$ and $\mathcal{C}$ achieve their maximum value, 1 and 4, respectively. Thus, we recovered the K-S equation, namely,

$$F^0_{t_1} + \nabla^2 F^0 + 4\nabla^4 F^0 + \frac{1}{2}|\nabla F^0|^2 = 0. \tag{4.186}$$

When $\alpha = \alpha_{c_1}$, $\mathcal{B} \approx 0$ and $\mathcal{C}_c \equiv \mathcal{C} \approx 1.069194$. Hence, equation (4.184) reduces to

$$F^0_{t_1} + \mathcal{C}_c\nabla^4 F^0 + \frac{1}{2}|\nabla F^0|^2 = 0. \tag{4.187}$$

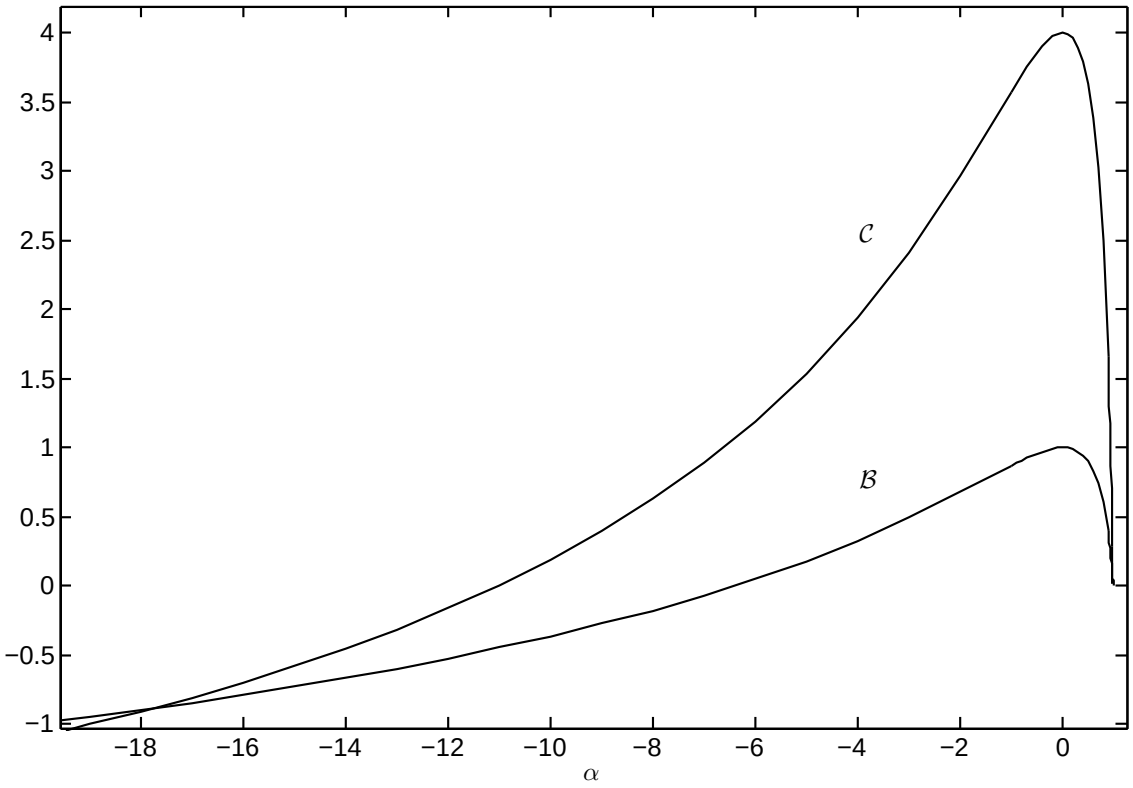

Figure 4.8 The coefficients $\mathcal{B}$ and $\mathcal{C}$ in equation (4.184) as a function of the modified Soret diffusion coefficient, α, as determined from equations (4.182) and (4.183).

We also observe that coefficient $\mathcal{B}$ is negative while $\mathcal{C}$ is positive in the range $\alpha_{c_2} \equiv -11.033770 < \alpha < \alpha_{c_1}$. When $\alpha = \alpha_{c_2}$, $\mathcal{B}_c \equiv \mathcal{B} \approx -0.450297$ and $\mathcal{C} \approx 0$. Consequently, equation (4.184) reduces to

$$F^0_{t_1} + \mathcal{B}_c \nabla^2 F^0 + \frac{1}{2}|\nabla F^0|^2 = 0. \tag{4.188}$$

Finally, in the range $-\infty < \alpha < \alpha_{c_2}$, both coefficients $\mathcal{B}$ and $\mathcal{C}$ are negative.

We have shown there to be eight somewhat different cases depending on the value of the parameter α in equation (4.184). Table 4.1 summarizes the coefficients $\mathcal{B}$ and $\mathcal{C}$, and the evolution equation for the perturbed flame front F^0 and its order for these cases.

In some sense there actually are only three cases: if $\alpha_{c_1} \leq \alpha \leq 1$, both coefficients $\mathcal{B}$ and $\mathcal{C}$ are nonnegative; if $\alpha_{c_2} \leq \alpha < \alpha_{c_1}$, coefficient $\mathcal{B}$ is negative and coefficient $\mathcal{C}$ is nonnegative; and if $-\infty < \alpha < \alpha_{c_2}$, both coefficients $\mathcal{B}$ and $\mathcal{C}$ are negative. Furthermore, we note that the evolution equation for the flame front is fourth-order in the range: $-\infty < \alpha < \alpha_{c_2}$ and $\alpha_{c_2} < \alpha < 1$. It is also worth mentioning that the order of the flame front equation is reduced for two particular choice of α, namely, it reduces to first-order and second-order when $\alpha = 1$ and $\alpha = \alpha_{c_2}$, respectively.

Table 4.1 The Coefficients $\mathcal{B}$ and $\mathcal{C}$, the Evolution Equation for the Flame Front F^0 and its Order, for Soret Diffusion Coefficient in the Range $-\infty < \alpha < 1$ ($\alpha_{c_1} = -6.389056$, $\alpha_{c_2} = -11.033770$, $\mathcal{B}_c = -0.450297$ and $\mathcal{C}_c = 1.069194$).

α	$\mathcal{B}$	$\mathcal{C}$	Evolution Equation for the Flame Front	Order
1	0	0	$F^0_{t_1} + \lvert\nabla F^0\rvert^2/2 = 0$	1
$0 < \alpha < 1$	positive	positive	$F^0_{t_1} + \mathcal{B}\nabla^2 F^0 + \mathcal{C}\nabla^4 F^0 + \lvert\nabla F^0\rvert^2/2 = 0$	4
0	1	4	$F^0_{t_1} + \nabla^2 F^0 + 4\nabla^4 F^0 + \lvert\nabla F^0\rvert^2/2 = 0$	4
$\alpha_{c_1} < \alpha < 0$	positive	positive	$F^0_{t_1} + \mathcal{B}\nabla^2 F^0 + \mathcal{C}\nabla^4 F^0 + \lvert\nabla F^0\rvert^2/2 = 0$	4
α_{c_1}	0	$\mathcal{C}_c$	$F^0_{t_1} + \mathcal{C}_c\nabla^4 F^0 + \lvert\nabla F^0\rvert^2/2 = 0$	4
$\alpha_{c_2} < \alpha < \alpha_{c_1}$	negative	positive	$F^0_{t_1} + \mathcal{B}\nabla^2 F^0 + \mathcal{C}\nabla^4 F^0 + \lvert\nabla F^0\rvert^2/2 = 0$	4
α_{c_2}	$\mathcal{B}_c$	0	$F^0_{t_1} + \mathcal{B}_c\nabla^2 F^0 + \lvert\nabla F^0\rvert^2/2 = 0$	2
$-\infty < \alpha < \alpha_{c_2}$	negative	negative	$F^0_{t_1} + \mathcal{B}\nabla^2 F^0 + \mathcal{C}\nabla^4 F^0 + \lvert\nabla F^0\rvert^2/2 = 0$	4

4.7 Linear Stability Analysis of the Evolution Equation for the Perturbed Flame Front in High Density Fluids

In the previous section, we have derived a nonlinear evolution equation for the perturbed flame front. Now, we will analyze the flame front equation, (4.184) by following the usual procedure of a linear stability analysis. For simplicity we will only consider the planar flame in two-dimension, namely,

$$F^0_{t_1} + \mathcal{B}F^0_{\eta\eta} + \mathcal{C}F^0_{\eta\eta\eta\eta} + \frac{1}{2}(F^0_\eta)^2 = 0 \tag{4.189}$$

where

$$\mathcal{B} = \frac{1-\alpha}{2-\alpha}\big(2 - \ln(1-\alpha)\big), \tag{4.190}$$

and

$$\mathcal{C} = -1 - \frac{5l_c}{2} + \alpha(2-\alpha)^{-1} + (1-\alpha)(2-\alpha)^{-1}\int_{-\infty}^{0} \ln(1-\alpha e^{\bar{\xi}})d\bar{\xi}. \tag{4.191}$$

There is an obvious basic state

$$F^s = 0 \tag{4.192}$$

which satisfies equation (4.189) and this corresponds to a disturbance-free planar flame. We can now examine its linear stability by introducing a small perturbation to the basic state, writing

$$F^0 = F^s + \epsilon\tilde{F} \tag{4.193}$$

where ϵ is a small parameter. Now substitute the perturbed form (4.193) into equation (4.189). At $O(\epsilon)$,

$$\tilde{F} + \mathcal{B}\tilde{F}_{\eta\eta} + \mathcal{C}\tilde{F}_{\eta\eta\eta\eta} = 0. \tag{4.194}$$

We now express $\tilde{F}$ in the form

$$\tilde{F} = \exp(\omega t + ik\zeta). \tag{4.195}$$

Substituting this into the linearized equation (4.194) to yield the following expression for the growth rate

$$\omega = \mathcal{B}k^2 - \mathcal{C}k^4. \tag{4.196}$$

The neutral stability curves that separate stable from unstable solutions is sketched in Figure 4.9, 4.10 and 4.11. We see that there is a range of α, namely, $\alpha_{c_2} < \alpha < \alpha_{c_1}$, such that the flame is stable to all disturbances as shown in Figure 4.9. Furthermore, we observe that there are two critical values, α_{c_1} and α_{c_2}, for which the basic state first becomes linearly unstable.

Figure 4.10 shows the neutral stability curve in the range $\alpha_{c_1} < \alpha < 1$ in more detail. If $\alpha > \alpha_{c_1}$, then there always exists a finite band of wave numbers that grow exponentially. The length of this band of wave numbers increases as α increases and reaches its maximum at $\alpha = 0$. Then it decreases as α increases and terminates as $\alpha \to 1$. Therefore, the flame front F is unstable for the perturbations characterized by sufficiently large wavelengths.

On the other hand, if $\alpha < \alpha_{c_2}$, then there is an infinite band of unstable wavelengths as shown in Figure 4.11. We note that there is a turning point located at $k = 0.8936$ and $\alpha = -37.5$. Furthermore, the stable solutions region is to the left of this stability boundary. As a result, for large negative value of α, the flame front F is stable under small perturbations.

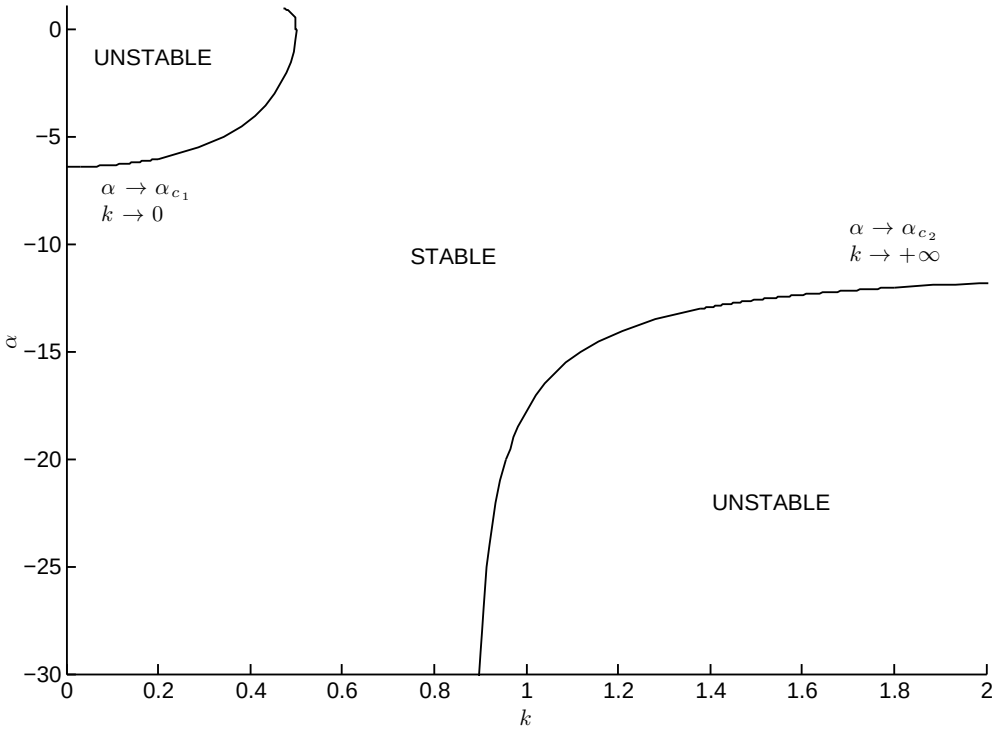

Figure 4.9 Neutral Stability curve.

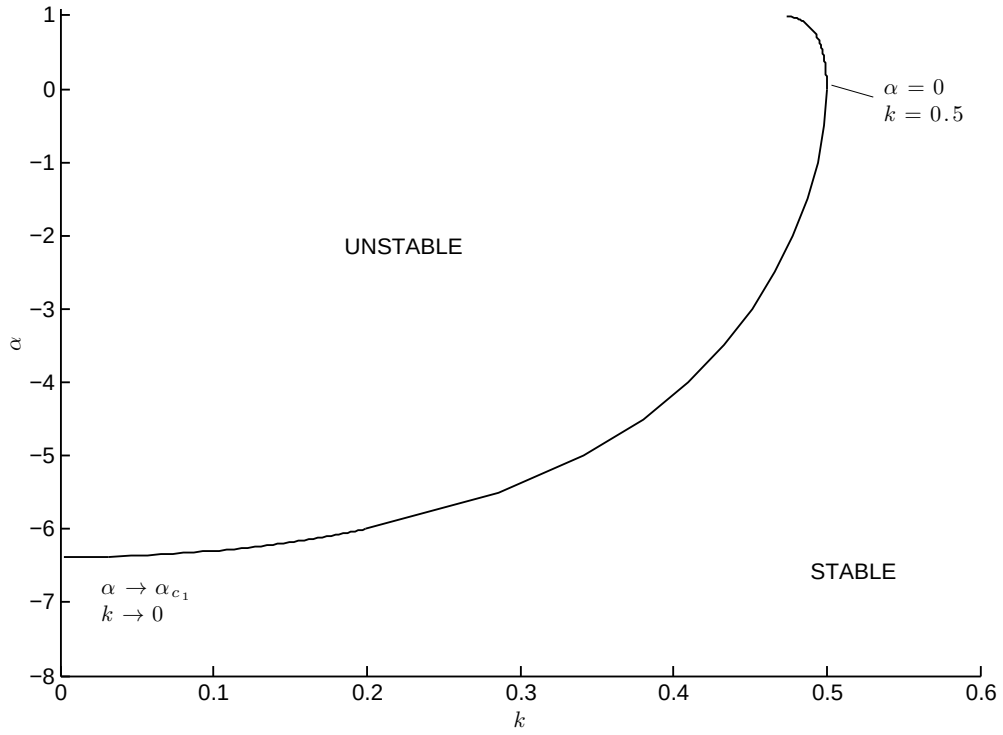

Figure 4.10 Neutral Stability curve.

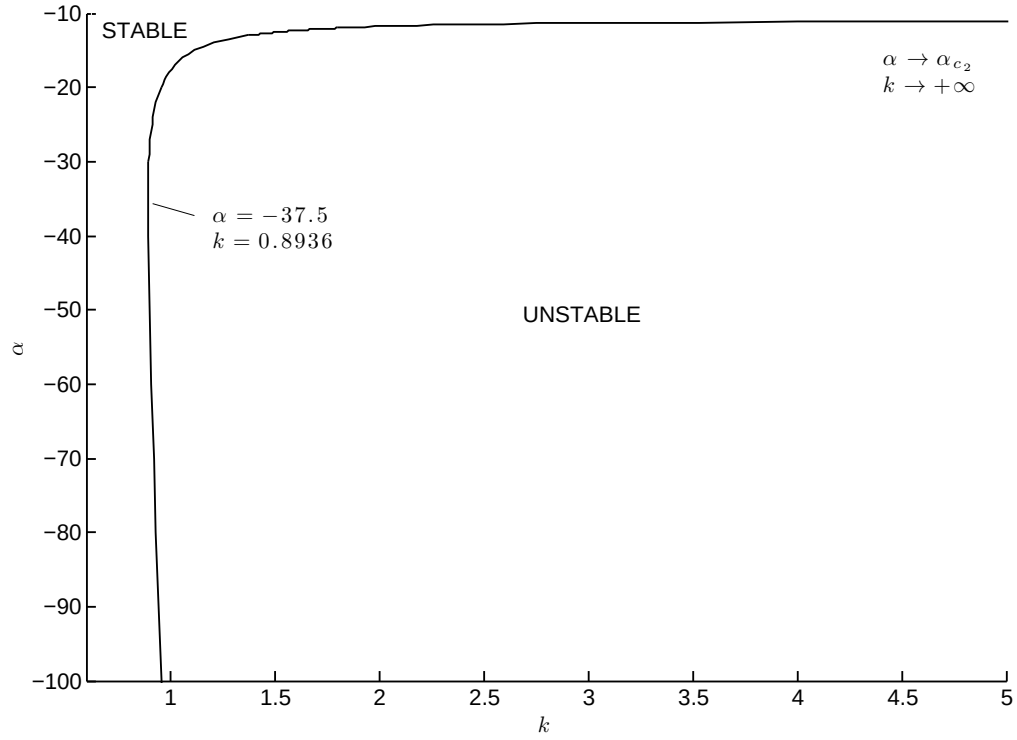

Figure 4.11 Neutral Stability curve.

4.8 Concluding Remarks

We have derived an asymptotic model of premixed flames propagating in high density fluids, where the transport of fuel is primarily through thermal diffusion, while the oxidant undergoes normal Fickian diffusion. Our model, (4.98) - (4.104), (4.107) and (4.108) has an explicit dependence on Lewis numbers, Le_O, equivalence ratio, ϕ, and modified Soret diffusion coefficient, α. It is worth mentioning that the local analysis of the reaction zone revealed that Soret effect gives rise to a completely new balance within the flame structure, namely, a balance between convection, Fickian diffusion, Soret diffusion and reaction has to be achieved. The model was used to analyze the basic structure of steady planar flames in a uniform flow with high density. The limited diffusion of fuel results in a discontinuous outer profile, and a rapid consumption within the reaction zone. The Soret effect, in which the fuel is transported toward the hot reaction zone, results in excess fuel mass concentrations on the upstream side of the reaction sheet. In addition, we find that the adiabatic flame speed increases as a function of the modified Soret diffusion coefficient.

We also examined the linear stability of the steady planar flame to arbitrary disturbances. The derived dispersion relation for the growth rate of a disturbance identifies a range of stable Lewis numbers and two distinct stability boundaries (similar to the ordinary gas flame), one corresponding to a cellular branch and the other to a pulsating regime. We have analyzed the effect of the Soret diffusion coefficient on these boundaries. For positive and small negative values of α, it is shown that a planar flame front is stable if the Lewis number corresponding to the oxidant, Le_O exceeds some critical value close to unity (but $Le_O < 1$). For large negative values of α, the cellular branch can be extended into the regime of $Le_O > 1$, suggesting that cellular instability may be observed in this regime. We note that light fuels, e.g., hydrogen typically has value of $\alpha < 0$, and the present theory suggests that cellular instability may be observed even when $Le_O > 1$.

In addition, the model was used to derive a nonlinear partial differential equation that describes the evolution of the flame front in the vicinity of the cellular stability boundary. This new evolution equation has an explicit dependence on the modified Soret diffusion coefficient, α and it can be reduced to the K-S equation in the limiting case $\alpha = 0$. We also carried out a linear stability analysis of the evolution equation. We find that the flame front is unstable with respect to long-wave instability in a range of Soret diffusion coefficient corresponds to no and weak Soret effect. Moreover, the analysis reveals that the flame front is unconditionally stable for moderate Soret effect and becomes unstable again under perturbations of sufficiently short wavelength.

CHAPTER 5

CONCLUSIONS

In the present work, we have used asymptotic and perturbations methods, supplemented by numerical methods to investigate the structure and dynamical properties of flames at high pressure and/or high density fluids. As the work covers two distinct topics, conclusions from each study are presented below.

5.1 Diffusion Flames

In Chapter 3, we have analyzed the asymptotic structure of a laminar diffusion flame residing in a counterflow of a fluid fuel stream and a gaseous oxidant. The oxidant undergoes Fickian diffusion, while the fuel diffuses primarily as a result of temperature gradients, i.e., the Soret effect. We adopt a constant density approximation, and pursue a large activation energy limit. As a result of our novel transport mechanism, appropriate for sufficiently high pressure and/or high density fluids, the local structure equations are substantially different from those discovered by Liñán for ideal gas streams. Temperature and concentration profiles are determined, and the fundamental flame properties of flame temperature and location are found explicitly as a function of Soret diffusion coefficient, ratio of temperature of the two streams, and the Damköhler number.

Our model predicts that the flame resides on the fuel side of the stagnation plane, although it moves closer to the oxidant stream as the value of the Soret coefficient is decreased. Exact solution of the structure problem, for the case when the temperature of the fuel supply stream equals the adiabatic flame temperature ($\beta = 1 + q/\phi$), shows a monotonic decreases in flame position with Damköhler number. However, for lower values of fuel stream temperature, computation of the local structure problem determines explicit extinction conditions, characterized by

turning points in response curves of flame location and temperature as a function of Damköhler number.

5.2 Premixed Flames

In Chapter 4, we have derived an asymptotic model of premixed flames propagating in high density fluids, where the transport of fuel is primarily through thermal diffusion, while the oxidant undergoes normal Fickian diffusion. Our model, (4.98) - (4.104), (4.107) and (4.108) has an explicit dependence on Lewis numbers, Le_O, equivalence ratio, ϕ, and modified Soret diffusion coefficient, α. It is worth mentioning that the local analysis of the reaction zone revealed that Soret effect gives rise to a completely new balance within the flame structure, namely, a balance between convection, Fickian diffusion, Soret diffusion and reaction has to be achieved. The model was used to analyze the basic structure of steady planar flames in a uniform flow with high density. The limited diffusion of fuel results in a discontinuous outer profile, and a rapid consumption within the reaction zone. The Soret effect, in which the fuel is transported toward the hot reaction zone, results in excess fuel mass concentrations on the upstream side of the reaction sheet. In addition, we find that the adiabatic flame speed increases as a function of the modified Soret diffusion coefficient.

We also examined the linear stability of the steady planar flame to arbitrary disturbances. The derived dispersion relation for the growth rate of a disturbance identifies a range of stable Lewis numbers and two distinct stability boundaries (similar to the ordinary gas flame), one corresponding to a cellular branch and the other to a pulsating regime. We have analyzed the effect of the Soret diffusion coefficient on these boundaries. For positive and small negative values of α, it is shown that a planar flame front is stable if the Lewis number corresponding to the oxidant, Le_O exceeds some critical value close to unity (but $Le_O < 1$). For large negative values of α, the cellular branch can be extended into the regime of $Le_O > 1$,

suggesting that cellular instability may be observed in this regime. We note that light fuels, e.g., hydrogen typically has value of $\alpha < 0$, and the present theory suggests that cellular instability may be observed even when $Le_O > 1$.

In addition, the model was used to derive a nonlinear partial differential equation that describes the evolution of the flame front in the vicinity of the cellular stability boundary. This new evolution equation has an explicit dependence on the modified Soret diffusion coefficient, α and it can be reduced to the K-S equation in the limiting case $\alpha = 0$. We also carried out a linear stability analysis of the evolution equation. We find that the flame front is unstable with respect to long-wave instability in a range of Soret diffusion coefficient corresponds to no and weak Soret effect. Moreover, the analysis reveals that the flame front is unconditionally stable for moderate Soret effect and becomes unstable again under perturbations of sufficiently short wavelength.

APPENDIX A

INTERIOR LAYER ANALYSIS OF THE CHEMISTRY-FREE EQUATION FOR FUEL CONCENTRATION

In this section, we will construct the asymptotic solution to the chemistry-free equation for fuel concentration in the region $z < z_f$. Let $()'$ denotes the derivative of the function, $\frac{d}{dz}()$. Thus equation (3.16) can be written as

$$\alpha_D Y'' + \alpha_s \left(Y \frac{T'}{T} \right)' + zY' = 0 \tag{A.1}$$

with the boundary conditions

$$Y = \begin{cases} 0, & z \to -\infty \\ Y^-, & z \to z_f^- \end{cases}, \tag{A.2}$$

where $T = 1 + A[2 - erfc(z/\sqrt{2})]$, $A = (T_f - 1)/(2 - E)$ and $E = erfc(z_f/\sqrt{2})$.

A.1 Outer Solution

The solution in this region can be expanded in powers of α_D,

$$Y = Y_{out} + \alpha_D Y^1_{out} + \cdots . \tag{A.3}$$

Substituting the above expansion into equation (A.1), we obtain the leading order equation

$$\left(z + \alpha_s \frac{T'}{T} \right) Y'_{out} + \alpha_s \left(\frac{T'}{T} \right)' Y_{out} = 0, \tag{A.4}$$

and the outer solution is

$$Y_{out} = \begin{cases} 0, & \infty < z < z_0 \\ Y^- \exp\left\{ \int_{z_f}^{z} \left[\frac{\alpha_s \frac{T'}{T}(\xi + \frac{T'}{T})}{\xi + \alpha_s \frac{T'}{T}} \right] d\xi \right\}, & z_0 < z < z_f^- \end{cases}, \tag{A.5}$$

where $z_0 = -\alpha_s T(z_0)'/T(z_0)$ is the singular point of equation (A.4).

The outer solution is not valid in the neighborhood of z_0, the rapid transition in this region is characteristic of an interior layer. Moreover, the outer solution is not even continuous when z is near z_0 for $\alpha_s < 0$. To determine the behavior near the interior layer, it is require a new expansion. To obtain this interior layer expansion, which together with the outer expansion will yield a composite expansion that is valid everywhere.

A.2 Interior Layer

To investigate the interior layer, we introduce the stretched variable

$$\bar{z} = \frac{z - z_0}{\alpha_D^{1/2}}, \tag{A.6}$$

expand T'/T in terms of the stretched variable $\bar{z}$ about z_0

$$\frac{T'}{T} \sim \frac{T'(z_0)}{T(z_0)} \left\{ 1 - \alpha_D^{1/2} \bar{z} \left(z_0 + \frac{T'(z_0)}{T(z_0)} \right) \right\}, \tag{A.7}$$

and expand the interior layer solution as

$$Y = Y_{in} + \alpha_D^{1/2} Y_{in}^1 + \cdots . \tag{A.8}$$

Now, substituting equations (A.6) – (A.8) into equation (A.1) yields the leading order problem

$$\left(z_0 + \alpha_s \frac{T'(z_0)}{T(z_0)} \right) Y_{in}' = 0, \tag{A.9}$$

We note that equation (A.9) is automatically satisfied by the fact that $z_0 = -\alpha_s T'(z_0)/T(z_0)$. Thus we have to go to the next order, $O(\alpha_D^{1/2})$ and the equation is

$$Y_{in}'' + a\bar{z} Y_{in}' + b Y_{in} = 0. \tag{A.10}$$

where

$$a = 1 + z_0^2(1 - \alpha_s^{-1})$$

and

$$b = z_0^2(1 - \alpha_s^{-1}).$$

The general solution of equation (A.10) can be written in terms of a linear combination of the confluent hypergeometric function ${}_1F_1$:

$$Y_{in}(\bar{z}) = c_{11}F_1\left(\frac{b}{2a}, \frac{1}{2}, -\frac{a}{2}\bar{z}^2\right) + c_2\bar{z}_1F_1\left(\frac{a+b}{2a}, \frac{3}{2}, -\frac{a}{2}\bar{z}^2\right) \tag{A.11}$$

where c_1 and c_2 are arbitrary constants.

A.3 Matching

We can determine the unknown constant c_1 and c_2 in the first approximation of the interior layer solution (A.11) by requiring that the inner solution matches with the outer solution (A.5).

$$\lim_{\bar{z}\to-\infty} Y_{in}(\bar{z}) = \lim_{z\to z_0^-} Y_{out}(z), \tag{A.12}$$

$$\lim_{\bar{z}\to+\infty} Y_{in}(\bar{z}) = \lim_{z\to z_0^+} Y_{out}(z). \tag{A.13}$$

The matching conditions are derived by expanding the outer solution Y_{out} (A.5) in terms of the inner variable $\bar{z}$, to yield

$$\lim_{z\to z_0^-} Y_{out}(z) \sim 0, \tag{A.14}$$

$$\lim_{z\to z_0^+} Y_{out}(z) \sim Y^-\left(\frac{\alpha_D^{1/2}\bar{z}}{z_f - z_0}\right)^p, \tag{A.15}$$

where

$$p = \frac{z_0^2(1-\alpha_s)}{\alpha_s - z_0^2(1-\alpha_s)}.$$

Since $a > 0$ in equation (A.10), the asymptotic expansion of the inner solution Y_{in} (A.11) for large $|\bar{z}|$ is

$$Y_{in} \sim \sqrt{\pi}\left(\frac{a}{2}\right)^{-b/2a}\left\{c_1\frac{1}{\Gamma\left(\frac{a-b}{2a}\right)}|\bar{z}|^{-b/a} + c_2\frac{1}{\Gamma\left(\frac{2a-b}{2a}\right)}\left(\frac{a}{2}\right)^{-1/2}\bar{z}|\bar{z}|^{-(a+b)/a}\right\} \quad \text{(A.16)}$$

where Γ is the gamma function. Applying the matching conditions (A.12) and (A.13) yield

$$\sqrt{\pi}\left(\frac{a}{2}\right)^{-b/2a}\left\{c_1\frac{1}{\Gamma\left(\frac{a-b}{2a}\right)} - c_2\frac{1}{\Gamma\left(\frac{2a-b}{2a}\right)}\left(\frac{a}{2}\right)^{-1/2}\right\} = 0$$

and

$$\sqrt{\pi}\left(\frac{a}{2}\right)^{-b/2a}\left\{c_1\frac{1}{\Gamma\left(\frac{a-b}{2a}\right)} + c_2\frac{1}{\Gamma\left(\frac{2a-b}{2a}\right)}\left(\frac{a}{2}\right)^{-1/2}\right\} = Y^-\left(\frac{\alpha_D^{1/2}}{z_f - z_0}\right)^p$$

from which it follows that

$$c_1 = \frac{Y^-}{2\sqrt{\pi}}\left(\frac{a}{2}\right)^{b/2a}\Gamma\left(\frac{a-b}{2a}\right)\left(\frac{\alpha_D^{1/2}}{z_f - z_0}\right)^p \quad \text{(A.17)}$$

and

$$c_2 = \frac{Y^-}{2\sqrt{\pi}}\left(\frac{a}{2}\right)^{(a+b)/2a}\Gamma\left(\frac{2a-b}{2a}\right)\left(\frac{\alpha_D^{1/2}}{z_f - z_0}\right)^p. \quad \text{(A.18)}$$

A.4 Composite Expansion

We have constructed the inner and outer asymptotic solutions in two different regions. The last step is to combine the two solutions into a single expression. The basic idea is to add expansions and then subtract the overlap part, i.e.

$$Y_{comp} = Y_{out} + Y_{in} - Y_{overlap}.$$

Thus, the leading order composite expansion for $z_0 \le z \le z_f^-$ is given by

$$
\begin{aligned}
Y_{comp} \;\sim\; & Y^- \exp\left\{\int_{z_f}^{z_0}\left[\frac{\alpha_s\frac{T'}{T}(\xi+\frac{T'}{T})}{\xi+\alpha_s\frac{T'}{T}}\right]d\xi\right\} \\
+ \;& \frac{Y^-}{2\sqrt{\pi}}\left(\frac{a}{2}\right)^{b/2a}\left(\frac{\alpha_D^{1/2}}{z_f-z_0}\right)^p \\
& \left\{\Gamma\left(\frac{a-b}{2a}\right){}_1F_1\left(\frac{b}{2a},\frac{1}{2},-\frac{a}{2}\frac{(z-z_0)^2}{\alpha_D}\right)+\right. \\
& \left.\left(\frac{a}{2}\right)^{1/2}\Gamma\left(\frac{2a-b}{2a}\right)\frac{(z-z_0)}{\alpha_D^{1/2}}{}_1F_1\left(\frac{a+b}{2a},\frac{3}{2},-\frac{a}{2}\frac{(z-z_0)^2}{\alpha_D}\right)\right\} \\
- \;& Y^-\left(\frac{z-z_0}{z_f-z_0}\right)^p, \qquad\qquad (A.19)
\end{aligned}
$$

and for $-\infty < z \leq z_0$ is

$$
\begin{aligned}
Y_{comp} \;\sim\; & \frac{Y^-}{2\sqrt{\pi}}\left(\frac{a}{2}\right)^{b/2a}\left(\frac{\alpha_D^{1/2}}{z_f-z_0}\right)^p \\
& \left\{\Gamma\left(\frac{a-b}{2a}\right){}_1F_1\left(\frac{b}{2a},\frac{1}{2},-\frac{a}{2}\frac{(z-z_0)^2}{\alpha_D}\right)+\right. \\
& \left.\left(\frac{a}{2}\right)^{1/2}\Gamma\left(\frac{2a-b}{2a}\right)\frac{(z-z_0)}{\alpha_D^{1/2}}{}_1F_1\left(\frac{a+b}{2a},\frac{3}{2},-\frac{a}{2}\frac{(z-z_0)^2}{\alpha_D}\right)\right\}. \qquad (A.20)
\end{aligned}
$$

Figures A.1 and A.2 shows the outer, inner and uniformly valid asymptotic approximations to the solution for $\alpha_D = 0.001$, clearly showing the boundary layer structure and how the uniformly valid solution captures both solutions regimes. The value of α_s is -0.4 in Figure A.1 and 0.4 in Figure A.2, with $\phi = 1$, $q = 5$, $\beta = 1+q/\phi$, and $Y^- = 0.2$.

The composite expansion gives a very good approximation to the numerical solution in the region $z < z_f$ as shown in Figures A.3 and A.4. For comparison purposes, the values used in Figures A.3 and A.4 are the same as the one used in Figures A.1 and A.2.

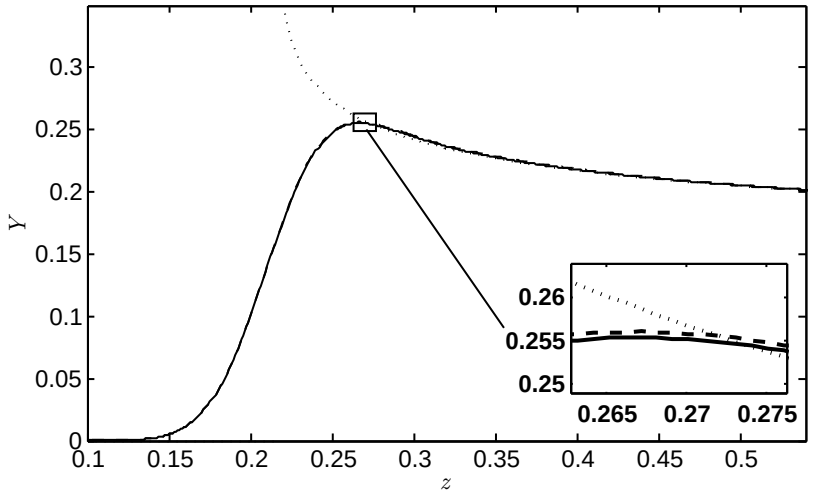

Figure A.1 Asymptotic solution of (A.1) showing interior layer near z_0 for $\alpha_D = 0.001$ with $\phi = 1$, $q = 5$, $\beta = 1 + q/\phi$, $Y^- = 0.2$ and $\alpha_s = -0.4$. The dotted curve corresponds to the outer solution (A.5). The dashed curve corresponds to the inner solution (A.11). The solid curve corresponds to the composite solution (A.19) and (A.20).

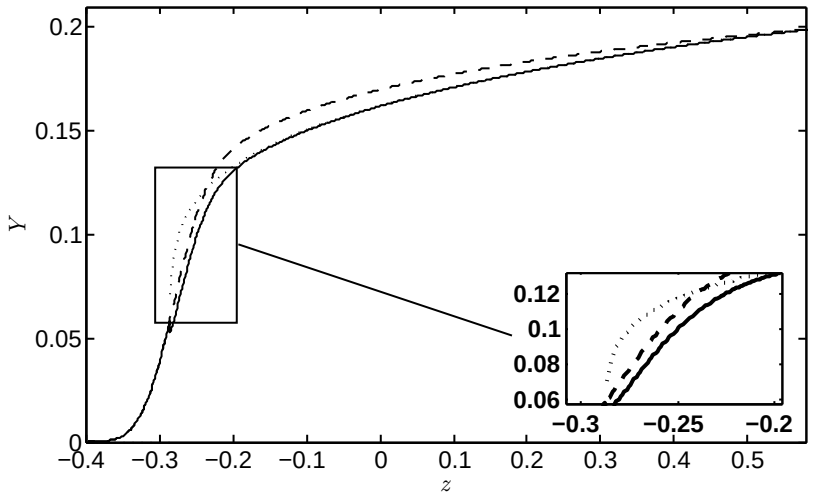

Figure A.2 Asymptotic solution of (A.1) showing interior layer near z_0 for $\alpha_D = 0.001$ with $\phi = 1$, $q = 5$, $\beta = 1 + q/\phi$, $Y^- = 0.2$ and $\alpha_s = 0.4$. The dotted curve corresponds to the outer solution (A.5). The dashed curve corresponds to the inner solution (A.11). The solid curve corresponds to the composite solution (A.19) and (A.20).

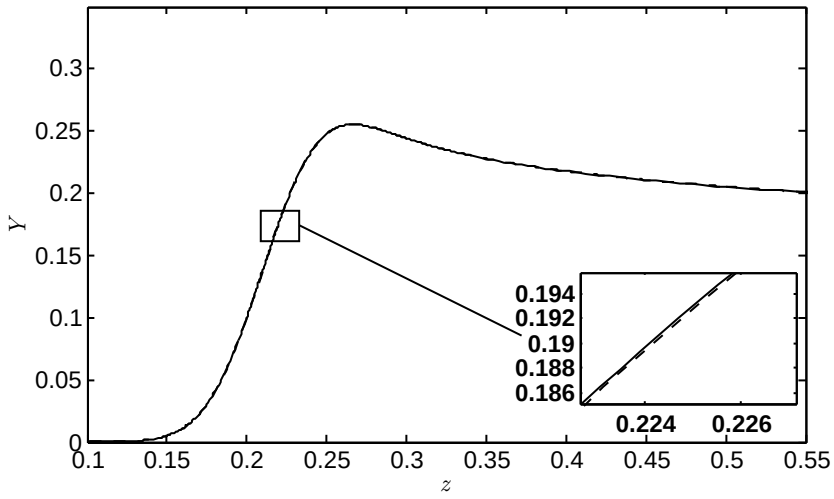

Figure A.3 The dashed curve corresponds to the composite solution (A.19) and (A.20). The solid curve corresponds to the numerical solution of (A.1). The differences between the composite and numerical solution are so small that the two are almost indistinguishable. The value of $\alpha_D = 0.001$ with $\phi = 1$, $q = 5$, $\beta = 1 + q/\phi$, $Y^- = 0.2$ and $\alpha_s = -0.4$.

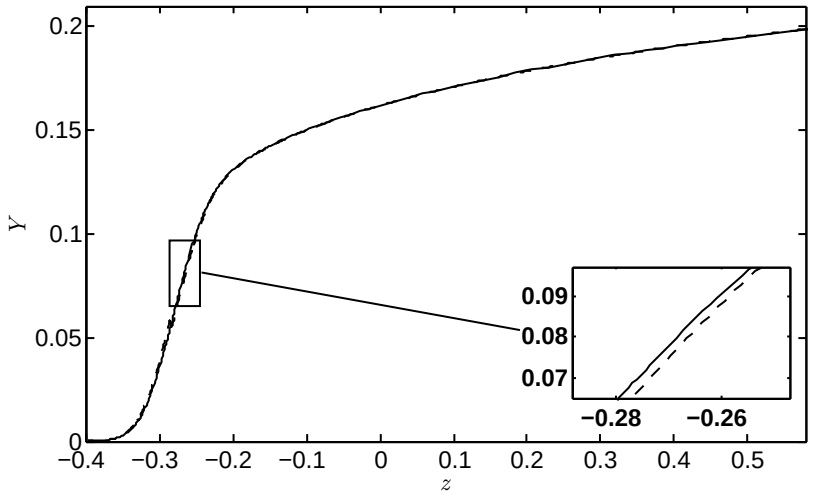

Figure A.4 The dashed curve corresponds to the composite solution (A.19) and (A.20). The solid curve corresponds to the numerical solution of (A.1). The differences between the composite and numerical solution are so small that the two are almost indistinguishable. The value of $\alpha_D = 0.001$ with $\phi = 1$, $q = 5$, $\beta = 1 + q/\phi$, $Y^- = 0.2$ and $\alpha_s = 0.4$.

BIBLIOGRAPHY

[1] Antoniou, E. S., Bechtold, J. K., and Matalon, M. A diffusional-thermal theory of near-stoichiometric premixed flames. *SIAM Journal of Applied Mathematics 64* (2004), 1434–1456.

[2] Arias-Zugasti, M., and Rosner, D. E. Soret transport, unequal diffusivity, and dilution effects on laminar diffusion flame temperatures and positions. *Combust. Flame 153* (2008), 33–44.

[3] Bechtold, J. K., and Margolis, S. B. The structure of supercritical diffusion flames with arrhenius mass diffusivities. *Combust. Sci. and Tech. 83* (1992), 257–290.

[4] Bechtold, J. K., and Matalon, M. Effects of stoichiometry on stretched premixed flames. *Combust. Flame 119* (1999), 217–232.

[5] Buckmaster, J. D. Slowly varying laminar flames. *Combust. Flame 28* (1977), 225–239.

[6] Buckmaster, J. D., and Ludford, G. S. S. *Theory of Laminar Flames.* Cambridge University Press, 1982.

[7] Burke, S. P., and Schumann, T. E. W. Diffusion flames. *Industrial and Engineering Chemistry 20* (1928), 998–1004.

[8] Cheatham, S., and Matalon, M. A general asymptotic theory of diffusion flames with application to cellular instability. *J. Fluid Mech. 414* (2000), 105–144.

[9] Clavin, P., and Williams, F. Effects of molecular diffusion and of thermal expansion on the structure and dynamics of premixed flames in turbulent flows of large scale and low intensity. *J. Fluid Mech. 116* (1982), 251–282.

[10] Dakhlia, R. B., Giovangigli, V., and Rosner, D. E. Soret effects in laminar counterflow spray diffusion flames. *Combust. Theory Modelling 6* (2002), 1–17.

[11] Daou, J., and Rogg, B. Convective burning of gaseous fuel pockets and supercritical droplets. *Combust. Flame 115* (1998), 1450157.

[12] Darrieus, G. Propagation d'un front de flamme. In *La Technique Moderne* (1938).

[13] Ern, A., and Giovangigli, V. Thermal diffusion effects in hydrogen-air and methane-air flames. *Combust. Theory Modelling 2* (1998), 349–372.

[14] Ern, A., and Giovangigli, V. Impact of detailed multicomponent transport on planar and counterflow hydrogen-air and methane-air flames. *Combust. Sci. and Tech. 149* (1999), 157–181.

[15] Foster, J. W., and Miller, R. S. *Fundamentals of High Pressure Combustion*. ProcessEng Engineering GmbH, 2010, ch. High Pressure Processes in Chemical Engineering, pp. 53–75.

[16] García-Ybarra, P., Nicoli, C., and Clavin, P. Soret and dilution effects on premixed flames. *Combust. Sci. and Tech. 42* (1984), 87–109.

[17] García-Ybarra, P. L., and Clavin, P. Cross-transport effects in nonadiabatic premixed flames. In *7th International Colloquium on Gasdynamics of Explosions and Reactive Systems* (1981), pp. 463–481.

[18] Harstad, K., and Bellan, J. Interactions of fluid oxygen drops in fluid hydrogen at rocket chamber pressures. *Int. J. Heat Mass Transfer 41* (1998), 3551–3558.

[19] Harstad, K., and Bellan, J. Isolated fluid oxygen drop behavior in fluid hydrogen at rocket chamber pressures. *Int. J. Heat Mass Transfer 41* (1998), 3537–3550.

[20] Harstad, K., and Bellan, J. High-pressure binary mass diffusion coefficients for combustion applications. *Ind. Eng. Chem. Res. 43* (2004), 645–654.

[21] Harstad, K. G., and Bellan, J. An all-pressure fluid drop model applied to bindary mixture: heptane in nitrogen. *Int. J. Multiphase Flow 26* (2000), 1675–1706.

[22] Harstad, K. G., Miller, R. S., and Bellan, J. Efficient high pressure state equations. *A.I.Ch.E. J. 43* (1997), 1605–1610.

[23] Joulin, G., and Clavin, P. Linear stability analysis of nonadiabatic flames: Diffusional-thermal. *Combust. Flame 35* (1979), 139–153.

[24] Kim, J. S., and Williams, F. Diffusional-thermal instability of diffusion flames. *J. Fluid Mech. 327* (1996), 273–301.

[25] Kim, J. S., and Williams, F. Extinction of diffusion flames with nonunity lewis numbers. *Journal of Engineering Mathematics 31* (1997), 101–118.

[26] Kukuck, S., and Matalon, M. The onset of oscillations in diffusion flames. *Combust. Theory Modelling 5* (2001), 217–240.

[27] Landau, L. D. On the theory of slow combustion. *Acta Physicochim. 19* (1944), 77–85.

[28] Law, C. K. Asymptotic theory for ignition and extinction in droplet burning. *Combust. Flame* (1974).

[29] Law, C. K. *Combustion Physics*. Cambridge University Press, 2006.

[30] Liñán, A. The asymptotic structure of counterflow diffusion flames for large activation energies. *Acta Astronautica 1* (1974), 1007–1039.

[31] Margolis, S. B. Chaotic combustion of solids and high-density fluids near points of strong resonance. *Proc. R. Soc. Lond. A. 433* (1991), 131–150.

[32] Margolis, S. B., and Johnston, S. C. Multiplicity and stability of supercritical combustion in a nonadiabatic tubular reactor. *Combust. Sci. and Tech. 65* (1989), 103–136.

[33] Markstein, G. H. Experimental and theoretical studies of flame-front stability. *Journal of the Aeronautical Sciences* (1951), 199–209.

[34] Matalon, M., Cui, C., and Bechtold, J. K. Hydrodynamic theory of premixed flames: Effects of stoichiometry, variable transport coefficients and arbitrary reaction orders. *J. Fluid Mech. 487* (2003), 179–210.

[35] Matalon, M., and Ludford, G. S. S. On the near ignition stability of diffusion flames. *International Journal of Engineering Sciences 18* (1980), 1017–1026.

[36] Matalon, M., and Matkowsky, B. J. Flames as gasdynamic discontinuities. *J. Fluid Mech. 124* (1982), 239–259.

[37] Matkowsky, B. J., and Sivashinsky, G. An asymptotic derivation of two models in flame theory associated with the constant density approximation. *SIAM Journal of Applied Mathematics 37* (1979), 686–699.

[38] Miller, R. S., Harstad, K. G., and Bellan, J. Direct numerical simulation of a supercritical mixing layer. No. 2000-0195, 38th Aerospace Sciences Meeting.

[39] Miller, R. S., Harstad, K. G., and Bellan, J. Direct numerical simulation of supercritical fluid mixing layers applied to heptane-nitrogen. *J. Fluid Mech. 436* (2001), 1–39.

[40] Palle, S., and Miller, R. S. Analysis of high-pressure hydrogen, methane, and heptane laminar diffusion flames: Thermal diffusion factor modeling. *Combust. Flame 151* (2007), 581–600.

[41] Palle, S., Nolan, C., and Miller, R. S. On molecular transport effects in real gas laminar diffusion flames at large pressure. *Phys. Fluids 17*, 103601 (2005), 1–19.

[42] Peters, N. *Turbulent Combustion*. Cambridge University Press, 2000.

[43] Ribert, G., Zong, N., Yang, V., Pons, L., Darabiha, N., and Candel, S. Counterflow diffusion flames of general fluids: Oxygen/hydrogen mixtures. *Combust. Flame 154* (2008), 319–330.

[44] Rosner, D. E., Israel, R. S., and Mantia, B. L. Heavy species ludwig-soret transport effects in air-breathing combustion. *Combust. Flame 123* (2000), 547–560.

[45] Sivashinsky, G. On a distorted flame front as a hydrodynamic discontinuity. *Acta Astronautica 3* (1976), 889–918.

[46] Sivashinsky, G. Diffusional-thermal theory of cellular flames. *Combust. Sci. and Tech. 15* (1977), 137–146.

[47] Sivashinsky, G. On flame propagation under conditions of stoichiometry. *SIAM Journal of Applied Mathematics 39* (1980), 67–82.

[48] Sivashinsky, G., Law, C. K., and Joulin, G. On stability of premixed flames in stagnation - point flow. *Combust. Sci. and Tech. 28* (1982), 155–159.

[49] Williams, B. A. Sensitivity of calculated extinction strain rate to molecular transport formulation in nonpremixed counter flames. *Combust. Flame 124* (2001), 330–333.

[50] Williams, F. *Combustion Theory*, 2nd ed. Addison-Wesley, 1985.

[51] Yang, F., Law, C. K., Sung, C. J., and Zhang, H. Q. A mechanistic study of soret diffusion in hydrogen–air flames. *Combust. Flame 157* (2010), 192–200.

[52] Zel'dovich, Y. B., and Frank-Kamenetsky, D. A. A theory of thermal flame propagation (in russian). *Zhurnal Fizicheskoi Khimii 12* (1938), 100–105.